2010

Fatigue of polymer composites: Life prediction and environmental effects

David Brian Dittenber
West Virginia University

Fatigue of Polymer Composites: Life Prediction and Environmental Effects

David Brian Dittenber

Thesis submitted to the
College of Engineering and Mineral Resources at
West Virginia University in
partial fulfillment of the requirements
for the degree of

Master of Science
in
Civil Engineering

Approved by

Hota V. S. GangaRao, PhD, Chair
Ruifeng Liang, PhD
Udaya B. Halabe, PhD

Department of Civil and Environmental Engineering

Morgantown, West Virginia
2010

Keywords: strain energy, fatigue life prediction, GFRP, tension, salt water, absorption

ABSTRACT

Fatigue of Polymer Composites: Life Prediction and Environmental Effects

David Dittenber
Constructed Facilities Center, West Virginia University

Fiber reinforced polymer composites offer significant advantages over traditional structural materials, but also many challenges, particularly with regard to their long term behavior. The fatigue performance of composites has been explored for the last few decades but it is still difficult to predict the behavior of a particular material under different loading and environmental conditions. Many researchers have worked to develop fatigue life prediction models and others to characterize the effect of environmental changes on static composite material properties, but experimental work in both of these areas can be difficult to perform and thus many observations have not been fully understood.

In order to further explore the effect of environmental conditions on fatigue life, a regimen of test was performed on a glass / vinyl ester composite. The testing included bending fatigue tests, tension-tension fatigue tests, and immersion conditioned tension-tension fatigue tests, with each type being performed under varying environmental conditions in the forms of elevated temperatures and the presence of salt water. From the experimental data, it was observed that the presence of salt water caused as much as a 50% decrease in fatigue life but was dependent on the time of exposure and had little effect on short duration tests. Elevated temperatures had an even more detrimental effect and exhibited a linear relationship with the number of cycles to failure. Immersion conditioning at room temperature decreased the fatigue life of the material to around 50-65% while immersion conditioning at 100°F decreased the fatigue life to around 15-25%.

Additionally, a strain energy-based fatigue life prediction model proposed by researchers at the West Virginia University Constructed Facilities Center was evaluated by applying the model to data collected through the experimental work, as well as to a large amount of fatigue data from the DOE/MSU Composite Material Fatigue Database. Test results for 109 different composites (1254 individual tests) were analyzed. From the variety of coupon fatigue data used to evaluate the model, it was found that the model was able to fit GFRP materials with over 80% of the results falling within ±5% of the log number of cycles to failure. The model was also shown to be able to predict the fatigue life of polyester GFRPs to within ±5% of the log number of cycles to failure using only two experimental values with a success rate of over 75%; using three increased the success rate to over 80%, but using more had little effect on its accuracy. A single-sample estimation model based on resin volume fraction was also developed and had reasonable success with polyester GFRPs. Of the two component fatigue results tested, both were able to be predicted by the fatigue model to within ±2.5% log error. The strain energy fatigue model appears to provide both a good fit and a good prediction for the tension-tension fatigue life of GFRP composite materials.

ACKNOWLEDGEMENTS

Oh, the depth of the riches both of the wisdom and knowledge of God! How unsearchable are His judgments and unfathomable His ways! For who has known the mind of the Lord, or who became His counselor? Or who has first given to Him that it might be paid back to him again? For from Him and through Him and to Him are all things. To Him be the glory forever. Amen.

~ Romans 11:33-36 ~

I would like to thank my advisor, Dr. Hota GangaRao, for his guidance and encouragement over the course of this project, as well as for serving as the chair of my review board. I have his instruction to thank for much of what I have learned over the last two years, and I greatly appreciate his willingness to discuss plans and difficulties.

I would also like to thank Dr. Ruifeng Liang for his guidance and assistance in conducting the experimental work discussed in this report, as well as for serving on my review board. His recommendations often kept this research going in the right direction.

Additionally, I am grateful to Dr. Udaya Halabe for also agreeing to serve on my review board.

With regards to my experimental work, I am greatly indebted to Jerry Nestor for his help in preparing samples and his excellent work manufacturing custom testing fixtures; to Mark Skidmore for his frequent advice and instruction on equipment usage; and to Saurabh Batra for his help with understanding testing procedures.

I am particularly appreciative to Dr. Stephen Ayers and Dr. Alan Miller for their encouragement for me to pursue this area of research and their constructive feedback.

Finally, I am very thankful for my family and friends, and their constant support during my time at WVU.

Financial support for this work has been provided by Lockheed Martin Corporation.

TABLE OF CONTENTS

LIST OF FIGURES

LIST OF TABLES

CHAPTER 1 INTRODUCTION

1.1 Background

According to the 2009 survey by the American Society for Civil Engineering, America's infrastructure has an overall grade of a 'D' with $2.2 trillion in maintenance needed over the next five years. Liang and GangaRao (2004) proposed that fiber reinforced polymer (FRP) composites offer an opportunity to revolutionize and rehabilitate US infrastructure because of their advantages over traditional structural materials due to: higher strength and stiffness, higher fatigue and impact resistance, higher corrosive and environmental resistance, longer service life, lower installation and maintenance costs, and more consistent performance. Infrastructure applications for FRPs are becoming more common and industry acceptance is growing.

Fiber reinforced polymers are composites which have the reinforcement in the form of fibers and the matrix in the form of a polymeric material, such as epoxy, vinyl ester, or polyester. The most common fiber reinforcements are glass fibers and carbon fibers, but the higher cost of carbon fibers generally prohibits their use in most infrastructure applications. Glass FRPs (GFRPs) are lightweight and have a good combination of mechanical performance, corrosion resistance, and low cost (Barbero 1999).

One of the greatest challenges when working with composite materials is to understand their long term behavior. Predicting fatigue behavior for homogeneous materials, like metals, can often be difficult, and the complexity is compounded for composites. Changes in the microstructure of the materials involved, as well as changes in their interfaces and interactions can lead to different forms of damage accumulation and different modes of failure. Additionally,

small changes in the temperature, loading conditions, material properties, or environment can cause significant changes in the performance of the material.

Performing extensive experimental work is one way to fully characterize the performance of material under different conditions, but fatigue testing tends to be a time consuming process. Therefore, observed behavioral trends need to be combined with established physical relationships in order to produce mathematical fatigue life models that can predict the behavior of materials with reasonable accuracy within a range of conditions. Many researchers have developed fatigue life prediction models for composites in the past few decades, but none have been widely adapted in industry.

1.2 Objectives

The objectives of this study are:

- To review past researchers efforts at producing fatigue life prediction models and at understanding environmental effects on GFRPs.
- To characterize a particular GFRP under a wide variety of environmental and loading conditions.
- To evaluate a strain energy-based fatigue life prediction model using a large amount and variety of fatigue data.

1.3 Organization of Thesis

A visual description of the organization of the thesis is shown in Figure 1-1.

Chapter 2 provides a review of published literature on topics related to the experimental objectives of this research. Aspects of composite materials are discussed, particularly fatigue

behavior, fatigue modeling, environmental effects, and environmental effects on fatigue. Additionally, a short review is provided on related research done at the West Virginia University Constructed Facilities Center (WVU-CFC) as well as a background on the strain energy-based fatigue life prediction model.

Chapter 3 introduces the material to be fatigue tested, and describes all of the manufacturing processes used to prepare the samples for testing. The experimental program is covered in detail, and the results are reported and analyzed. The tests conducted include fiber content tests, bending static tests, tension static tests, bending fatigue tests (with and without environmental conditions), tension-tension fatigue tests (with and without environmental conditions), absorption tests, and post-immersion conditioning tension-tension fatigue tests (with and without environmental conditions). These variables are intended to simulate the environmental conditions that will be encountered by composites intended for seawater use.

Chapter 4 discusses the evaluation procedure that was performed on the proposed strain energy-density fatigue life prediction model. Data from the DOE/MSU Composite Material Fatigue Database was used to show its accuracy at predicting fatigue life for a variety of GFRP materials. Additionally, the model was applied to the tests results from Chapter 3 and to component fatigue data collected previously by the WVU-CFC.

Chapter 5 summarizes the results found in the previous chapters, draws general conclusions, and provides some recommendations for further work in this area of research.

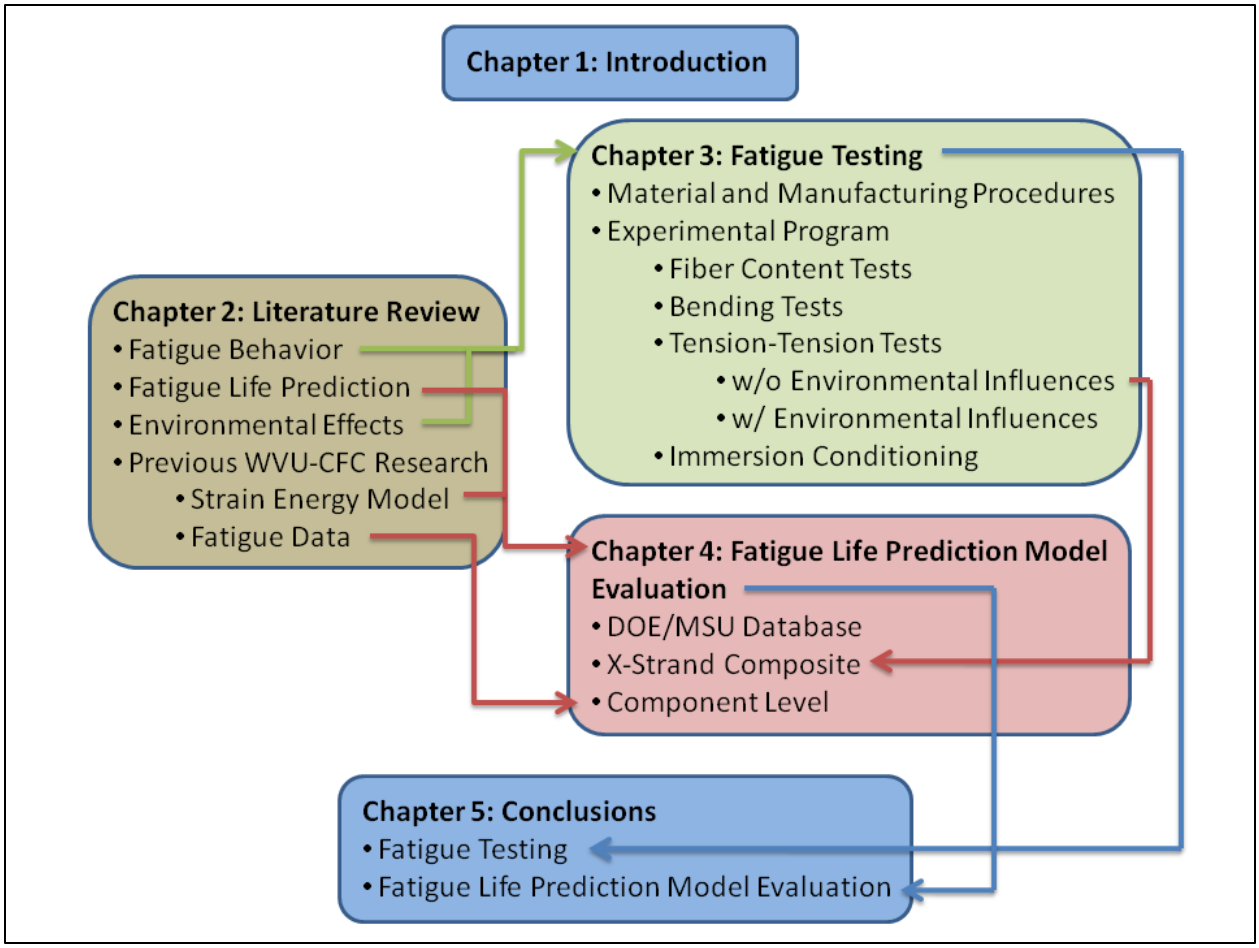

Figure 1-1 - Thesis Organization

CHAPTER 2 LITERATURE REVIEW

2.1 Introduction

Physics and mechanics, through mathematical tools, can be combined to accurately represent and predict homogeneous materials' responses under controlled loading and environmental conditions, as evidenced by many types of behavior of structural members and systems (Reifsnider 1990b). With composite materials, the challenge goes far beyond that of homogeneous materials, as the controlled inhomogeneity (and anisotropy) of composites introduces numerous complexities. The individual responses of the constituent materials in composites to loading conditions, environmental influences, and long-term behavior, as well as the performance of the internal boundaries within the material require new and different approaches to understanding fracture, fatigue, aging, and other performances. The fact that composites generally seem to behave well under fatigue loading makes it all the more important that their fatigue response be understood, in order to fully exploit their advantages over traditional, homogeneous materials. According to Reifsnider (1990b), "The subject we must understand consists of the mechanisms and processes which reduce the strength, stiffness, and life of composite materials and material systems subjected to long-term, time-variable, external mechanical, thermal, and chemical influences with levels of intensity which are useful for the purpose of performing engineering functions effectively and efficiently."

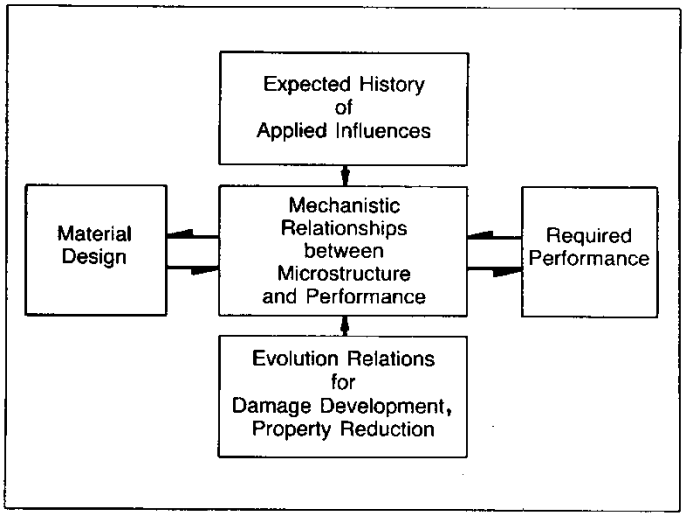

Figure 2-1 - Composite Design Process (Reifsnider 1990b)

In the future of fatigue design, as engineers are able to predict precisely how a composite will behave under a variety of conditions, the design process will reverse from its current state. Instead of designing a material and then taking into account all of the expected influences and damage development to design a component to meet with the required performance (progressing from left to right in Figure 2-1), the design process will be able to begin with establishing the required performance and end with an appropriate, specifically tailored material design (progressing from right to left in Figure 2-1) (Reifsnider 1990b).

The remainder of this chapter explores the published literature regarding the fatigue behavior of composite materials, as it relates to the research conducted later in this thesis. First, the fatigue behavior of composites is examined, including its typical modes of damage accumulation and their influences on testing methodology. Next, the difficulties associated with producing an accurate fatigue model are explained, followed by a review of several of the most commonly cited fatigue life prediction models. In the next section, the influence of environmental effects, particularly temperature and moisture content, is examined. Finally, the

fatigue life prediction model applied to experimental data later in this thesis is introduced and a short review of the related previous work done by the WVU-CFC is provided.

2.2 Fatigue Response of FRP Composites

2.2.1 Fatigue Behavior

Due to their anisotropy, composite materials are more complicated in their fatigue behavior than isotropic materials mainly due to the different types of damage that can occur and how they interact. Fatigue performance of composites is affected by the fiber type, matrix type, reinforcement structure, stacking sequence, environmental conditions, loading conditions, boundary conditions, among other influences (Degrieck and Van Paepegem 2001).

The simplest composite material is one that has fibers all aligned in the test direction (unidirectional laminates). In unidirectional composites, the fibers carry virtually the entire load; one would expect that the fatigue behavior would depend solely on the fibers, which have good resistance to fatigue. However, experimental results have shown that the fatigue behavior is determined principally by the strain in the matrix (Curtis 1989). This is because all non-metallic fibers have a statistical distribution of strength, depending on the presence of damage and manufacturing defects. Talreja (1990) presents a number of statistical considerations used to assess the strength and fatigue reliability of unidirectional composites. He concludes that a Weibull distribution seems to adequately describe the statistical strength, but also that development is still needed before the fatigue reliability is really understood.

When the weakest location in a composite fails, the surrounding fiber/matrix interface experiences increased local stresses, which can lead to eventual fatigue damage. The weakest location is, more often than not, caused by material defects, such as misaligned fibers, voids, or

resin-rich regions. As fatigue damage progresses, cracks in either the resin or the resin / matrix interface develop between the fibers, causing many to become locally overloaded and fail. This matrix or interface damage is responsible for the longitudinal splitting that often occurs in unidirectional composites, which results in "brush-like" fiber failures. It has been shown experimentally that using higher performance fibers in the same matrix generally results in little improvement in fatigue behavior when compared to using the same fibers in a higher performance matrix system (see Figure 2-2); therefore, the fatigue behavior of the resin is of primary concern (Curtis 1989). As composite strength and stiffness is increased through the use of high-performance fibers and toughened matrix materials, usually the fatigue behavior is poorer, resulting in steeper slopes on the S-N curves.

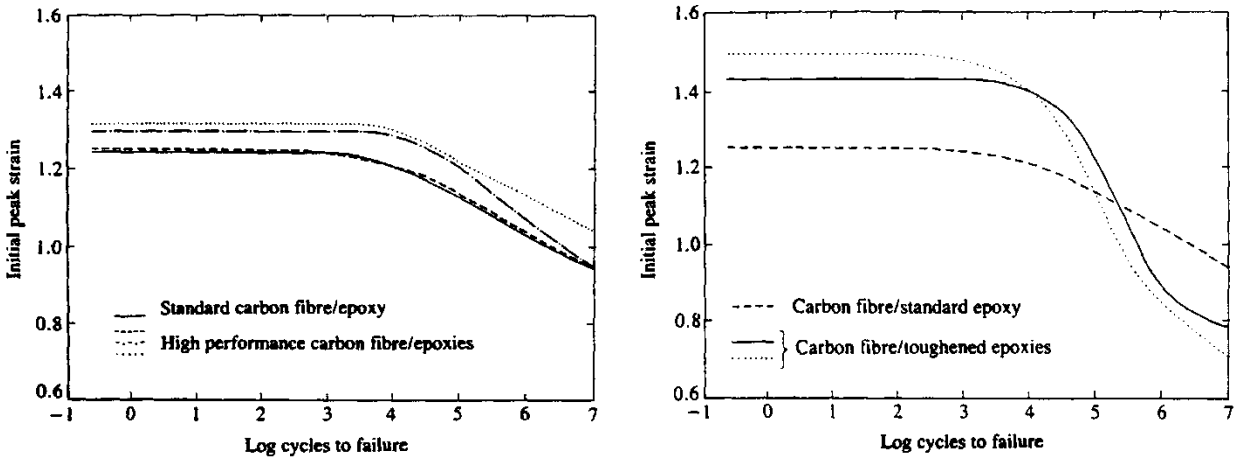

Figure 2-2 - Plots varying fibers (left) or matrix materials (right) (Curtis 1989)

Introducing non-axial fibers in a laminate (with otherwise the same fiber type, matrix type, and manufacturing process) greatly reduces the static tensile strength and stiffness, but is necessary in order to provide reinforcement against multi-directional loads, as are experienced in nearly every end-use application (Curtis 1989). Transverse layers, with fibers at 90º to the test

direction, develop transverse cracks early on in testing due to the matrix's inability to carry the load, but usually have little effect on axial strength or stiffness since they have little support in that direction anyway (Curtis 1989). Angled-ply layers can also develop intra-ply damage, which may introduce stress concentrations that lead to eventual delaminations. This often leaves the 0°-fiber layers as the principle load bearing layers, which in itself is not a problem, but delamination can also lead to a reduction in properties and integrity of a part, leading to susceptibility to environmental attack, and a severe reduction in strength. The unidirectional fibers still ultimately control the tensile fatigue behavior of a composite laminate; therefore, multi-directional composites usually exhibit similar fatigue behavior to unidirectional composites with identical unidirectional fiber contents (Curtis 1989). Woven composites, composed to interlaced fibers instead of the layered straight strands of non-woven composites, offer advantages in handling, fabrication, and impact absorption, but generally result in poorer static and fatigue behavior (Curtis 1989).

2.2.2 Damage Accumulation

Homogeneous fatigue damage is initiated by localized crack growth introduced by a stress concentration, and metals are therefore more sensitive to tensile loading after cracking. Composite fatigue damage is more widespread, usually consisting of interlayer damage and reduced fiber support; composites are therefore more sensitive to compressive loading after cracking (Curtis 1989). Composites accumulate damage as a combination of matrix cracking, delamination, and fiber fracture (Sendeckyj 1990).

For laminates with off-axis plies, the first and most significant observable damage mode is usually matrix cracking (Reifsnider 1990a). Called primary cracks, these cracks form through the thickness of plies in a direction perpendicular to the dominant load axis or parallel to the

fibers, depending on fiber architecture. Several widely-used failure theories can predict the appearance of these cracks in static loading (Reifsnider 1990a). In fatigue loading, however, the first incident of crack formation in the weakest plies (called first ply failure) is much more difficult to accurately predict. The formation of the primary matrix cracks in fatigue loading is the beginning of a sequence of micro-damage events that will eventually lead to the ultimate fatigue failure (Reifsnider 1990a).

After the formation of the primary cracks and the initial damage to the matrix, the following mode of damage accumulation is through fiber fractures in adjacent plies near the crack tips (Reifsnider 1990a). These fractures are particularly significant since the fibers are responsible for most of the strength of the composite. Once fiber fracture has taken place, secondary cracks form perpendicular to the primary cracks in the adjacent plies (Reifsnider 1990a). Where the primary and secondary cracks meet at a ply boundary, localized delamination commences and continues until eventual fracture (Reifsnider 1990a). See Figure 2-3 for an illustration of the damage accumulation process.

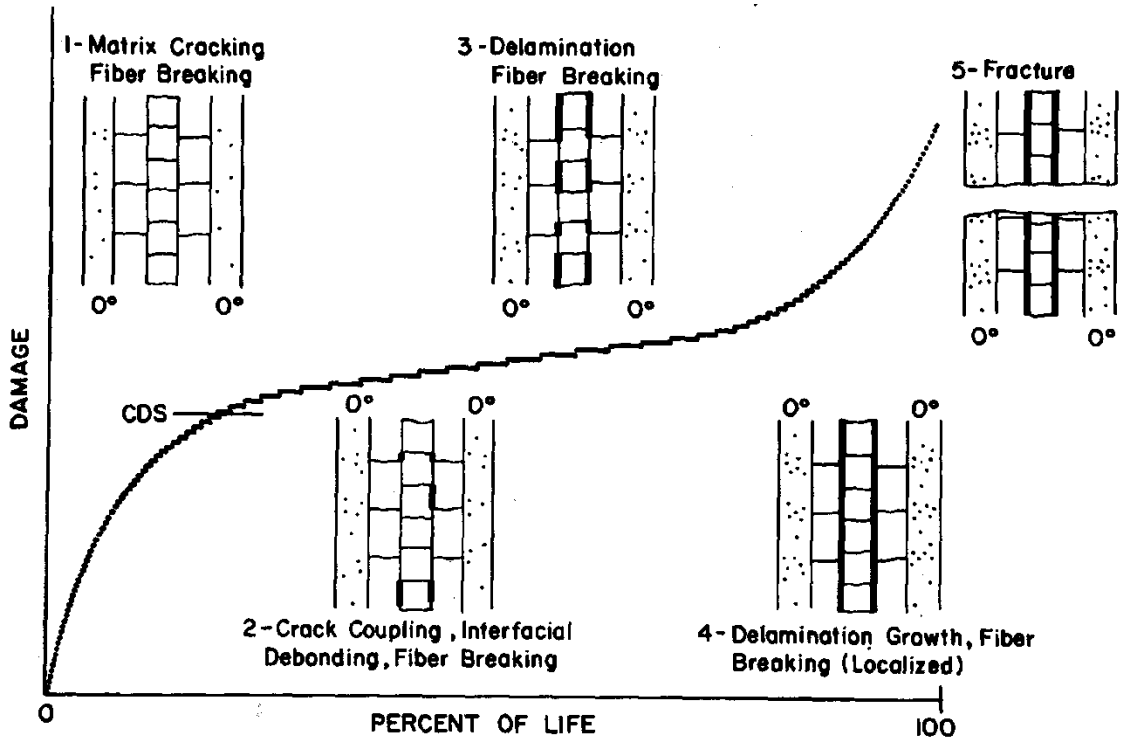

Figure 2-3 - Development of Damage Modes during Fatigue Life (Reifsnider 1990a)

2.2.3 Testing

The main concern in conducting a fatigue test is that the coupon should fail in a manner similar to that in which the material will fail in the intended end-use structural component. For test coupons, this means that the failure ought to occur in the gage length, where the stresses induced by the fixture method will not cause premature failure. Dog bone or reduced-waist profiles usually cause static failure to occur in the gage length, but not necessarily fatigue failure. A constant cross-section, rectangular specimen most frequently yields the longest fatigue lives and best fatigue behavior (Curtis 1989). Even though failure still often occurs in the grips with rectangular specimens, the frequency of occurrence can be reduced by care in coupon preparation and the use of additional end reinforcement.

Flexural fatigue testing is often used instead of axial fatigue testing because it is easier to perform, not requiring support guides or higher-capacity testing machines. However, the information gathered from flexural tests is difficult to analyze because of the complex stress distribution through the thickness of the specimen. Therefore, axial fatigue testing is preferred unless the end-use application involves significant flexural loads (Curtis 1989).

During fatigue testing, care should be taken to minimize hysteresis heating of the material (often in the resin or fiber/resin interface, due to repeated direction changes during testing). Laminates dominated by axial fibers usually have small strains and therefore less hysteresis heating, thus frequencies of up to 10 Hz are suitable (Curtis 1989). For laminates dominated by the resin strength, resulting in larger strains and greater hysteresis heating, the frequency should be kept to less than 5 Hz. The effect of the loading rate on the fatigue properties, as long as the hysteresis heating is small, is usually negligible. However, in many glass fiber reinforced materials, a higher rate of testing results in deceptively high strengths. It is therefore important, when working with GFRPs, to carry out all fatigue tests at roughly the same rate in order to limit the introduction of erroneous strength variation due to testing rate induced heating (Curtis 1989).

2.3 Fatigue Life Prediction

In order to predict the fatigue behavior of a material, the remaining strength or the remaining number of cycles, the material properties and the environmental/loading conditions must be related to the damage modes that the material is likely to experience. The fatigue behavior of resin-matrix composites depends on the interlaminar and intralaminar shear resistance, which in turn depends on the lamina properties, laminate stacking sequence, the environmental conditions (moisture, temperature), the testing frequency, and the stress ratios

(min/max and max/ultimate) (Sendeckyj 1990). Under long-term, time-variable accrual of damage (physical aging), the state of a material may change significantly. The mechanical properties and geometric constraints may change, as well as the state of the stress through loading conditions, directions, and bearing surfaces (Reifsnider 1990b). Particularly with composite materials, there are several ways that a component may achieve ultimate failure; through study of the changes in the state of stress and the state of the material, a model including both micro-mechanical and macro-mechanical information must be used to develop a failure mode criterion (Reifsnider 1990b). This failure mode criterion can then usually be used to establish the strength/life relationship, and thus the fatigue behavior of the material (see Figure 2-4).

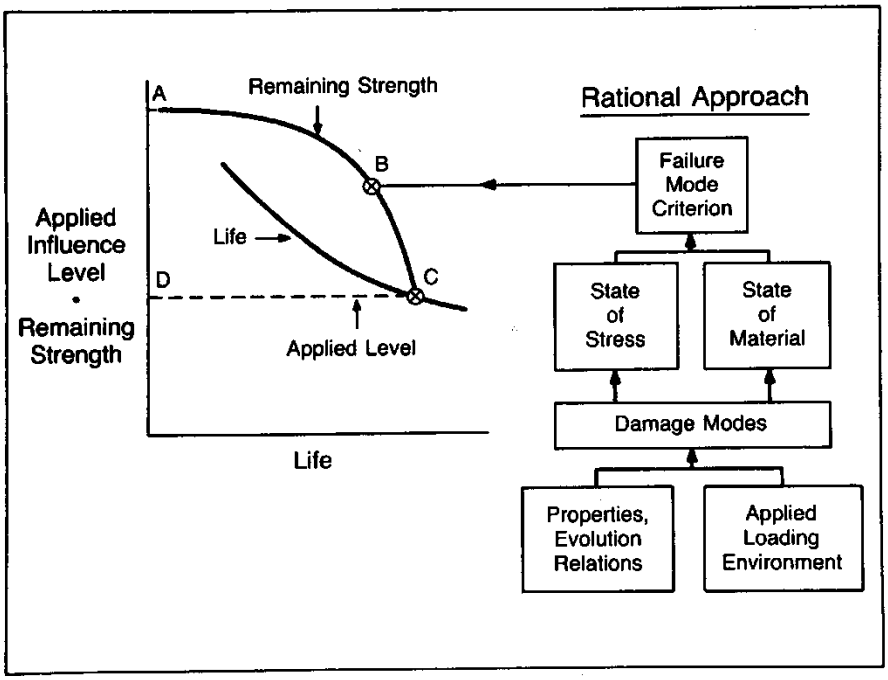

Figure 2-4 - Approach to Fatigue Life Prediction (Reifsnider 1990b)

Sendeckyj (1990) introduces a general process that should be followed in order to develop a life prediction method for a material. First, the process of damage accumulation must

be observed, and an appropriate damage metric must be chosen to represent that accumulation. Next, experimental work must be done to characterize the parameters so that a fatigue damage accumulation model can be formed. Finally, the life prediction capability of the model must be verified experimentally. This approach has been successful for metallic structures, but has had difficulty in application to resin-matrix composites due to their lack of a single simple damage metric.

The linear elastic fracture mechanics approach is most often used (Curtis 1989) to predict composite fatigue life, but since this technique is based on the theory that the growth of a single flaw eventually leads to failure, its applicability is questionable. Curtis (1989) hypothesizes that an ideal life prediction technique would enable fatigue life and residual strength to be obtained with a minimum amount of testing, and would be able to extrapolate values for different lay-ups and testing conditions. Sendeckyj (1990) similarly proposes that the ideal fatigue theory would:

1. Be based on a damage metric that takes into account all of the damage accumulation processes
2. Include all material, test, and environmental variables
3. Be able to relate the data to a large class of materials
4. Permit the prediction of laminate fatigue behavior from lamina fatigue data
5. Be extendable to more complex forms of loading than just constant amplitude loading
6. Account for the appearance of data scatter in fatigue tests

While Sendeckyj (1990) classifies fatigue theories only in general terms, Degrieck and Van Paepegem (2001) provide an extensive review of over 50 specific fatigue damage models published prior to 2001. While a number of models have been established with regards to a

particular material and stacking sequence, the challenge is to extrapolate those models to real structures with different stacking sequences and more complex loads. Some unique models also include considerations for load frequency effects, the combined effect of creep and fatigue, or impact-damaged materials.

According to Curtis (1989), no truly successful technique exists for the prediction of fatigue life in composite materials; however, two kinds of prediction models have been developed specifically for use with composites: Empirical models and wear-out models. Empirical models assume that strengths of coupons would rank in the same order statically (initial strength) and in fatigue (aged strength – the strength-life-equal rank assumption), and require large amounts of data in order to predict residual strengths and fatigue life at any number of cycles. Wear-out models depend on the measurement of the reduction of some mechanical property, such as stiffness or strength, and often also depend on the collection of large amounts of data to develop trend curves. In essence, both types of models are empirical.

Sendeckyj (1990) better classifies failure theories into four categories: Empirical fatigue theories, residual strength degradation-based fatigue theories, stiffness change-based fatigue theories, and actual damage mechanism-based fatigue theories.

Degrieck and Van Paepegem (2001) instead group the theories into three categories, combining the mechanical property change-based models: fatigue life models, phenomenological models for residual strength/stiffness, and progressive (measureable) damage models. This grouping seems to be the most current trend, and correlates well with the following literature review. The first category contains all models which generally rely on some form of traditional S-N curves, often require significant experimental work, and do not consider actual specific damage mechanisms. The second category, phenomenological models, encompasses all models

which describe a gradual deterioration in a macroscopically observable mechanical property irrespective of the specific damage. The third category, progressive damage models, contains models which attempt to describe the extent of actual damage taking place in the material. Since the model highlighted later in this report falls within the first category, the majority of this literature review will focus on other models within that category.

2.3.1 Fatigue Life Models

According to Degrieck and Van Paepegem (2001), "The main drawback of the fatigue life models is their dependency on large amounts of experimental input for each material, layup, and loading condition." Most of these models are fairly straightforward to use, not requiring knowledge of the actual damage mechanisms.

2.3.1.1 Hashin-Rotem Failure Model

One of the first and best known life prediction models is the one proposed by Hashin and Rotem in 1973. Because of the large variety of laminates, it is impossible to determine general fatigue failure criteria by experiments only, unless a specific laminate is chosen and tested. According to Hashin and Rotem (1973), a better approach is to establish a fatigue failure criteria based on the constituting laminae. In this approach, a lamina relationship was derived from the failure criteria using modified maximum stress and Tsai-Hill criterion where the failure mode (fiber or matrix) is taken into consideration. The particular failure mode is determined based on the angle between the applied load and the reinforcement for each lamina, as shown in Equation 2-1, where τ^s and σ^s_A stand for the static shear and axial strengths, while the other functions are along the same directions, and related to the stress ratio ($\sigma_{min}/\sigma_{max}$), R, the number of cycles, N, and the testing frequency, v.

$$tan(\theta_c) = \frac{\tau^S}{\sigma^S{}_A} \frac{f_\tau(R,N,\nu)}{f\prime(R,N,\nu)} \tag{2-1}$$

Since the failure criterion is dependent on one of two failure modes, it has two forms, as seen in Equations 2-2 and 2-3. In the equations, the *U* superscript denotes the fatigue failure stress, and the *T* subscript indicates the stress is transverse to fiber orientation, due to Poisson's effect.

$$\sigma_A = \sigma_A^U \tag{2-2}$$

$$\left(\frac{\sigma_T}{\sigma_T^U}\right)^2 + \left(\frac{\tau}{\tau^U}\right)^2 = 1 \tag{2-3}$$

Hashin and Rotem's testing was conducted on unidirectional reinforcement only, at various off-axis angles. Their specimens were made from E-glass roving with an epoxy matrix. Using the failure criterion of Equation 2-3, the critical angle (which separates the two failure modes) can be calculated after several static tensile tests. After fatigue testing, it was found that this critical angle was approximately the same regardless of fatigue or static testing conditions. The researchers concluded that plane stress fatigue failure of unidirectional laminates and laminae can be reasonably predicted using their failure criterion (Hashin and Rotem 1973).

2.3.1.2 Ellyin-El-Kadi Failure Model

Ellyin and El-Kadi proposed a fatigue failure criterion based on strain energy density, and applied it to predicting fatigue life in 1990. For elastic plane stress problems, the strain energy density, *W*, is calculated as shown in Equation 2-4. Their method takes into account the 3x3 stress-strain compliance matrix (see Equation 2-5) in its calculation of the strain energy density in order to get it in terms of stress only, as shown in Equation 2-6.

$$W = \left(\sigma_x \varepsilon_x + \sigma_y \varepsilon_y + \tau_{xy} \gamma_{xy}\right)/2 \tag{2-4}$$

$$\begin{Bmatrix} \varepsilon_x \\ \varepsilon_y \\ \gamma_{xy} \end{Bmatrix} = \begin{bmatrix} \bar{S}_{11} & \bar{S}_{12} & \bar{S}_{16} \\ \bar{S}_{21} & \bar{S}_{22} & \bar{S}_{26} \\ \bar{S}_{61} & \bar{S}_{62} & \bar{S}_{66} \end{bmatrix} \begin{Bmatrix} \sigma_x \\ \sigma_y \\ \tau_{xy} \end{Bmatrix} \tag{2-5}$$

$$W = \left(\bar{S}_{11}\sigma_x^2 + 2\bar{S}_{12}\sigma_x\sigma_y + \bar{S}_{22}\sigma_y^2 + 2\bar{S}_{16}\sigma_x\tau_{xy} + 2\bar{S}_{26}\sigma_y\tau_{xy} + \bar{S}_{66}\tau_{xy}^2\right)/2 \tag{2-6}$$

Assuming that the stress-strain relationship for a lamina is elastic, ΔW can then be simplified (for the uniaxial case) to Equation 2-7, where R is the stress ratio.

$$\Delta W = \bar{S}_{11}[\Delta\sigma_x^2/2(1 - R_x)^2] \tag{2-7}$$

Ellyin and El-Kadi (1990) believed that ΔW related well to the number of cycles to failure, N_f, through a power law, as shown in Equation 2-8.

$$\Delta W = \kappa N_f^{\alpha} \tag{2-8}$$

This relationship is dependent on the coefficients κ and α, which are themselves dependent on the fiber orientation angle and five other material constants (two static and three fatigue). While the method does show that the strain energy is a viable damage metric for predicting fatigue life through its ability to predict fatigue failure with some reliability, it relies on obtaining individual lamina properties and conducting ply mechanic calculations, in addition to needing a number of experimentally determined coefficients. The plots of strain energy density vs. number of cycles are also difficult to relate to clear physical meanings.

2.3.1.3 Reifsnider-Gao Failure Model

Since many failure theories depend on empirical data fitting, they should therefore be limited in their correlation only to the range of data within the limits of the data used to derive them. In 1991, Reifsnider and Gao established a systematic micromechanics model, not empirically-based, using the Mori-Tanaka method, which has been used to predict the effective thermal, electrical, and mechanical properties of composites.

The concept of using an "average field" was used to attempt to include the interaction between the fibers and the matrix material. A stress tensor containing the average stresses in the fibers and matrix was developed for the material using a modification of Eshelby's solution (Reifsnider and Gao 1991). Once the stress tensors, $\langle \sigma_{ij}^{f} \rangle$ and $\langle \sigma_{ij}^{m} \rangle$, had been defined, a fatigue criterion similar to that used by Hashin and Rotem (1973) was used to establish failure limits (see Equations 2-9 and 2-10).

$$\langle \sigma_{11}^{f} \rangle = X^{f} \tag{2-9}$$

$$\left(\frac{\langle \sigma_{22}^{m} \rangle}{X^{m}}\right)^{2} + \left(\frac{\langle \sigma_{12}^{m} \rangle}{S^{m}}\right)^{2} = 1 \tag{2-10}$$

In the above equations, X^f and X^m are fatigue failure functions under tensile loading for the fibers and matrix, respectively, and S^m is the fatigue failure function of the matrix under shear loading (Reifsnider and Gao 1991). Obtaining these fatigue functions requires the collection of experimental data individually for the fibers and the matrix material, instead of a lamina operating as a whole. While Reifsnider and Gao are able to, within reason, re-predict the fatigue life of Hashin and Rotem's fatigue data, the trade-off between the complexity of the development of the stress tensor and the ability to calculate the fatigue life based only on the experimental data of the individual components of a composite material seems like it would only be worthwhile in particular situations.

2.3.1.4 Fawaz-Ellyin Failure Model

In 1994, Fawaz and Ellyin proposed a general multi-axial fatigue failure theory which would take into account general loading parameters such as the bi-axiality ratios, the cyclic stress ratio, and the off-axis angles, since the fatigue strength of a given laminate largely depends on

the type and orientation of the constituent laminae. To predict the fatigue life of differently oriented laminates, Fawaz and Ellyin introduced the concept of elementary blocks.

An elementary block is simply either a single lamina or a common laminae groupings ([0, 90] or [-60, 0, 60], for example), which has its static and fatigue performance already characterized experimentally. The performance of a laminate composed of these elementary blocks can then be predicted by assuming a semi-log linear relationship between the stress, *S*, and the number of fatigue cycles for each lamina, *N*, as shown in Equation 2-11.

$$S = m\log(N) + b \tag{2-11}$$

The material coefficients, m and b, in the semi-log relationship are determined by accounting for the combined interaction of all of the laminates and the application of a failure criterion, such as the Tsai-Hill criterion. The model additionally relies on an established reference S-N curve. It is possible to include the effects of bi- and multi-axial loading in the determination of the semi-log coefficients, as shown in the experimental results of the paper (Fawaz and Ellyin 1994).

The experimental data shown by Fawaz and Ellyin (1994) correlated well with their prediction method for several unidirectional composites under uni-axial loads, and a woven composite under bi-directional loads. However, the methodology is arduous and it seems like a significant amount of experimental characterization work is needed for each material and type of elementary block before it becomes particularly useful. For complex laminates or loading techniques, the calculations would quickly become even more complicated, but are at least theoretically sound as long as the assumptions of a semi-log relationship and in-plane stresses are accurate.

2.3.1.5 Philippidis-Vassilopoulos Failure Model

One major problem with some fatigue criterion is their focus on uni-axial performance, which is unable to consider the complex stress states that arise from multi-directional composites and/or multi-axial stresses. In their 1999 work, Philippidis and Vassilopoulos focused on macroscopic strength fatigue theories (fatigue life models) because they considered those to be the only practical approach to predict failure under complex stress states.

Philippidis and Vassilopoulos intended to demonstrate the efficiency in accurately predicting fatigue life using a failure tensor polynomial modified for fatigue, as shown in Equations 2-12 and 2-13, where F_{ij} and F_i are failure tensors, which are functions of the number of cycles, N, the stress ratio, R, and the frequency of loading, v. For a full solution, their method requires the determination of five failure stresses experimentally to determine the failure tensors, but they have shown that only three are needed to yield satisfactory predictions (Philippidis and Vassilopoulos 1999).

$$F_{ij}\sigma_i\sigma_j + F_i\sigma_i - 1 \leq 0 \quad i,j = 1,2,6 \tag{2-12}$$

$$F_{ij} = F_{ij}(N,R,v) \text{ and } F_i = F_i(N,R,v) \tag{2-13}$$

The material tested was an E-glass/polyester with 0 and ±45 reinforcement, cut at 0, 30, 45, 60, and 90 degree off-axis directions. The researchers conducted comparisons between their results, Hashin-Rotem results, and Fawaz-Ellyin results. While their model was often more accurate than the other two, it did not seem to provide a good prediction in every case. They do extend their theory to include a variable amplitude loading case, but did not experimentally verify its accuracy. The ability to use laminate properties instead of lamina properties makes the theory more applicable for complex lay-ups.

2.3.1.6 Epaarachchi-Clausen Failure Model

In 2003, Epaarachchi and Clausen proposed an empirical fatigue model intended to accurately account for the effects of the load stress ratio and the load frequency. Their model, shown in Equation 2-14, takes into account the ultimate and maximum fatigue testing stress, the fiber angle, θ, the frequency, f, and an angle function, ψ, which is defined as R for tension-tension or full-reversal tests, and $1/R$ for compression-compression tests.

$$\left(\frac{\sigma_u}{\sigma_{max}} - 1\right)\left(\frac{\sigma_u}{\sigma_{max}}\right)^{0.6-\psi|\sin\theta|} \frac{1}{(1-\psi)^{1.6-\psi|\sin\theta|}} f^{\beta} = \alpha\left(N^{\beta} - 1\right) \tag{2-14}$$

The model requires determining α and β experimentally for each material and loading frequency (or just average loading frequency), using an unspecified number of data points (Epaarachchi and Clausen 2003). The model seemed to fit experimental data for a number of different materials and loading conditions quite well.

Epaarachchi (2005) also proposed a method of combining static-fatigue (creep) effect and fatigue effect to predict the life of composite materials, based on the above fatigue model. While the explanations behind this combined model seem reasonable, it does not seem to consistently match the data.

2.3.1.7 Other Recent Fatigue Life Models

In 1999, Sarkani et al. used a combination of a standard semi-log model function and a damage accumulation law known as the Palmgren-Miner rule. Since their fatigue data was, for the most part, conducted on a variety of joints, their results may have been better for simple laminates. However, the method was only adequate at predicting the fatigue life for some of the configurations, and the researchers concluded that it should be used with caution as it tends to

yield unconservative results and that it does not significantly improve with a two-segment approach (Sarkani et al. 1999).

Mouritz proposed a modification to the common semi-log linear S-N model to account for the presence of z-direction reinforcement in a 2005 publication. His model, shown in Equation 2-15 requires only three easily obtainable material properties – the ultimate strength of the 3D composite, σ_{3D}, the ultimate strength of the 2D laminate, σ_{2D}, and the slope of the fatigue life curve of the 2D laminate, m.

$$S_{3D} = \frac{\sigma_{3D}}{\sigma_{2D}}(\sigma_{2D} + m \log N) \tag{2-15}$$

This simple method seems to provide a good estimate of the increase/decrease in tensile, compressive, or flexural fatigue life due to 3D stitching. Mouritz acknowledges that the model only applies to composites that exhibit fairly linear semi-log S-N curves. The model's other major limitation is that the fatigue damage mechanism must be the same in the 2D and 3D versions of the composite in order for the prediction to be accurate.

In 2006, Qiao and Yang proposed a Goodman-Line-based fatigue prediction model for a urethane based GFRP composite, with a modification to include the stress level, stress ratio, and frequency. It requires significant experimental testing and works best for composites that exhibit linear semi-log S-N behavior.

Mahadevan and Mao also proposed a damage accumulation model which would account for both fatigue and creep effects, based on several experimentally-obtained coefficients, in 2004. It is difficult to judge whether they were successful at modeling or not from their presented results.

2.3.2 Phenomenological Models Based on Residual Strength/Stiffness

It is impossible to measure the residual strength nondestructively; however, models based on the residual strength method do have a simple failure criterion: failure occurs when the residual strength is less than the applied stress. Residual stiffness can be measured without destroying a sample and it has less scatter than residual strength; however, the determination of an accurate failure criterion can be more difficult (Degrieck and Van Paepegem 2001).

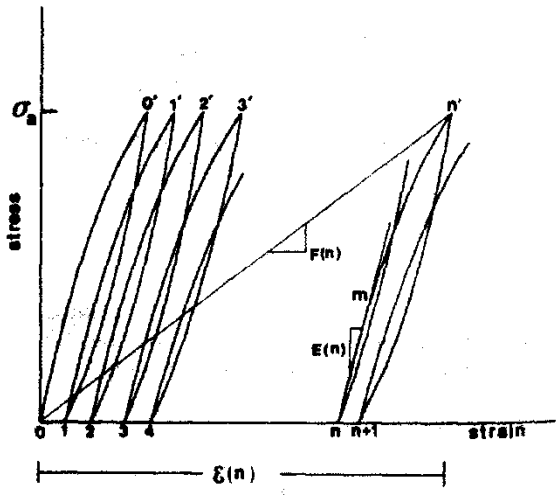

Figure 2-5 - Fatigue Modulus Concept (Hwang and Han 1986)

In an attempt to provide a more practical and applicable equation for predicting the fatigue life of a composite material, the new concept of "fatigue modulus" was introduced by Hwang and Han in 1986. The fatigue modulus, *F*, is calculated as the slope of the line between the initial stress/strain coordinate (origin) and the stress/strain coordinate at the peak of the nth loading cycle (see Figure 2-5). Assuming that the fatigue modulus degradation rate, *dF/dn*, adheres to a power function relationship with the loading cycle, *n*, (seen in Equation 2-16) the number of cycles to failure for a material can be predicted using the applied stress ratio, *r*, and two material constants, *B* and *c* (seen in the final equation, shown below as Equation 2-17).

$$\frac{dF}{dn} = -Acn^{c-1} \tag{2-16}$$

$$N = [B(1-r)]^{1/c} \tag{2-17}$$

Hwang and Han's testing was performed on a glass/epoxy material at stress levels ranging from 0.6-0.9. The experimental fatigue life at each stress level was compared to the predicted fatigue life using the proposed fatigue modulus method, a straight-line method on the S-N curve, and Basquin's relation (an exponential relationship). The fatigue modulus of elasticity was found to have a coefficient of correlation with the experimental data of 0.9952, while the S-N curve and Basquin's relation had coefficients of -0.9851 and -0.9745, respectively (Hwang and Han 1986). Hwang and Han concluded that, even though their method provided better results than the other two tested, the non-linear, viscous nature of the stress/strain relationship during fatigue cycling was responsible for the error that they had. They believed that viscoelastic and viscoplastic studies could provide more exact analyses, and that a general strain failure law could be established through experimental research on different materials.

In 2001, Khan et al. proposed that the elastic modulus of a material at any point in time was a function of undegraded modulus multiplied by a factor related to the accumulated damage, as shown in Equation 2-18. Their method required collecting a significant amount of data in order to establish the damage function, $g(D)$, which could then be related to the number of cycles to failure using the stress range, $\Delta\sigma$, and stress ratio, R, as shown in Equation 2-19. Their stiffness degradation model seems to do a reasonable job predicting material fatigue life for mid-length (10^5 – 10^6 cycles) tests, but it does not seem able to very accurately predict the fatigue life of much shorter or longer tests. The accuracy is certainly not good enough to indicate that this modulus degradation method should be preferable to more simple empirical methods, since there are constants that still need to be determined experimentally.

$$E = E_o g(D) \tag{2-18}$$

$$N_f = \int_{D_i}^{D_f} \frac{dD}{f(\Delta\sigma,R,D)} \tag{2-19}$$

Also in 2001, Kim and Zhang applied a stiffness degradation theory very similar to that used by Khan et al. to their fatigue data. Their results seemed to be better (or at least more easily observed) than Khan et al.'s, but they also exhibit a tendency to be somewhat more conservative than necessary.

In a 2007 publication, Varvani-Farahani and Shirazi proposed a stiffness-degradation based model which was able to calculate the fatigue life for laminates composed of 0º and 90° plies, as long as the mechanical properties of those plies were already known. In its prediction, the model considered the stress ratio, the stress magnitude, the number of cycles to failure, the off-axis angle, and a parameter relating to the interfacial efficiency. It is easy to see that their proposed damage evolution model seems to fit the data well, but it is not as easy to see the relationship to observable properties or eventual final failure criterion.

2.3.3 Progressive Damage Models

It is the opinion of Degrieck and Van Paepegem (2001) that the progressive damage models (the third category), have the most promising capability to predict fatigue life due to their quantitative handling of damage progression. However, it seems like most of the models within this category are an order of magnitude more complicated than some of the fatigue life models and phenomenological models, making them less likely to be useful outside the academic realm unless directly incorporated into software.

Kim and Zhang, in addition to their 2001 work developing a stiffness-degradation model, conducted a study on the development of micro-cracks, in which they counted the number of cracks appearing in a particular region of the sample at intervals during fatigue testing. They

concluded that most micro-cracks formed perpendicular to the loading (tension) direction and that the surface micro-crack density increased with the applied number of cycles exponentially. They did not yet attempt to develop a model relating the micro-crack density to the fatigue life.

One example of a fully-developed progressive damage is the one proposed by Sun et al. in 2003. Their complex, crack-density-based progressive damage model used a "Monte Carlo simulation" approach and compared the number of cracks to a "probability density function".

2.4 Environmental Effects on FRP Composite Mechanical Properties

Increased temperature and the presence of moisture both have similar effects on polymeric composites – both induce stress by swelling and both relax stress by softening (Weitsman 1990). As a result of these similarities, the simultaneous presence of temperature and moisture can make it much more difficult to analyze the impact they are having on results. Due to its relevancy to the testing conducted as a part of this research, the environmental effect focused on will be that of moisture absorption, with the understanding that both moisture absorption and increased temperature cause similar behaviors.

It is well established that polymeric composites absorb moisture in hot, humid environments (Bradley and Grant 1995). Weitsman (1990) summarizes previous polymeric moisture research as the following basic findings:

1. The moisture saturation level depends mostly on the humidity, but may partly depend on temperature (if a saturation level even exists)
2. Diffusion(or absorption) is highly sensitive to temperature
3. The presence of moisture accelerates creep effects
4. Moisture induces internal stresses due to swelling

5. Moisture lowers the T_g (glass transition temperature)
6. Moisture degrades mechanical properties, particularly shear and compression
7. The above findings can vary significantly between different materials

2.4.1 Moisture Uptake

Bradley and Grant found that moisture uptake data showed that saturation content was less in salt water solutions than in fresh water solutions (by 5-25%) (Bradley and Grant 1995). This is likely because the salt is not as easily absorbed into the composite as fresh water, and therefore would begin to build up at the surface of the composite, slowing additional moisture uptake. Immersion in pressurized salt water (3000 psi) resulted in only slightly more moisture absorption – the effect of higher pressure is likely almost cancelled by the volume reduction (Bradley and Grant 1995).

Liao et al. (1999) tested an E-glass/vinyl ester material for tensile properties under the condition of fresh water aging. With regard to absorption rates, they also found that higher salt concentrations lead to lower change in mass when compared to fresh water uptake. Oddly, they found that the aging conducted in the elevated temperature fresh water led to a much faster and higher mass increase, but after a short time those samples dropped in mass absorbed to below the samples kept at room temperature (see Figure 2-6).

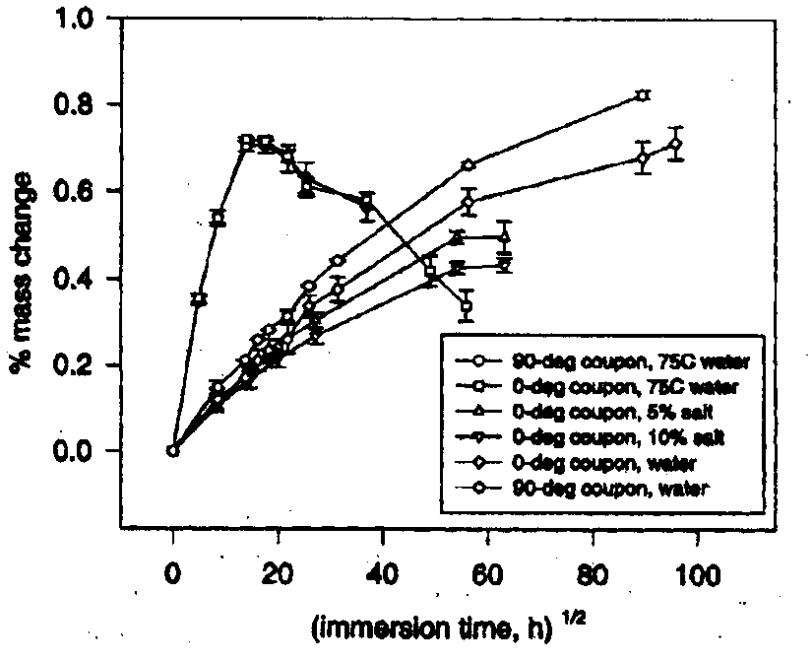

Figure 2-6 - Absorption Test Results (Liao et al. 1999)

Murthy et al. (2009) researched the difference between the effect of salt water absorption on epoxy and vinyl ester matrix composites. They were able to show that both the saturation level and rate were lower for vinyl ester-based composites than for epoxy-based composites (see Figure 2-7). Due to its superior chemical stability in seawater, the use of vinyl ester over other possible matrix materials was recommended for moisture-exposed applications. They were also able to observe by SEM the interfacial debonds due to moisture penetration.

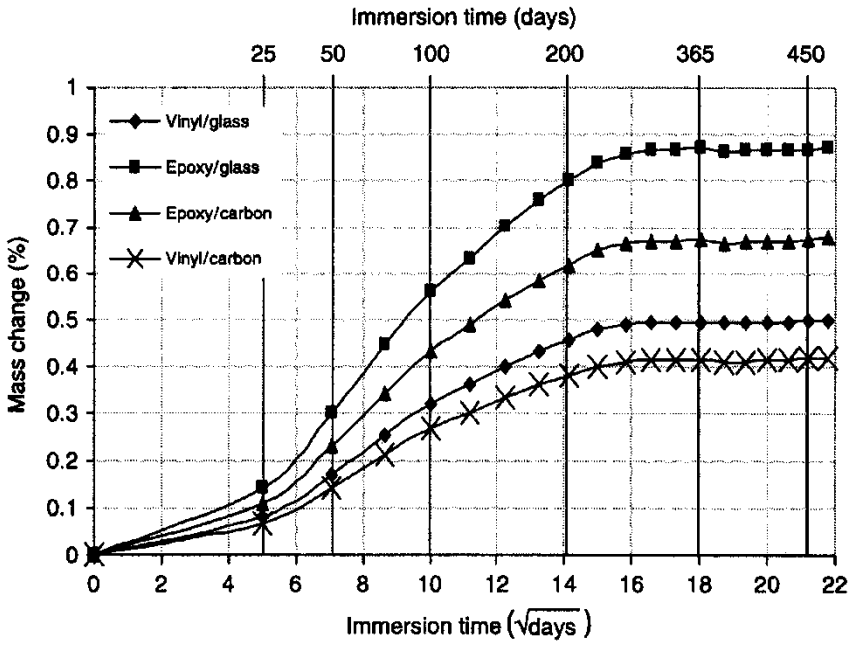

Figure 2-7 - Absorption Rates of Epoxy and Vinyl Ester Composites (Murthy et al. 2009)

McBagonluri et al. (1999) examined the effect of moisture absorption and cycling. They studied comparative fatigue tests in dry, fresh water, and salt water environments for a glass/vinyl ester composite. They found that absorption took, on average, 28 days in a water bath and desorption took 3 days in an oven.

Weitsman (1990) found that polymers often deviate from classical diffusion prediction models in the following ways:

1. Saturation may never occur, as some materials will just continuously gain weight and others will have an apparent pause in the process, and then continue gaining weight again
2. The concentration as the weight gain process
3. The process of weight gain may depend on previous absorption-desorption cycles.

Weitsman's findings were focused on graphite/epoxy systems, and may not be extendable to other material systems.

2.4.2 Moisture Damage

Moisture absorption is usually limited to the matrix and the fiber/matrix interface; while glass fibers rarely absorb much moisture, they are susceptible to stress cracking (Bradley and Grant 1995). The stability of the interface between the fibers and the matrix is a major factor in the strength and lifetime of a composite material – when thermoset plastics are exposed to moisture, they often have a tendency to plasticize and cause debonding at the fiber/matrix interface (Murthy et al. 2009). At this interface, moisture can both directly reduce the chemical bond and change the internal residual stresses. The relaxation of compressive stress at the interface also reduces the interfacial shear strength (Bradley and Grant 1995).

Composites with brittle matrices promote damage via matrix cracking and thus have low strengths. These composites show an increase in strength after saturation because of plasticization. Those that exhibited the most significant changes in strength also seemed to have a change in damage mode from matrix cracking to interface damage (Bradley and Grant 1995). Composites with more ductile matrices generally develop damage at the fiber/matrix interface, and therefore generally remain unchanged after saturation since damage is always concentrated in the same, unaffected region. Minimal void content also helps reduce the effect of exposure to moisture. Generally the tensile strength of unidirectional composites is unaffected by moisture absorption. However, Bradley and Grant (1995) found that the compressive and transverse tensile strengths can reduce by as much as 10-50%.

Liao et al. (1999) studied the reduction in mechanical properties in an e-glass/vinyl ester composite due to environmental aging. They tested the material for flexural properties under the

conditions of as-received, fresh water aging, 5% salt solution aging, 10% salt solution aging, and 75ºC fresh water aging. The flexural properties were, for the most part, found to be slightly lower for the aging methods, yet still within a reasonable error limit (within 10% less for flexural modulus and 13% less for flexural strength). The exception to this was the flexural strength of the sample aged in the elevated temperature fresh water; it exhibited a decrease of 40% on average (see Figure 2-8). The effect of aging on the tensile properties was more pronounced, with a decrease in tensile modulus of 23% and a decrease in tensile strength of 29% (for the given composite material; see Figure 2-9).

Vijay and GangaRao (1999) measured the effect of aging in a 3% salt solution on tensile properties as a reduction in tensile strength of 18.5-24.5% and an increase in tensile modulus of 4-5%.

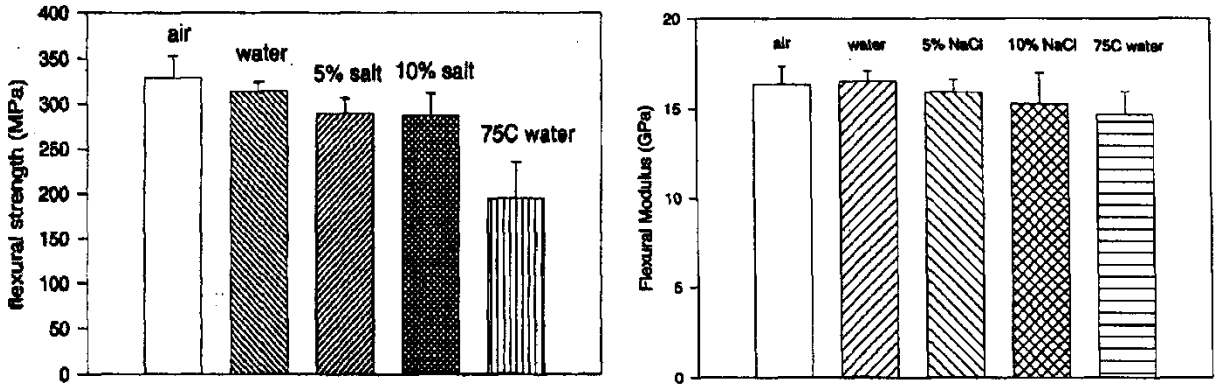

Figure 2-8 - Flexural Properties Before/After Absorption (Liao et al. 1999)

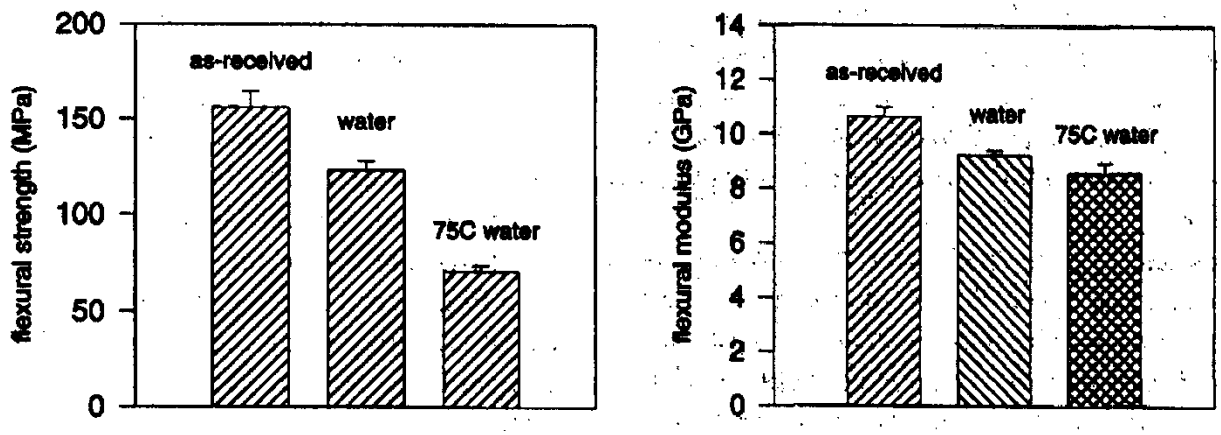

Figure 2-9 - Tensile Properties Before/After Absorption (Liao et al. 1999)

McBagonluri et al. (19990 found that the tensile modulus of elasticity decreased by about 11% and the strength by about 32%, regardless of whether the material absorbed fresh water or salt water (see Figure 2-10). Using SEM, damage was found both in the fibers and in the interface region after cyclic absorption-desorption. They also concluded that the fatigue failure process was unaffected by short-term exposure to fresh water or salt water, testing frequency, and temperature of exposure (one assumes they are referring to long-term environmental exposure, and not temperature while testing).

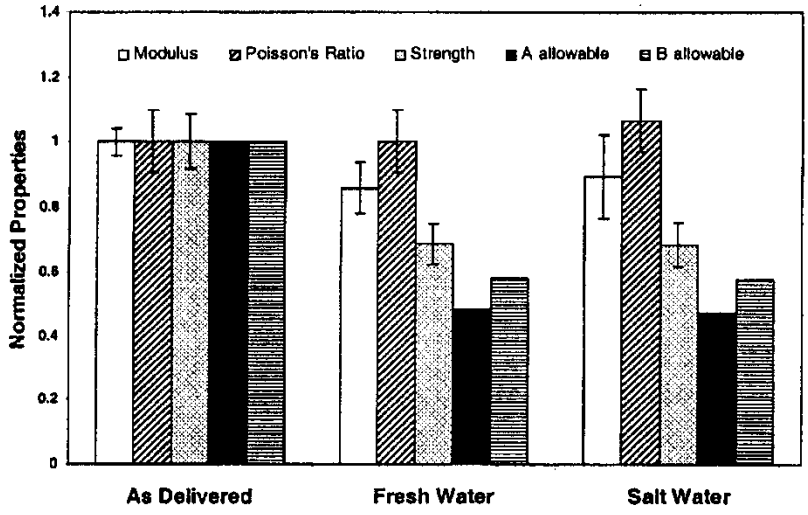

Figure 2-10 - Effect of Absorption on Material Properties (McBagonluri et al. 1999)

Liao et al. (1999) agree with other researchers that the damage caused by absorption and desorption to the matrix is of secondary concern to the damage caused to the fibers and particularly the fiber/matrix interface region. In general, higher temperatures and longer exposures can also cause significant reduction in mechanical properties. Their general conclusions were that aging in water and salt solutions results in degraded mechanical properties (both flexural and tensile), and that the salt concentration did not seem to noticeably affect the flexural properties (although it did affect the moisture uptake).

Moisture cycling has the ability to induce additional damage in a material over constant moisture exposure. The damage begins with small debonds at the fiber-matrix interfaces. At early stages, these debonds are restricted to individual fibers, but as the cycling continues, they may coalesce into continuous cracks. As with all damage results, wide scatter in the data exists regarding the formation of these cracks. Regarding moisture cycling in a graphite/epoxy system, Weitsman (1990) concludes:

1. Moisture induces damage in the forms of cracks at fiber-matrix interfaces
2. Damage increases with moisture cycling (with more damage occurring during desorption)
3. A higher average moisture content resulted in greater damage
4. Damage always initiated along outer surfaces
5. Cracks grew parallel to free surfaces
6. Damage tends to be localized

2.5 Environmental Effects on FRP Composite Fatigue Life

Including environmental effects in fatigue testing introduces complications due to the long period of time the tests often need. If the tests are going to be relatively short and conducted at room temperature, then coupons previously exposed to moisture are less likely to dry out. If tests are going to be extensive or conducted at elevated temperatures, precautions must be taken to preserve the moisture content of the specimen. One solution is to test in a chamber with both humidity and temperature controls, but due to cost this is not always feasible. Alternative approaches involve enclosing the specimen in a water-filled bag or wrapping it in moist towels. McBagonluri et al. (1999) used a transparent Plexiglas fluid cell, which was sealed onto each specimen's gage length using a silicone adhesive.

The environmental effect on fatigue behavior is most pronounced in materials where the matrix controls, since the matrix and fiber-matrix interface are usually more affected by absorbed moisture than the fibers. If tested at room temperature, moisture effects are usually small; testing at elevated temperatures can produce much poorer fatigue behavior (Curtis 1989).

Khan et al. (2002) explored the impact of temperature on the fatigue life of carbon fabric composites. They expected fatigue life enhancement at higher temperatures due to visco-elastic matrix behavior, but instead found that there was a severe reduction in fatigue life due to the thermal degradation of the matrix and the weakening of the fiber/matrix interfaces. They proceeded to develop a model relating temperature to stiffness degradation in order to incorporate the temperature effect into their own damage accumulation model. They found that the damage accumulation sequence was essentially the same at each temperature level they tested (ranging between -20ºC and 150°C) but the rate of accumulation increased with temperature. A more significant impact on fatigue life was found to occur when the

environmental temperature was above the glass transition temperature of the matrix, as one might expect.

As technology advances and more thorough understandings of fatigue failure are achieved, materials are continuously being exposed to harsher loads and environmental conditions. Reifsnider (1990b) concludes that "it is becoming increasingly difficult to analyze the fatigue performance of materials by concentrating on a primary influence such as mechanical loads and ignoring or "correcting for" any secondary influences such as temperature, chemical activity, or damage development." If possible, establishing the impact of environmental effect on fatigue life as only a factor to be included in fatigue life predictions (similar to the approach taken by Khan et al. (2002)) would advance the applicability of composites in fatigue applications with harsh environments.

2.6 Previous WVU-CFC Research Work

Several researchers at the West Virginia University Constructed Facilities Center have done work on fatigue in composites. Their research has focused on finding a fatigue life prediction model for glass fiber reinforced polymers.

2.6.1 Development of Fatigue Life Prediction

The GFRP fatigue life model proposed by Natarajan et al. (2005) uses the internal strain energy of the material as the damage metric; this energy is expended due to damage in the forms of matrix cracking, fiber/matrix interface failure, delaminations, or fiber breakage before rupture (Natarajan 2003; Natarajan et al. 2005; GangaRao 2009; Dittenber and GangaRao 2010). Strain energy was chosen as the damage metric because of its ability to represent a variety of damage modes through one measurement and its high sensitivity to damage accumulation due to the

squaring of the stress/strain term. While Ellyin and El-Kadi (1990) have previously used the strain energy to predict fatigue life, the following strain energy model differs in the following ways:

1. It is laminate-derived instead of lamina-derived, meaning no ply mechanic calculations need to be made
2. It focuses on utilizing a minimum number of experimental tests to determine material coefficients
3. It relates the strain energy back to the S-N curve in order to provide clear physical meaning
4. It is intended for use in industry, thereby attempting to simplify the life prediction process as much as possible, while still providing a reasonable life prediction

The expenditure of strain energy occurs in three stages (as shown in Figure 2-11): Stage I is a steep curve of energy loss as the material is initially loaded, and generally lasts for about 15% of the fatigue life; Stage II is nearly linear, with the slope a characteristic of the material and testing conditions, and generally lasts for about 75% of the fatigue life; Stage III is again a steep curve leading to material failure over the last 10% of the fatigue life (Kelkar 2001; Natarajan et al. 2005; Dittenber and GangaRao 2010; Stinchcomb and Bakis 1990).

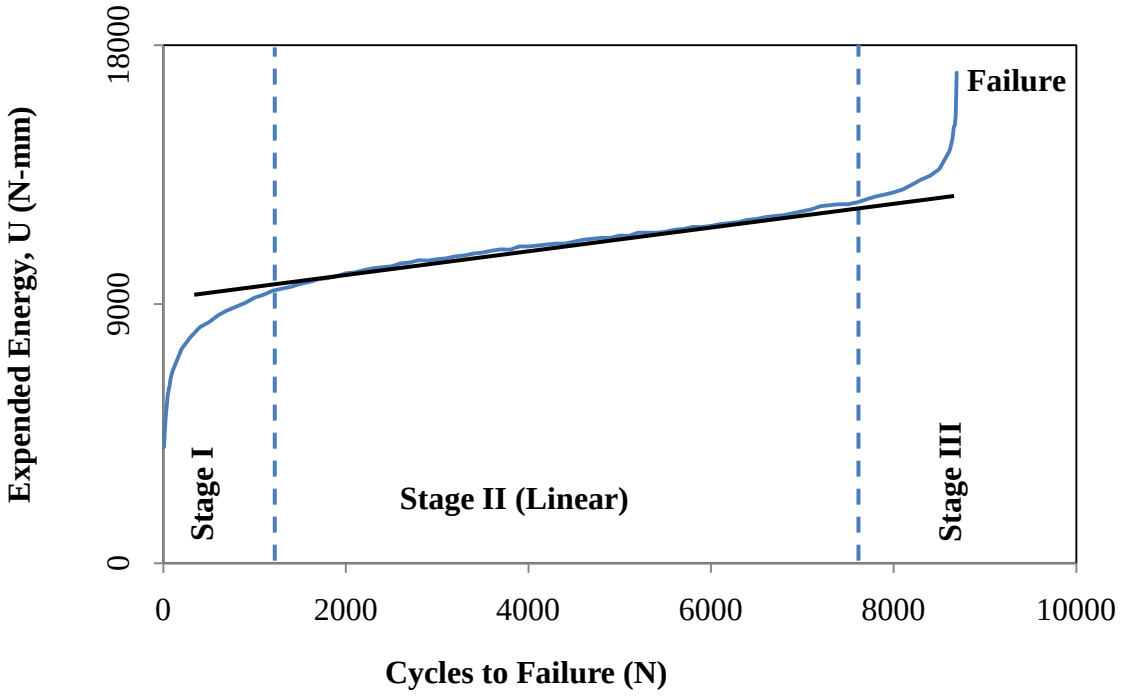

Figure 2-11 - Three Stages of Energy Expenditure in Fatigue (Dittenber and GangaRao 2010)

Equation 2-20 describes the rate of the release of strain energy, U_j, with respect to the number of cycles, N_j, as being a function of the mean strain, ε_m, the strain range, ε_r, the amount of expended strain energy corresponding to the current cycle count, and the particular composite material type, C_t. If the material type is kept constant, then this relationship supposes that the rate of the release of strain energy with respect to the number of cycles is a function of the loading conditions.

$$\frac{dU_j}{dN_j} = f\left(\varepsilon_m, \varepsilon_r, U_j, C_t\right) \tag{2-20}$$

The strain energy at any cycle of a fatigue test can be determined from the deflection (or strain) and loading data; for a tension-tension fatigue test this is, in its simplest form:

$$U_n = \frac{P_n \delta_n}{2} \tag{2-21}$$

where P_n is the load and δ_n is the deflection for any cycle n. To account for more complex material properties, it would likely be acceptable to use different versions of the strain energy equation, such as those used by Ellyin and El-Kadi in Equations 2-4 and 2-6. Natarajan et al. (2005) calculated the initial strain energy U_o using the mean loading stress just prior to initiating fatigue, as shown in Equation 2-22.

$$U_o = \frac{{\sigma_{mean}}^2 AL}{2E_{static}} \tag{2-22}$$

After analyzing experimental strain energy release results for a few dozen GFRP fatigue tests, Natarajan et al. (2005) observed that the strain energy expended at≈90% of the fatigue life (the end of Stage II) was consistently close to 1.5 times the initial strain energy, U_o. The data point at the end of Stage II can therefore be defined as (N_f, U_f), shown in Equations 2-23 and 2-24.

$$U_f \cong 1.5U_o \tag{2-23}$$

$$N_f \cong 0.9N_{ult} \tag{2-24}$$

The energy release rate per cycle is relatively constant within Stage II (for tests between approximately 20% and 85% of the ultimate strength), and is dependent on the material type and loading conditions. Plotting the normalized strain against the energy release rate, the data can be curve-fitted with a power law as shown below:

$$\frac{dU}{dN} = a\left(\frac{\varepsilon_{max}}{\varepsilon_{ult}}\right)^b \tag{2-25}$$

where *a* and *b* are the fatigue coefficients. Because of the linearity of the Stage II energy release, *dU/dN* can be approximated as *ΔU/ΔN*, as shown in Equation 2-26. If we assume the strain ratio can be approximated as equivalent to the stress ratio (Equation 2-27), the number of cycles to the

end of Stage II, or ≈90% of the number of cycles to failure, can be calculated as shown in Equation 2-28.

$$\frac{dU}{dN} = \frac{\Delta U}{\Delta N} = \frac{1.5U_o - U_o}{N_f} = \frac{U_o}{2N_f} \tag{2-26}$$

$$\frac{\varepsilon_{max}}{\varepsilon_{ult}} \cong \frac{\sigma_{max}}{\sigma_{ult}} \tag{2-27}$$

$$N_f = \frac{U_o}{2\left(\frac{dU}{dN}\right)} = \frac{U_o}{2\left(a\left(\frac{\sigma max}{\sigma_{ult}}\right)^b\right)} \tag{2-28}$$

The application of this model to experimental data will be discussed in a later section.

2.6.2 Earlier Stages of Related Work

Master's Theses by V. Natarajan in 2003 and by P. Munagala in 2005 were both earlier stages of the fatigue model work contained within this thesis. Brief reviews of their studies follow.

2.6.2.1 Natarajan's Research

Natarajan's research (2003) was intended to be an overview of the fatigue response of GFRP composites, with a focus on the expenditure of strain energy throughout the process. Testing was performed on both coupons and modular bridge decks.

For the coupon testing, three different composite materials were used. All three were glass/vinyl ester plates formed by pultrusion. Two of the materials were tested in tension-tension fatigue, while the third was tested in flexural fatigue. The testing was conducted at rates of 4 Hz and 0.5 Hz for the tension-tension and flexural tests, respectively. Using the procedure of strain energy calculations previously mentioned, Natarajan found that the expenditure of strain energy between the first cycle and the cycle at the end of Stage II (called N_f) was consistently near 50% of the first cycle strain energy. Using that characterization, he was able to derive the simplified

version of the model shown above. For his three different materials, he calculated the fatigue coefficients *a* and *b* as shown in Table 2-1. He drew some preliminary conclusions regarding the effects of fiber content, fiber architecture, loading type, and specimen thickness on these fatigue coefficients, but due to the small sample size these are merely case-specific observations. Natarajan was eventually able to fit his experimental data with his predicted model with reasonable success.

Table 2-1 - Natarajan Fatigue Coefficients (Natarajan 2003)

Material	*a*	*b*
MAT 1	6.29	13.15
MAT 2	33.1	10.11
MAT 3	1.58	11.17

The two modular bridge decks tested both contained glass reinforcement, but one used a vinyl ester matrix while the other used a polyester matrix. Each deck was composed of five modules and thus had four joints. The decks were each tested in flexural fatigue (using a 10 x 20 inch patch load) at a frequency of 2 Hz up to two million cycles. The decks were not tested to failure, but instead were checked for modulus degradation at half million cycle increments; therefore, the strain energy model was not applicable to the test data. The polyester deck failed in 230,000 cycles due to punching shear failure and the vinyl ester deck did not show any degradation after the full 2,000,000 cycles.

2.6.2.2 Munagala's Research

Munagala's research (2005) was similar to Natarajan's, in that he worked to fit the strain energy model to GFRP composites at both the coupon and the component level. For coupon testing, he again tested three materials, all in tension-tension fatigue, in order to observe their

strain energy expenditure behavior. However, due to some inconsistencies in his coupon data, it was not considered usable for the database analysis conducted later in this report.

At the component level, Munagala tested glass/vinyl ester single-cell and multi-cell bridge decks at a variety of loading levels. However, the multi-cell bridge deck was not tested to failure, so only the single-cell bridge deck data can be used to verify the simplified strain energy model. Munagala showed that for the single cell deck, the model was able to fit the data reasonably well. The research conducted by another WVU-CFC graduate student, V. Nagaraj, in 1994, provided more usable component fatigue data.

2.7 Conclusions

The fatigue behavior of composites is far more complex than the fatigue behavior of metals and has many contributing factors to be considered: fiber type, matrix type, reinforcement structure, stacking sequence, environmental conditions, loading conditions, boundary conditions, and others. Fatigue damage usually begins with matrix cracking and later progresses into fiber failure and delamination; a good fatigue model should be able to account for these different damage modes. Axial fatigue is the preferred testing method, due to its ease of analysis and its relatively more simple stress distributions. Testing conditions can have a significant effect on the fatigue results, and most researchers recommend using rates no more than 5-10 Hz (research conducted at the WVU-CFC generally assumes 4-6 Hz as a more appropriate maximum rate).

Fatigue life prediction models generally can be divided into three categories: fatigue life models, phenomenological models for residual strength/stiffness, and progressive damage models. The fatigue life models are relatively easy to apply, but usually require extensive fatigue testing. Many start with an established failure criterion and then apply factors to account for

fatigue conditions. Phenomenological models present difficulties either in their establishment of an accurate failure criterion or in the measurement of the mechanical properties on which they are based. Progressive damage models depend on the presence of observable damage and share some of the limitations of establishing failure criterion and measuring damage; additionally, they generally seem to be more complex.

Both increased temperature and the presence of moisture have similar effects on the composite materials, swelling and softening the matrix. Moisture absorption can vary widely depending on the materials and the manufacturing process. Generally, composites exposed to salt water do not absorb as much moisture as those exposed to fresh water, but the salt solution has a slightly greater impact on mechanical properties. At elevated temperatures or in a high-moisture environment, the accumulation of fatigue damage goes through the same sequence, just at an increased rate.

The strain energy-based fatigue model proposed by Natarajan et al. (2005) uses the expenditure of strain energy as the damage metric because of its ability to represent various damage modes. Using a few simplifications, the model can easily be applied to wide variety of fatigue data. Several other researchers at the WVU-CFC have done work involving the fatigue model, but this paper is intended to provide a much better evaluation of the model's success at predicting fatigue life.

CHAPTER 3 FATIGUE TESTING OF COUPONS

3.1 Introduction and Scope

In order to characterize the fatigue behavior of a composite material under different environmental conditions (particularly those expected to be encountered by seawater use), the following testing regimen was followed between fall 2008 and spring 2010 at the West Virginia University Constructed Facilities Center (WVU-CFC).

First, the material to be tested is introduced and a thorough explanation is given of the manufacturing processes used to prepare the material for the various tests. Included in this section is a newly developed procedure for making a liquid enclosure for a tension test coupon. In the following section, the results of the following tests are presented and analyzed: fiber content test, static tests, bending fatigue tests, tension-tension fatigue tests, and accelerated immersion conditioning tests. The conclusions from these individual tests are discussed within each subsection. Finally, a summary of all of the conclusions reached during testing are presented at the end of the chapter.

3.2 Materials and Manufacturing Processes

3.2.1 Material

The material tested was provided to WVU-CFC in the form of three 10 inch x 10 inch x ¼ inch thick laminates (see Figure 3-1). They were manufactured by Owens-Corning, specimen #M111008. The composite is composed of X-Strand fiber, MCW21 sizing, and vinyl ester resin cured with Ashland's non-foaming recipe. Owens-Corning confirmed good compatibility and

bonding of resin and fibers in room temperature tests. It was made by filament-winding over a flat mandrel, followed by press cure at elevated temperature and pressure. It has a 75/25 ratio of tows in the two principle directions, with the direction containing 75% of the tows considered the 0°-direction.

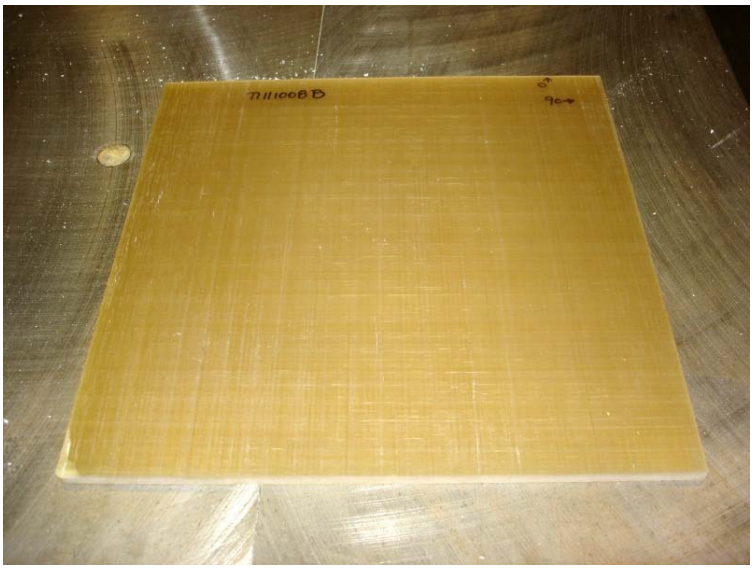

Figure 3-1 - Material Before Samples were Cut

3.2.2 Bending Test Coupons

Coupon specimens were cut by a table saw with a carbide blade. Each specimen measured approximately 8 inches long x ¼ inch thick x ½ inch wide (see Figure 3-2). The long dimension was cut in the 0-direction, so that each sample was tested in the 75% fiber direction. Individual coupon dimensions were measured and are shown in Table 3-1.

Figure 3-2 - Bending Test Coupons

Table 3-1 - Bending Test Sample Dimensions

Sample ID	Avg. Width (in)	Avg. Thickness (in)	CSA (in^2)	Length (in)	Gage Length (in)
1.1	0.493	0.235	0.116	10	6
1.2	0.502	0.239	0.120	10	6
1.3	0.506	0.239	0.121	10	6
1.4	0.496	0.240	0.119	10	6
1.5	0.490	0.239	0.117	10	6
1.6	0.493	0.241	0.119	10	6
1.7	0.494	0.238	0.118	10	6
1.8	0.493	0.240	0.118	10	6
1.9	0.496	0.242	0.120	10	6
1.10	0.496	0.241	0.120	10	6
1.11	0.496	0.243	0.120	10	6
1.12	0.498	0.243	0.121	10	6

3.2.3 Tension Test Coupons

Coupon samples were cut by table saw with a carbide blade. Each sample measured approximately 10 inches long x ¼ inch thick x ½ inch wide. The long dimension was cut in the

0-direction, meaning each sample was tested in the 75% fiber direction. Individual coupon dimensions were measured and are recorded in Table 3-2.

Table 3-2 - Tension Test Sample Dimensions

Sample ID	Avg. Width (in)	Avg. Thickness (in)	CSA (in^2)	Length (in)	Gage Length (in)
1.13	0.495	0.245	0.121	8	2.70
1.14	0.496	0.245	0.121	8	2.70
1.15	0.494	0.246	0.121	8	2.72
2.1	0.502	0.241	0.121	10	4.71
2.2	0.502	0.241	0.121	10	4.70
2.3	0.507	0.243	0.123	10	4.70
2.4	0.508	0.243	0.123	10	4.69
2.5	0.505	0.243	0.123	10	n/a
2.6	0.504	0.244	0.123	10	4.69
2.7	0.500	0.244	0.122	10	4.70
2.8	0.508	0.244	0.124	10	4.70
2.9	0.508	0.244	0.124	10	4.72
2.10	0.509	0.245	0.125	10	4.70
2.11	0.509	0.244	0.124	10	4.70
2.12	0.506	0.243	0.123	10	4.72
2.13	0.508	0.242	0.123	10	4.70
2.14	0.506	0.242	0.122	10	4.72
2.15	0.509	0.240	0.122	10	4.70
2.16	0.508	0.239	0.121	10	4.71
3.1	0.509	0.271	0.138	10	4.71
3.2	0.507	0.269	0.136	10	4.68
3.3	0.510	0.269	0.137	10	4.66
3.4	0.507	0.267	0.135	10	4.66
3.5	0.507	0.268	0.136	10	4.66
3.6	0.507	0.259	0.131	10	4.73

As per ASTM D3039 for tensile testing, each sample underwent a process of affixing steel tabs to each end. The flat-side surfaces on each end were lightly roughed with a grinding wheel, cleaned, and adhered to 1/8 inch thick steel plates (see Figure 3-3) using Ashland's PlioGrip (Structural Adhesive 7779/220). Each sample was allowed a minimum of 24 hours cure time before undergoing testing. As described below, in order to affix the bottles onto the samples to be tested in salt water, the lower steel tabs were made longer (~3.3 inches instead of 2 inches

for the upper tabs) so as to extend beyond the gripping area. For consistency in gage length, even those samples not tested in salt water were tested with the long lower tabs. For the samples which were exposed to the immersion conditioning / accelerated aging, the tabs were not applied until after the samples had reached saturation and been removed from the pressurized absorption cylinder.

Figure 3-3 - Steel tabs attached to sample

3.2.4 Tension Test Coupons with Water Containment Vessel

The samples to be fatigue tested in salt water were prepared in a similar manner to the dry samples, with an additional procedure to attach a water containment vessel (see Figure 3-4). This procedure was devised specifically for this application and was used in the place of much more expensive water containment options.

Figure 3-4 - Completed water containment sample on testing machine

The tabs to be attached to the lower end of the sample were cut about 1 ¼ inches longer than the top tabs (see Figure 3-5). Once again, the steel tabs were affixed to the sample using Pliogrip, clamped, and allowed to cure for 24 hours.

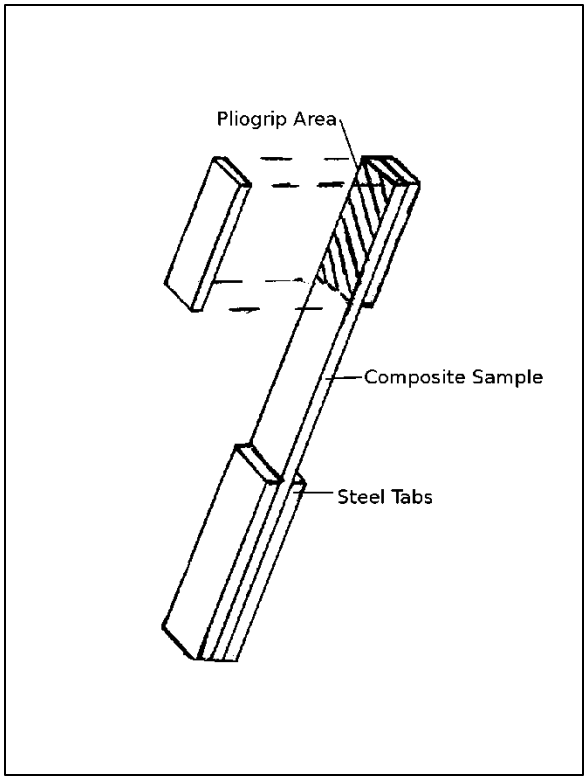

Figure 3-5 - Composite sample with grip placement

After the Pliogrip was fully cured, a regular plastic (PETE) 24 oz (710 ml) soda bottle was cleaned with acetone. Large grit sandpaper was used to rough up the material on the inside of the neck, followed by another cleaning with acetone. The bottle was positioned next to the sample, such that the lower tabs would extend up through the neck of the bottle (see Figure 3-6). The position of the bottom of the lower tabs was marked on the bottle and cut through. The half of the bottle not containing the neck was disposed.

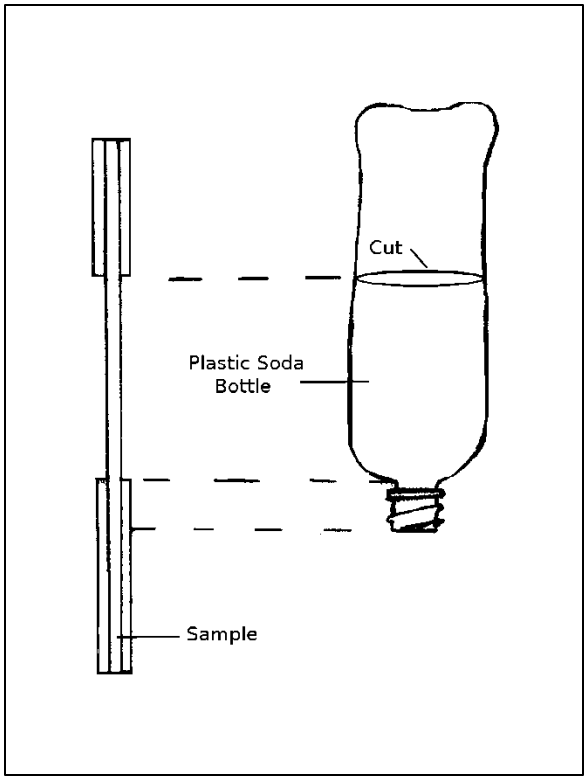

Figure 3-6 - Composite sample with bottle alignment

Using electrical tape, the bottle was affixed in position around the sample (see Figure 3-7). Care was taken to make sure that the electrical tape formed a seal below the mouth of the bottle, so that none of the foam sealant would leak out. If, after taping, the bottle ended up not being properly aligned with the sample, an additional piece of tape could be used on the other end of the bottle to hold it in position.

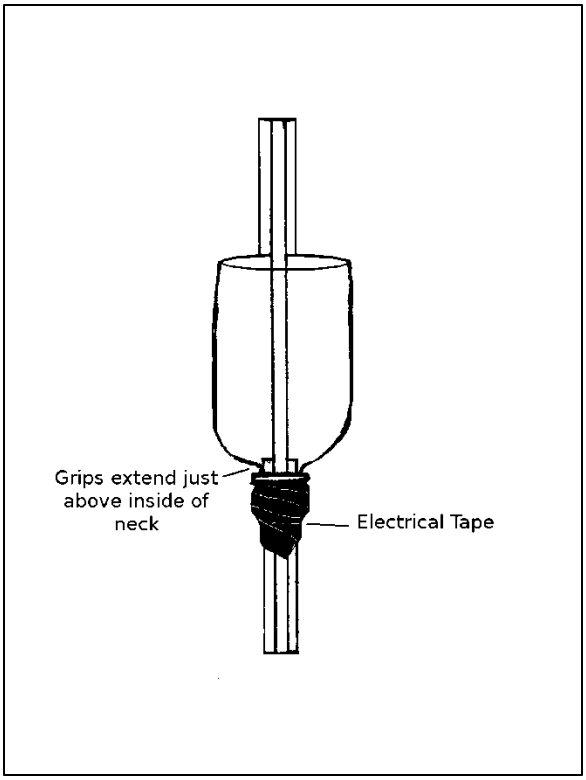

Figure 3-7 - Bottle positioning and taping

After the bottle was correctly positioned, the lower tabs were lightly clamped in a vice such that the sample was kept vertical. Dow's *Great Stuff* Polyurethane Sealant was applied in between the neck of the bottle and the sample (see Figure 3-8). The long straw applicator included with the sealant was sufficient to reach the neck from the open top of the bottle fixture. Care was taken not to allow the sealant to contact the sample, except in the gripping area contained in the neck of the bottle, which was completely filled. The sealant was then allowed to cure the recommended amount of time before proceeding.

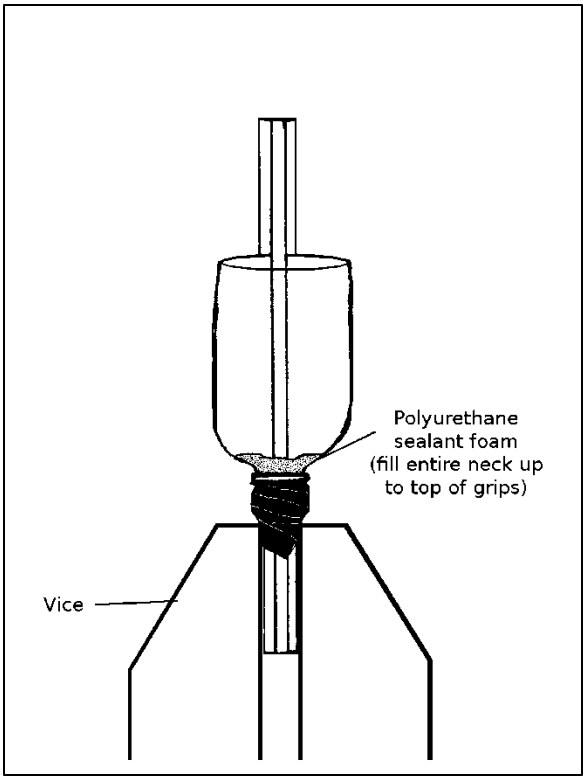

Figure 3-8 - Application of foam sealant

The cured sealant provided a rigid interface between the bottle and the sample. As a result, the sample could be released from the vice and the tape removed. If any sealant had leaked out through the tape, it was cut off. A layer of Loctite Clear Silicone Adhesive Sealant was applied inside of the bottle, on top of the sealant. Care was taken to ensure that the silicone formed a continuous layer, contacting the entire circumference of the bottle and the perimeter of the sample just above the tabs (see Figure 3-9). Silicone was also applied around the outside of the mouth of the bottle. The silicone was then allowed to cure the recommended amount of time before fatigue testing. After testing several samples, it was found that they often failed in delaminations that extended into the tabs, letting the water leak out through the lower grip area. A layer of silicone was then applied around the entire exposed surface of the sample between the

lower tabs, where it would not interfere with the testing clamps (see Figure 3-10). An isometric view of the final design can be seen in Figure 3-11.

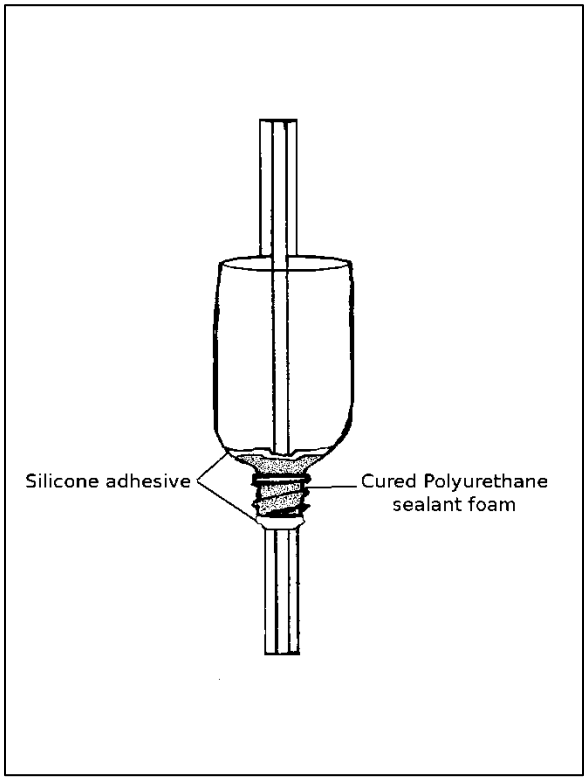

Figure 3-9 - Application of Silicone adhesive

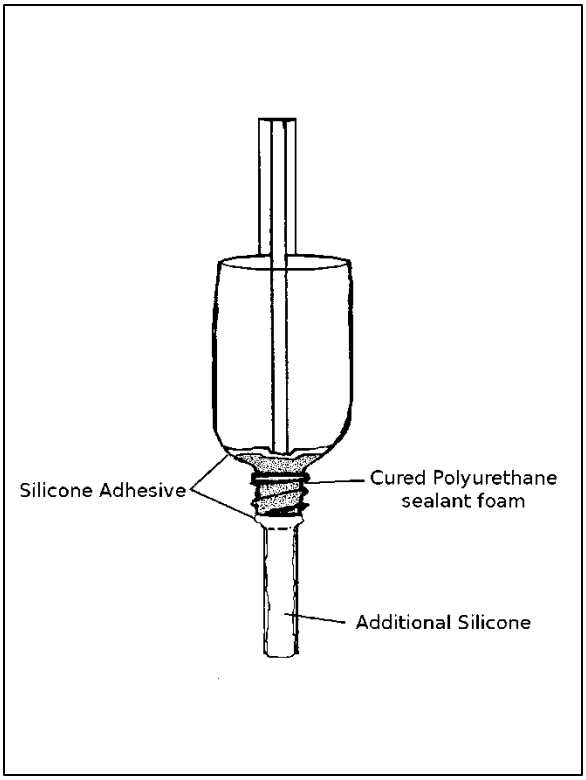

Figure 3-10 - Modified Silicone adhesive placement

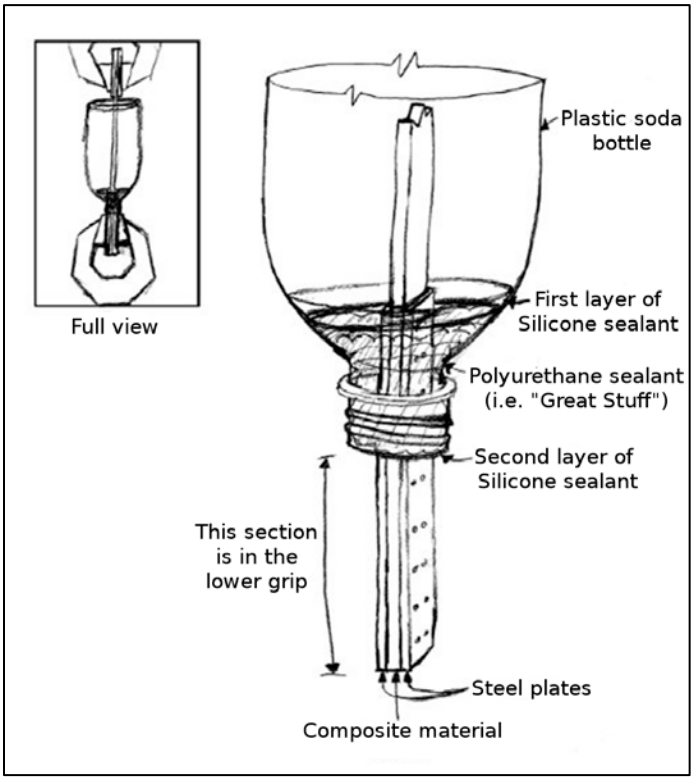

Figure 3-11 - Completed water containment sample

3.3 Experimental Methodology

3.3.1 Fiber Content Test

The fiber volume fraction test was performed roughly following the procedure outlined in ASTM D2584. Three samples were cut to approximately the recommended size (1 inch x 1 inch x the thickness of the material). Each sample was weighed in its respective crucible before ignition (see Table 3-3). The crucibles were then heated in an oven up to 450°C for four hours. The crucibles were then allowed to cool to room temperature before being reweighed.

Table 3-3 - Fiber Content Test Sample Dimensions

Sample	Width (in)	Length (in)	Thickness (in)	Volume (in^3)	Weight (g)
A	0.871	1.039	0.243	0.220	6.871
B	0.856	1.044	0.242	0.216	6.786
C	0.878	1.037	0.245	0.223	6.916

3.3.2 Static Tests

The objective of the static three-point bending and tension tests was to determine the material failure load and deflection at room temperature in a dry environmental condition. This failure load could then be used as the ultimate load against which the stress level of the fatigue tests could be measured. Additionally, the flexural and tensile strengths and moduli of the material could be established with reference to procedures in ASTM D790 and D3039, providing baseline values of the mechanical properties of the material.

The static bending tests were performed using a WVU-manufactured three-point bending test fixture installed on an Instron 8501 testing machine (Figure 3-12). The test span was 6 inches, leaving a 1 inch overhang on each outer support. The test conditions for static bending testing were room temperature and dry (not immersed in salt water), with a 0.15 inch/minute

crosshead speed. Coupons were loaded to failure, which was determined as the first point at which the coupon experienced a dramatic decrease in the amount of load it was resisting. The first coupon was continuously loaded through several stages of failures; subsequent tests only loaded the coupons until just after the first failure.

Figure 3-12 - Bending Test Fixture on Instron Machine

The static tensile tests were performed using an Instron 8501 testing machine (see Figure 3-13) with standard tensile clamps (see Figure 3-14). The gage length of the samples was 4.7 inches, with two inches of each end of the sample within each grip. The test conditions for static

testing were room temperature and dry (not immersed in salt water), with a 0.05 in/min crosshead speed as per ASTM D3039. Since the lower tabs extended an inch above the lower grips, a small C-clamp was applied to help keep tab separation from occurring in that area. Strain gauges were used to assess the tensile modulus of elasticity of the material. Samples were loaded to failure, which was determined as the first point at which the coupon experienced a dramatic decrease in the amount of load it was resisting.

Figure 3-13 - Instron 8501 Universal Testing Machine

Figure 3-14 - Tension Clamps (Shown with Water Containment Bottle)

3.3.3 Bending Fatigue

The objective of the fatigue three-point bending tests was to characterize the bending fatigue response of the material under different loading and environmental conditions. Plots of the load and deflection over number of cycles were collected and will be further used for theoretical characterization in the future. These fatigue tests are intended to serve as assessments of the general salt-water fatigue behavior of the material and to confirm the suitability of the test methods. Upon completion, we will establish if the conditioning environment change would result in a significant reduction in properties.

Fatigue tests were also performed using the same fixture, span, and testing machine as was used for static bending testing (see Figure 3-15). Using Instron's WaveMaker software, the specimens were ramp-loaded up to their mean value, and then sinusoidally loaded to the max and min load values repeatedly (see Figure 3-16). The max load divided by the ultimate load (from static testing) determined the load level, while the min load divided by the max load determined the R-Ratio value. The sensitive nature of fatigue tests usually required several attempts in adjusting the PID loop-feedback values in order to achieve the desired load levels, inevitably resulting in some tests having more accurate loading levels than others. The max/min load and deflection values (measured by the Instron's incorporated load cell and LVDT) were recorded for each cycle, and the tests were run until a failure or multistage failures were observed. A coupon was considered to have failed when its deflection experienced a dramatic increase over a very short number of cycles while it failed to maintain the required load, indicating that some level of delamination or splitting had taken place.

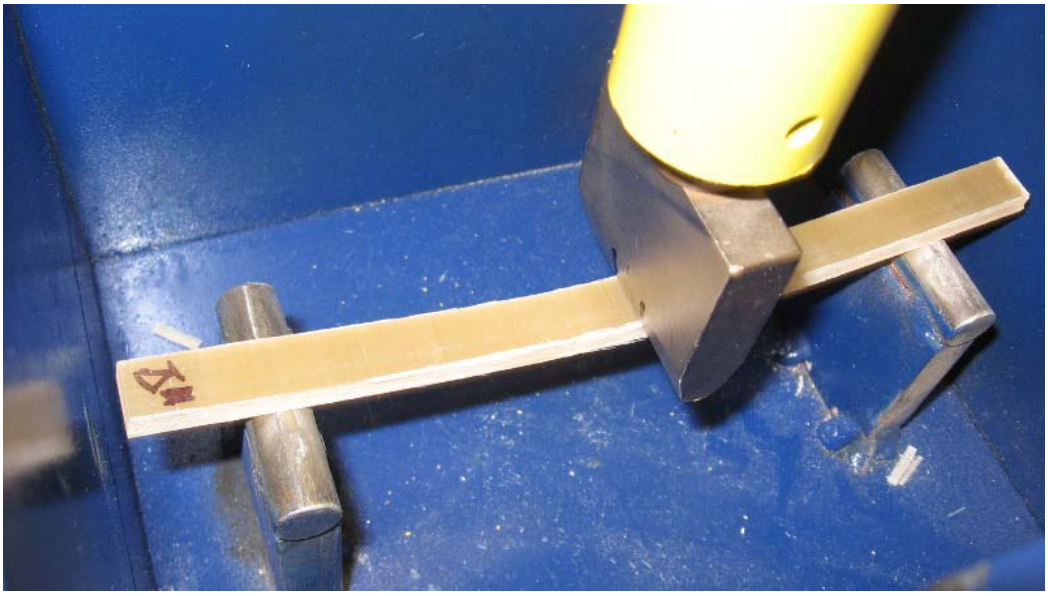

Figure 3-15 - Bending Test Fixture with Sample

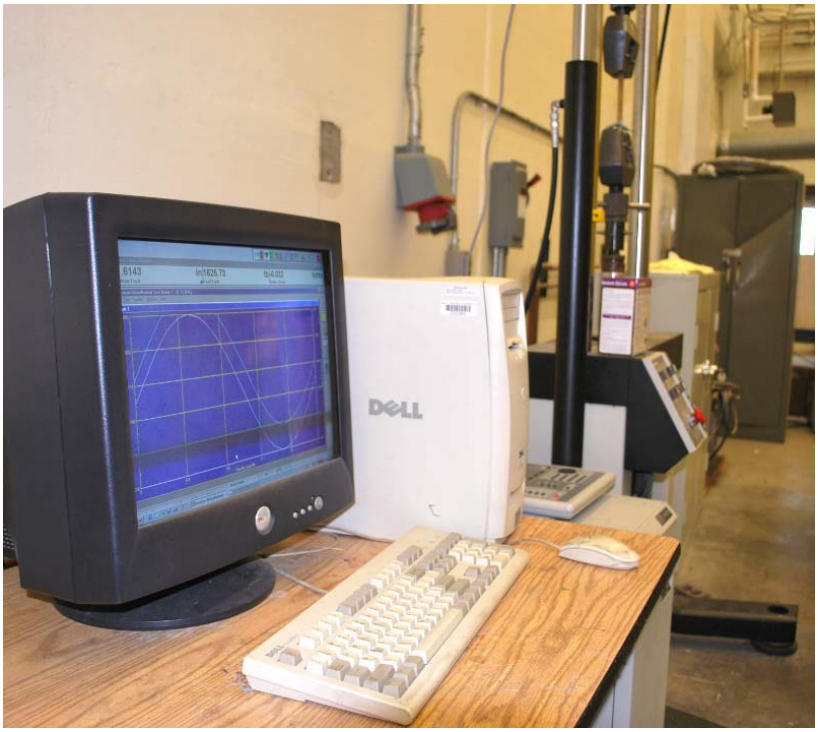

Figure 3-16 - Instron WaveMaker Software used with the Instron 8501

Temperature was controlled using an Instron environmental chamber, which encapsulated both the coupon and the entire test fixture (see Figure 3-17). For high temperature tests, the chamber, test fixture, salt water (if used), and coupon were all allowed to reach temperature before the test was begun.

Figure 3-17 - Instron Environmental Chamber

The WVU-manufactured bending test fixture had dimensions of 9” x 7” x 7” and was able to contain salt water. Salt water was made from mixing tap water and Instant Ocean® Sea Salt, using the mixing instructions provided with the sea salt.

The bending fatigue tests were run under a variety of environmental conditions and stress levels, as listed in Table 3-4.

Table 3-4 - Bending Test Condition Matrix

Sample ID	Test Type	Temperature (°F)	Environment	Stress Level (max/ultimate)
1.1	Static	70	Dry	n/a
1.2	Static	70	Dry	n/a
1.3	Static	70	Dry	n/a
1.4	Fatigue	70	Dry	60%
1.5	Fatigue	70	Dry	63%
1.6	Fatigue	150	Salt water	63%
1.7	Fatigue	70	Salt water	63%
1.8	Fatigue	70	Salt water	50%
1.9	Fatigue	70	Salt water	63%
1.10	Fatigue	125	Salt water	63%
1.11	Fatigue	100	Salt water	63%
1.12	Fatigue	70	Dry	50%

3.3.4 Tension-Tension Fatigue

The objective of the tension testing was to characterize the tensile fatigue response of the material under different loading and environmental conditions. Plots of the load and deflection over number of cycles were collected and will be used for theoretical characterization in the future. These fatigue tests are intended to serve as assessments of the general salt water fatigue behavior of the material and to confirm the suitability of the test methods. Upon completion, we will establish if the conditioning environment change would result in a significant reduction in properties.

Tensile fatigue tests were also performed using the same fixtures, gage length, and testing machine as used for static testing (Figure 3-14). Using Instron's WaveMaker software, the samples were ramp-loaded up to their mean value, and then sinusoidally loaded to the max and min load values repeatedly. The max load divided by the ultimate load (from static testing) determined the load level, while the min load divided by the max load determined the R-Ratio

value. The sensitive nature of fatigue tests inevitably resulted in some tests having more accurate loading levels than others. The max/min load and deflection values (measured by the Instron's incorporated load cell and LVDT) were recorded for each cycle, and the tests were run until a failure or multistage failures were observed. A coupon was considered to have failed when its deflection experienced a dramatic increase over a very short number of cycles while it failed to maintain the required load, indicating that some level of delamination or splitting had taken place.

Temperature was controlled using an Instron environmental chamber, which encapsulated both the coupon and the entire test fixture. For the elevated temperature test, the chamber, tension grips, salt water, and coupon were all allowed to reach temperature before the test began. Salt water was made from mixing tap water and Instant Ocean® Sea Salt, using the mixing instructions provided with the sea salt.

The tension-tension fatigue tests were run under a variety of environmental conditions, as outlined Table 3-5.

Table 3-5 - Tension Test Condition Matrix

Sample ID	Test Type	Temperature (°F)	Environment	Stress Level (max/ultimate)	Acclerated Immersion
1.13	Fatigue	70	Salt water	63%	n/a
1.14	n/a	n/a	n/a	n/a	n/a
1.15	Static	70	Dry	n/a	n/a
2.1	Static	70	Dry	n/a	n/a
2.2	Fatigue	70	Dry	63%	n/a
2.3	Fatigue	70	Salt water	63%	n/a
2.4	Fatigue	70	Dry	50%	n/a
2.5	n/a	n/a	n/a	n/a	70F, Atmospheric
2.6	Fatigue	70	Salt water	50%	n/a
2.7	Static	70	Dry	n/a	n/a
2.8	Fatigue	100	Salt water	63%	n/a
2.9	Fatigue	70	Dry	50%	70F, 2200 psi
2.10	Fatigue	70	Salt water	63%	70F, 2200 psi
2.11	Fatigue	70	Salt water	50%	70F, 2200 psi
2.12	Fatigue	70	Dry	50%	70/100F, 2200/1700 psi
2.13	Fatigue	70	Salt water	50%	100F, 1700 psi
2.14	Fatigue	70	Dry	50%	100F, 1700 psi
2.15	Fatigue	70	Salt water	63%	100F, 1700 psi
2.16	Fatigue	70	Salt water	50%	n/a
3.1	Fatigue	70	Dry	35%	n/a
3.2	Fatigue	70	Dry	55%	n/a
3.3	Fatigue	70	Dry	55%	n/a
3.4	Fatigue	70	Dry	70%	n/a
3.5	Fatigue	70	Dry	47%	n/a
3.6	Fatigue	70	Dry	47%	n/a

3.3.5 Accelerated Immersion Condition

The objective of the accelerated immersion conditioning was to determine the approximate material saturation percent weight and to quickly bring each sample to that

saturation point. Once each sample reached its immersion point, it could be tension-tension tested to determine if the absorption resulted in any loss of fatigue properties.

The objective of the fatigue testing was to characterize the saturated tension-tension fatigue response of the material under a few different loading and environmental conditions. Plots of the load and deflection over number of cycles were collected and will be used for theoretical characterization in the future. These fatigue tests are intended to serve as assessments of the long-term salt water fatigue behavior of the material. Whether or not the conditioning environment change resulted in a significant reduction in properties was established upon completion.

Accelerated immersion conditioning was carried out in a pressurized enclosure manufactured by the WVU-CFC (see Figure 3-18 and Figure 3-19). A steel piston was designed to enclose up to a dozen samples and the immersing salt water. An actuator was used to apply force to the shaft of the piston, resulting in an increased pressure throughout the immersing fluid. A 3000psi pressure gauge was used to monitor the internal pressure (see Figure 3-20). All internal surfaces of the pressure chamber were chromed to reduce corrosion.

Figure 3-18 - WVU-CFC Manufactured Pressure Chamber

Figure 3-19 - Pressure Chamber in Use

Figure 3-20 - Pressure Gauge

Samples were weighed using a balance with an accuracy of .0001g before being installed in the pressure chamber. All samples were removed weekly and allowed to air dry for ten minutes before additional weight measurements were taken. Once samples appeared to have significantly reduced in their absorption rate week-to-week, they were assumed to be close to their saturation point and considered ready for fatigue testing.

For the elevated temperature immersion conditioning, copper tubing was tightly wrapped around the outside of the section of the pressure chamber. A heated water circulator constantly flowed 104F (40C) water through the copper tubing throughout the entirety of the immersion conditioning (see Figure 3-21). Preliminary trials showed that the immersing fluid reached the target temperature of 100F after a short period using this method.

As a control, sample 2.5 was immersed in room temperature water at atmospheric pressure (Figure 3-22) and monitored several times a week for 319 days.

Figure 3-21 - Elevated Temperature / Pressurized Immersion Chamber

Figure 3-22 - Room Temperature / Pressure Sample

Before being fatigue tested, the samples removed from the accelerated immersion chamber still needed to have their steel tabs (and in those cases to be fatigue tested in salt water, their water containment bottles) attached. The samples were allowed to surface dry for a few hours, and then they underwent the same manufacturing processes described in the previous section.

The first round of accelerated immersion (samples 2.9, 2.10, 2.11, 2.12) was conditioned at room temperature and approximately 2200psi. The second round of accelerated immersion (samples 2.12 [again], 2.13, 2.14, 2.15) was conditioned at 100°F and approximately 1700psi (see Table 3-5 for the tension test condition matrix, including immersion conditions).

3.4 Results and Discussion

3.4.1 Fiber Content Test

The samples for the ignition loss test were assumed to have a negligible void content. Dimensions for each sample are available in Table 3-3. The fiber weight fraction can be calculated according to Equation 3-1 (where *m* is mass), which operates on the assumption that all of the resin/matrix material has combusted and burned off of the sample as a gas, leaving behind only the fibers.

$$FWF = \frac{m_{post}}{m_{pre}} \tag{3-1}$$

The fiber volume fraction can be obtained from the fiber weight fraction if the density of the fibers is known. In this case, the density of the fibers was assumed to be 2.55 g/cc, an average density for E-glass fibers (Barbero 1999). Equation 3-2 shows how to calculate the fiber volume fraction, where ρ_{tot} is the total composite material density and ρ_f is 2.55 g/cc. The fiber

weight and volume fractions are shown in Table 3-6. The average fiber weight fraction was found to be 76.1% and the average fiber volume fraction was found to be 56.8%.

$$FVF = \frac{\rho_{tot}}{\rho_f} FWF \tag{3-2}$$

Table 3-6 - Fiber Content Test Results

Sample	A	B	C	Average	Range
Pre-Ignition Mass (g)	6.87	6.79	6.92	6.86	-
Total Density (g/cc)	1.91	1.92	1.89	1.90	-
Post-Ignition Mass (g)	5.23	5.18	5.24	5.22	-
Fiber Weight Fraction	76.1%	76.3%	75.8%	76.1%	0.55%
Fiber Volume Fraction	56.9%	57.4%	56.2%	56.8%	1.19%

Additionally, after the resin had been burned off, the general fiber lay-up could be observed. It was easily seen that the composite consisted of 0° fibers in the center and along the top and bottom of the material, with thin layers of 90° fibers in between (see Figure 3-23).

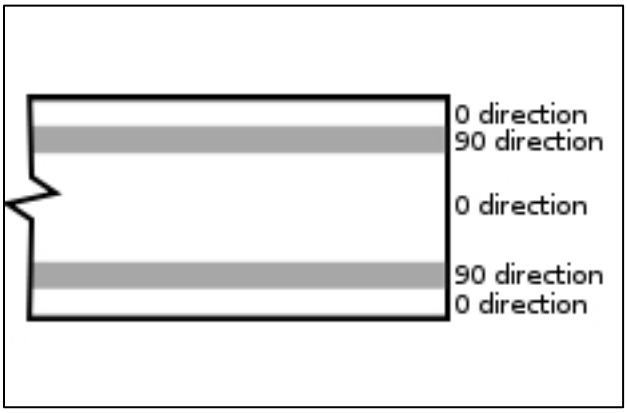

Figure 3-23 - Basic Fiber Architecture

3.4.2 Static Tests

3.4.2.1 Static Bending Results

The load and deflection of the static bending samples were recorded through the WaveMaker software using the testing machine's incorporated load cell and LVDT. The maximum load and deflection data was taken directly from the collected data. The bending modulus of elasticity, E_b, was calculated according to Equation 3-3, where P is the load, δ is the deflection, l is the span length, b is the width, and d is the depth of each sample. The (P/δ) term was acquired by fitting a regression line to the slope of the load/deflection plot.

$$E_b = \left(\frac{P}{\delta}\right)\frac{l^3}{4bd^3} \tag{3-3}$$

The flexural strength, S_b, was calculated according to Equation 3-4. In this case, P was taken as the maximum load (the load at failure).

$$S_b = \frac{3Pl}{2bd^2} \tag{3-4}$$

A summary of the static bending test results is shown in Table 3-7. The calculated modulus of elasticity value is shown in two forms: first, assuming the deflection is due to pure bending and the shear effect is negligible because of the span-to-depth ratio of 24, and second, adjusting for the shear effect by applying an estimated deflection factor of 7%. The average maximum load was calculated as 471.6 pounds, the average maximum deflection as 0.669 inches, the average unadjusted modulus as 6.04×10^6 psi, the average adjusted modulus as 6.47×10^6 psi, and the average flexural strength as 150.4 ksi. The failed static bending samples are shown in Figure 3-24.

Table 3-7 - Static Bending Test Results

Sample	1.1	1.2	1.3	Average
Max Load (lbs)	476.0	460.8	478.0	471.6
Max Deflection (in)	0.667	0.631	0.708	0.669
Modulus of Elasticity (psi)	6.34E+06	6.01E+06	5.78E+06	6.04E+06
Modulus of Elasticity, Adjusted (psi)	6.79E+06	6.43E+06	6.18E+06	6.47E+06
Flexural Strength (ksi)	156.9	145.0	149.2	150.4

Figure 3-24 - Failed Static Bending Samples

3.4.2.2 Static Tension Results

The load and deflection of the static tension samples were recorded through StrainSmart software using the testing machine's incorporated load cell and strain gauges applied to the samples. The maximum load was taken directly from the collected data; the maximum strain was beyond the capability of the strain gauge used. The tensile stress, σ_t, can be calculated at any time during the test from the load, P, and the cross sectional area, A, as shown in Equation 3-5. The tensile modulus of elasticity, E_t, could be calculated according to Equation 3-6, where σ_t is the tensile stress and ε_a is the axial strain, but was instead acquired by fitting a regression line to the slope of each stress/strain plot (Figure 3-25 for sample 2.1 and Figure 3-26 for sample 2.7). A

summary of the static bending test results is shown in Table 3-8. The average maximum load was calculated as 12.24 kips, the average modulus of elasticity as 5.51×10^6 psi, and the average tensile strength as 100.70 ksi. The tension test sample dimensions are shown in Table 3-2. A typical failed static test sample (sample 2.1) is shown in Figure 3-27.

$$\sigma_t = \frac{P}{A} \tag{3-5}$$

$$E_t = \frac{\sigma_t}{\varepsilon_a} \tag{3-6}$$

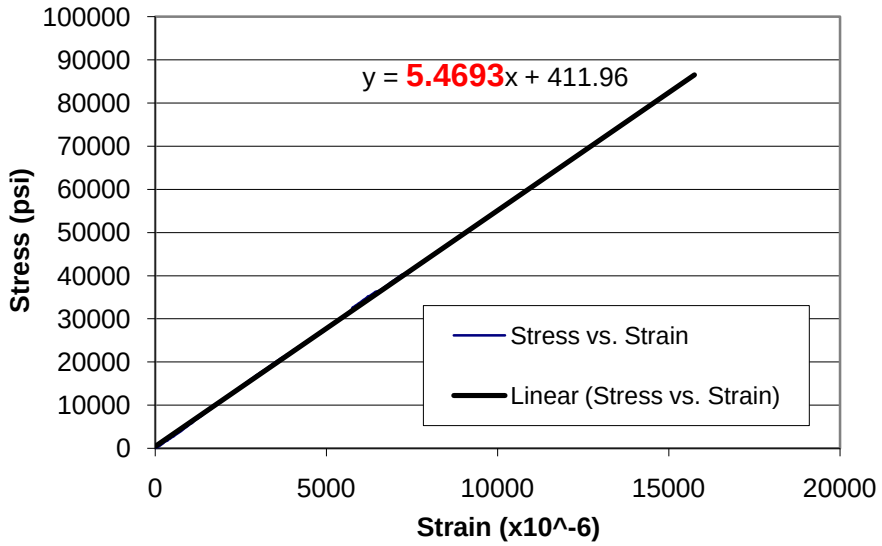

Figure 3-25 - Stress/Strain Plot for Sample 2.1

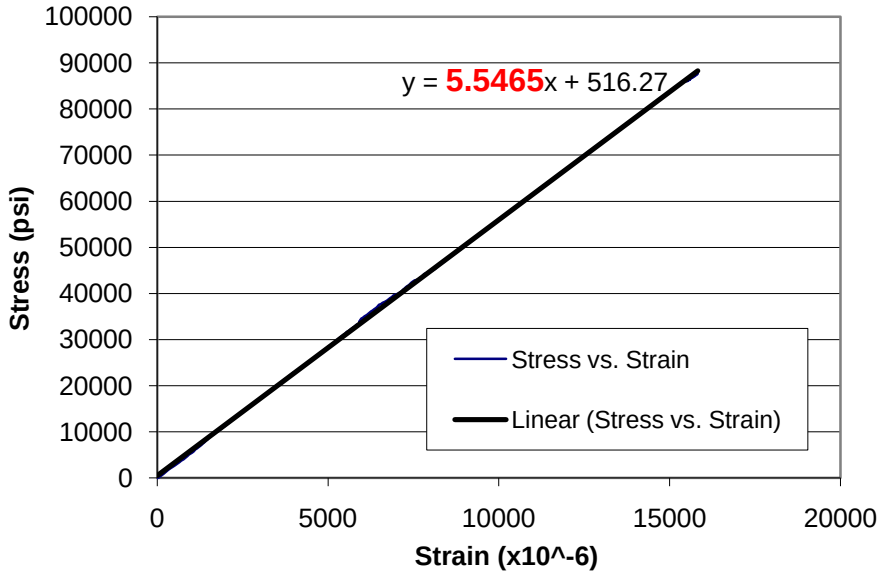

Figure 3-26 - Stress/Strain Plot for Sample 2.7

Table 3-8 - Static Tension Test Results

Sample ID	2.1	2.7	Average
Cross Sectional Area (in^2)	0.121	0.122	0.122
Max Load (kips)	12.23	12.24	12.24
Modulus of Elasticity (psi)	5.47E+06	5.55E+06	5.51E+06
Max Stress (ksi)	101.07	100.33	100.70

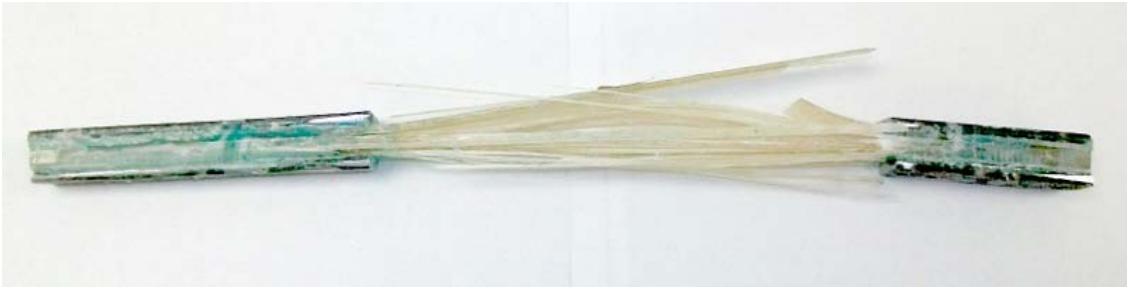

Figure 3-27 - Failed Static Tensile Sample (2.1)

3.4.3 Bending Fatigue

A summary of the bending fatigue test results is shown in Table 3-9. Deflection data was collected via internal LVDT; therefore, error introduced by depressions in the samples caused by friction at supports is included. The deflection data reported was obtained by subtracting the initial LVDT reading where each test began. Hence the max deflection and min deflection data should be considered as for reference only, but the deflection range (the difference between the max deflection and min deflection) is more accurate, reflecting the net deflection induced by the load range (difference between max load and min load).

Table 3-9 - Summary of Bending Fatigue Test Results

Sample ID	**1.5**	**1.6**	**1.8**	**1.9**	**1.10**	**1.11**	**1.12**
Temperature, °F	RT (65)	**HT (150)**	RT (65)	RT (72)	**MT2 (125)**	**MT1 (100)**	RT (72)
Salt Water	**No**	Yes	Yes	Yes	Yes	Yes	**No**
Rate	0.5 Hz	0.5 Hz	0.5 Hz	0.5 Hz	0.5 Hz	0.5 Hz	0.5 Hz
Load Level	63%	63%	**50%**	63%	63%	63%	**50%**
R-Ratio	0.2	0.2	0.16	0.2	0.2	0.2	0.18
Average Max Load, lbs	301.7	301.1	243.3	299.7	297.8	300.4	239.0
Average Min Load, lbs	59.3	60.7	39.4	60.7	62.2	60.2	43.0
Load Range, lbs	242.4	240.4	203.9	239	235.6	240.2	196.0
Deflection Range, inch	0.316	0.319	0.287	0.318	0.311	0.304	0.272
Full Number of Cycles	41,195	4,886	189,170	34,719	13,391	41,837	526,546
Cycles to First Failure	**34,445**	**4,824**	**153,749**	**28,845**	**13,031**	**17,802**	**284,360**

The “first failure” referred to in Table 3-9 is defined as the beginning of the increased slope on the deflection diagram that led to an inability to sustain the full load. In some cases, the sample experienced a clear first failure but had not yet tripped the deflection limit set on the

Instron testing machine, thereby continuing to run for the “full number of cycles” shown in Table 3-9.

For each fatigue test, data plots were generated over the number of cycles for the following quantities: max/min load, max/min deflection, load range, and deflection range. The results were compiled into the following composite plots (available in Appendix A): loading (Figure A-1), deflection maximum (Figure A-2), deflection minimum (Figure A-3), and deflection range (Figure A-4). Because the material was frequently tested in a salt water environment, underwent high amounts of strain, and frequently experienced surface failures before the true material failure, strain was not able to be collected through strain gauges. The strain could be calculated from the deflection data, but would contain the same errors and would not provide any additional useful information.

On nearly every test, black dust appeared around where the sample contacted the steel supports. It is believed that the dust was generated from the steel deteriorating under the friction from the sample, and was therefore not directly affecting the tests. However, depressions appeared in the sample over the supports (see Figure 3-28), which might lead to irregular fluctuations in max/min deflection versus number of cycle curves for some tests.

Figure 3-28 - Depressions at Supports on Bending Fatigue Samples

During a trial fatigue test for sample 1.4 (dry condition) at room temperature, temperature readings were taken on the surface of the coupon by infrared measurement at several intervals. The ambient temperature was around 55°F for the majority of the test. It appears that the overall specimen temperature had no significant change, indicating no hysteresis effect (see Table 3-10).

Table 3-10 - Sample Surface Temperature during Bending Fatigue Test

Cycles	Temp (°F)
Initial	54.6
250	54.6
750	56.1
1250	55.5
1750	54.8
2250	55.6
4000	55.9
6000	55.9
9000	56.1
12000	50.3

During testing of sample 1.9, the PID control settings were such that the testing machine vibrated at the natural frequency of the test fixture (filled with salt water) and created a harmonic vibration. This vibration can easily be seen in Figure A-1 between cycles 4000 and 6000. The water level was then reduced, and no further interference was noted throughout the duration of the test.

It appeared that there was a moment of interruption during overnight testing of sample 1.7 (salt water, room temperature, 63% loading). Data plots showed a very strange loading pattern around 7800 cycles, possibly due to either power fluctuations in the research building or another case of resonance. The sample was found fallen off its supports at approximately 9020 cycles. The sample apparently shifted away from its original loading position during the test, resulting in two pairs of wear marks from the lower supports. The test was repeated using sample 1.9.

The buoyancy force for immersed samples was considered negligible because of their small volume.

The failure mode under bending fatigue seemed to consistently be delamination on the lower surface (tension side), initiated near the midpoint of the specimen. On some specimens the delamination was visible only around the center of the specimen; on others it propagated from the center area to one or both of the lower supports, and on a few the delamination reached one end of the specimen (see Figure 3-29). It seems that delamination begins beneath the central loading fixture and propagates outward on subsequent cycles.

Figure 3-29 - Failed Bending Fatigue Samples (Tension Side)

Based on the data in Table 3-9, it was observed that the presence of salt water reduced the fatigue life of the material to 84% of the value of a dry test at room temperature and a stress level of 63% of ultimate load, i.e., from 34,445 cycles to 28,845 cycles. At a stress level of 50% of the ultimate load, the presence of salt water reduced the fatigue life of the material to 54% of the value of a dry test at room temperature (see Figure 3-31).

In an extreme case, the elevated temperature (150°F) reduced the fatigue life of the material to 17% of the value at room temperature, in salt water, and at a stress level of 63%, from 28,845 cycles to 4,824 cycles, because of the viscoelastic effect of the polymer resin. Midrange temperatures exhibited similar behavior, with a test run at 100°F reducing the fatigue life to 62% of the original value and a test run at 125°F reducing the fatigue life to 45% of the original value (see Figure 3-31). It seems that the increase of temperature (on the salt water samples) has a roughly linear effect on the number of cycles to failure, as seen in Figure 3-32.

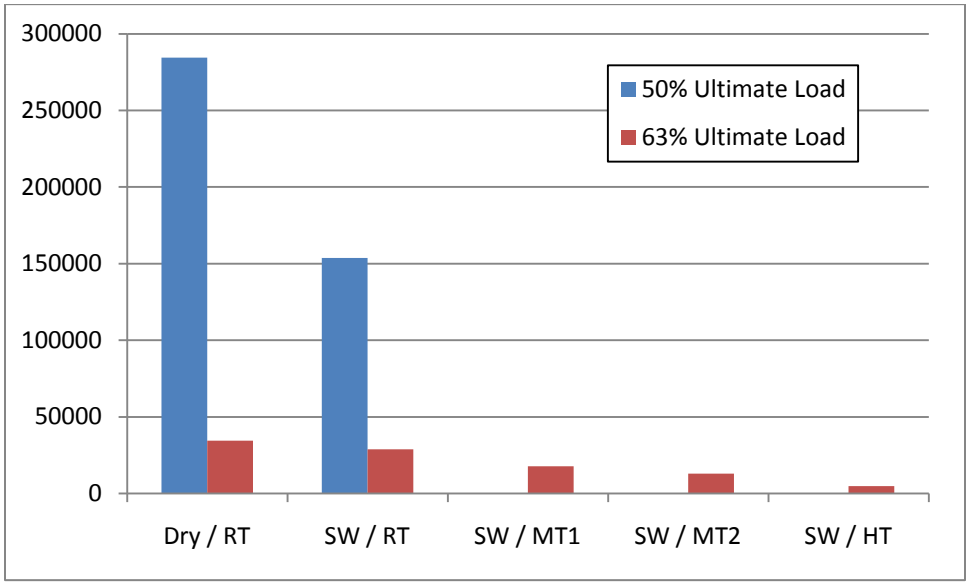

Figure 3-30 - Bending Fatigue Life Environmental Comparison

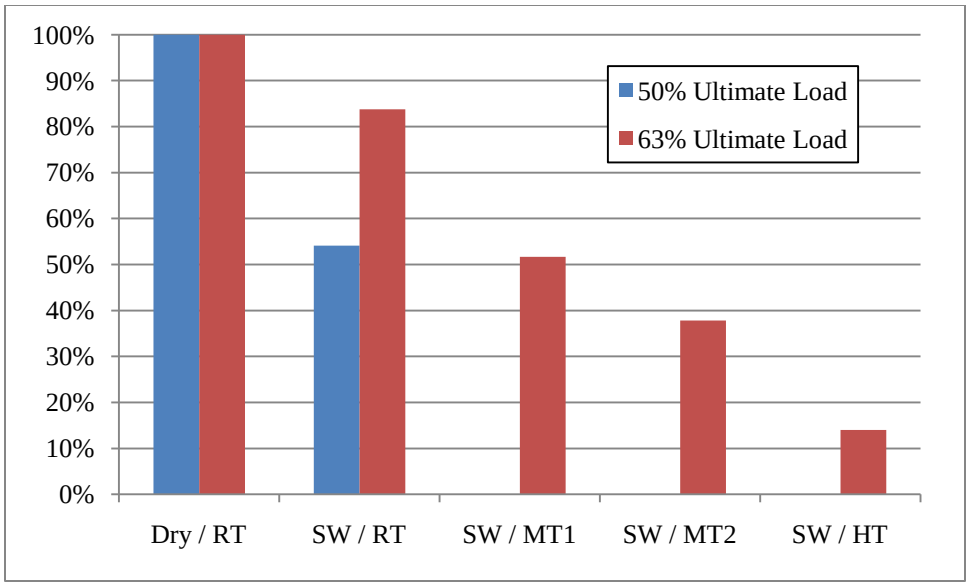

Figure 3-31 – Bending Relative % Fatigue Life Environmental Comparison

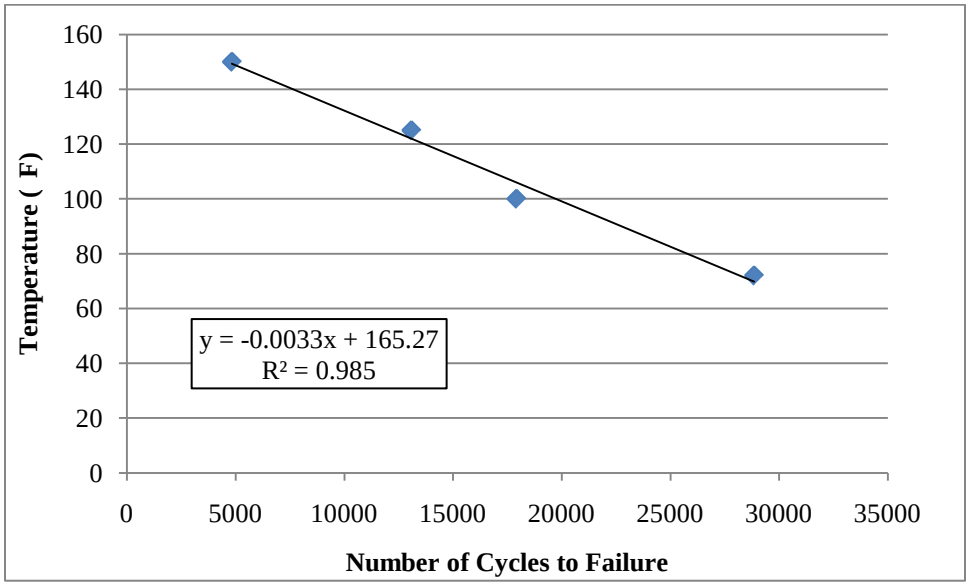

Figure 3-32 - Temperature Effect on Bending Fatigue Cycles to Failure

Under the same environmental conditions (room temperature, salt water), increasing the loading level from 50% to 63% resulted in a decrease in fatigue life to approximately 19% of the original value, i.e. from 153,749 cycles to 28,845 cycles. A dry test run at the same levels

resulted in a decrease of fatigue life to approximately 12% of the original value (see Figure 3-30).

As expected, the presence of salt water or elevated temperature significantly lowered the fatigue life of the material, while reducing the loading level greatly increased its fatigue life. It appears that the delamination was initiated by micro-cracking at the midpoint on the tension side and then propagated outward to both sides of the lower supports as the test progressed, leading to eventual failure.

3.4.4 Tension-Tension Fatigue

A summary of the tension-tension fatigue test results varying applied stress is available in Table 3-11; for the results varying environmental conditions see Table 3-12. Deflection data was collected via internal LVDT; therefore, error introduced by elongation or slipping in the grips is included. The deflection data reported was obtained by subtracting the initial LVDT reading where each test began. Hence the max deflection and min deflection data should be considered as for reference only, but the deflection range (the difference between the max deflection and min deflection) is more accurate, reflecting the net deflection induced by the load range (difference between max load and min load).

Table 3-11 - Tension-Tension Fatigue (Stress) Test Results

Sample ID	2.2	2.4	3.1	3.3	3.4	3.6
Temperature (°F)	RT (72)	RT (72)	RT (72)	RT (72)	RT (72)	RT (72)
Salt Water	No	No	No	No	No	No
Rate	0.5 Hz	0.5 Hz	2.0 Hz	1.0 Hz	0.5 Hz	2.0 Hz
Load Level	63%	50%	35%	55%	70%	47%
R-Ratio	0.2	0.2	0.1	0.1	0.1	0.1
Average Max Load (lbs)	7624.0	6046.0	4249.2	6649.3	8474.1	5708.7
Average Min Load (lbs)	1536.2	1196.4	402.0	648.8	842.8	550.8
Load Range (lbs)	6087.8	4849.6	3847.2	6000.5	7631.3	5157.9
Deflection Change (in)	0.0422	0.0693	0.0683	0.0460	0.0695	0.0676
Full Number of Cycles	2,979	70,774	5,636,130	49,510	1,159	145,611
Cycles to First Failure	2,925	70,772	5,627,500	32,860	1,159	145,611

Table 3-12 - Tension-Tension Fatigue (Environment) Test Summary

Sample ID	2.2	2.3	2.4	2.6	2.8	2.16
Temperature (°F)	RT (72)	RT (72)	RT (72)	RT (72)	**MT1 (100)**	RT (72)
Salt Water	**No**	Yes	**No**	Yes	Yes	Yes
Rate	0.5 Hz	0.5 Hz	0.5 Hz	0.5 Hz	0.5 Hz	0.5 Hz
Load Level	63%	63%	**50%**	**50%**	63%	**50%**
R-Ratio	0.2	0.2	0.2	0.2	0.2	0.2
Average Max Load (lbs)	7624.0	7618.0	6046.0	6049.0	7581.3	6050.6
Average Min Load (lbs)	1536.2	1528.2	1196.4	1194.0	1479.5	1202.0
Load Range (lbs)	6087.8	6089.8	4849.6	4855.0	6101.8	4848.6
Deflection Change (in)	0.0422	0.0357	0.0693	0.0543	0.0784	0.0847
Full Number of Cycles	2,979	3,580	70,774	21,485	1,365	30,454
Cycles to First Failure	**2,925**	**3,505**	**70,772**	**21,483**	**1,363**	**30,454**

The “first failure” referred to in Table 3-11 and Table 3-12 is defined as the beginning of the increased slope on the deflection diagram that led to an inability to sustain the full load. In some cases, the sample experienced a clear first failure but had not yet tripped the deflection limit set on the Instron testing machine, thereby continuing to run for the “full number of cycles.”

For each fatigue test, data plots were generated over the number of cycles for the following quantities: max/min load, max/min deflection, load range, and deflection range. The results varying stress level were compiled into the following composite plots (available in Appendix A): loading (Figure A-5), deflection maximum (Figure A-6), deflection minimum (Figure A-7), and deflection range (Figure A-8). The results varying environmental conditions were compiled into the following composite plots (available in Appendix A): loading (Figure A-9), deflection maximum (Figure A-10), deflection minimum (Figure A-11), and deflection range (Figure A-12). Because the material was tested in a salt water environment, underwent

high amounts of strain, and frequently experienced surface failures before the true material failure, strain was not able to be collected through strain gauges. The strain could be calculated from the deflection data, but would contain the same errors and would not provide any additional useful information.

The tests under the room temperature and dry environmental conditions, varying only the stress, were run in order to characterize the material for application of the strain energy fatigue life prediction model, which is discussed in the following chapter. The results of those tests are plotted on a semi-log S-N curve in Figure 3-33, where the stress is plotted as relative to the ultimate strength of the material.

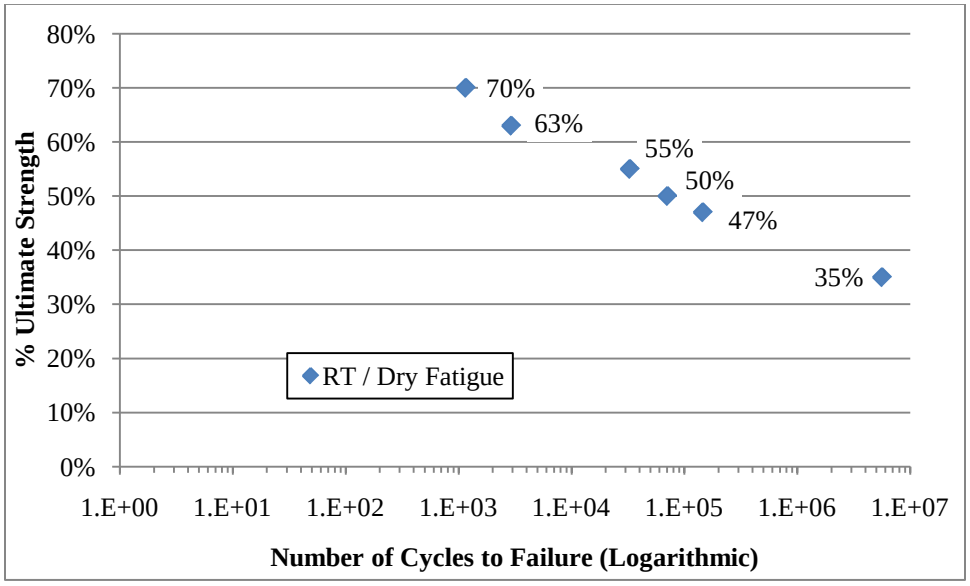

Figure 3-33 - Tension-Tension Fatigue (Stress) Cycles to Failure Plot

While samples 2.2 and 2.4 were tested at an R-ratio ($\sigma_{min}/\sigma_{max}$) of 0.2 and the rest of the stress-varying samples were tested at an R-ratio of 0.1, this minor variation does not seem to have had a major effect on the results. The ratio was changed for the last several tests so that the

data would be more comparable to the database analysis conducted in the next chapter, in which every test was run at an R-ratio of 0.1. The differences in the testing rate (0.5 Hz to 1-2 Hz), which were made to make the high-cycle tests more feasible, also do not seem to have had much effect on the results. Even though Curtis (1989) recommends running all fatigue tests on GFRP's at roughly the same rate in order to limit the introduction of strength variation, 2 Hz is still well below his recommended maximum testing rate of 5-10 Hz.

The results from the tests run on samples 3.2 and 3.5 were not reported because the adhesive between the samples and the steel tabs failed prior to sample failure in both cases. This was likely due to the age of the adhesive and an improper ratio of the two components as it reached the end of the tube. Samples 3.3 and 3.6 were run as replacement tests. The bond between the composite and the steel tabs was usually excellent and, other than the previously mentioned samples 3.2 and 3.5, no other samples seemed to have slipped in the grips.

Prior to the tension-tension fatigue tests in which the environmental conditions were varied, one trial fatigue run of the salt water containment procedure was conducted on an 8-inch long sample (sample 1.13) in order to verify the design. The results were not reported, since the gauge length was considerably shorter than the other tension-tension tests.

From examining data trends (particularly when the immersion test results, in the next section, were also considered), it was suspected that sample 2.6 had prematurely failed. Premature failure would likely be attributed to grinding the sample too aggressively prior to applying the adhesive and tabs, which would compromise the integrity of the outer 0° layers before the fatigue test was begun. To confirm that sample 2.6 had failed early, sample 2.16 was run under the exact same test conditions. The new sample lasted more than 1.4 times as long as

sample 2.6, which appeared to better fit the data trends. Therefore, the results of sample 2.6 were ignored for the rest of this analysis.

Figure 3-34 depicts several of the failed tension-tension fatigue samples, both those tested dry and in salt water. The failure mode for all of the tension-tension fatigue tests seemed to be a combination of lamina separation and fiber breaking. In every instance, the weakest lamina interface seemed to be between the outer 90° laminae and the thick 0° laminae of the inner layer (see Figure 3-23 for a simple diagram of fiber architecture).

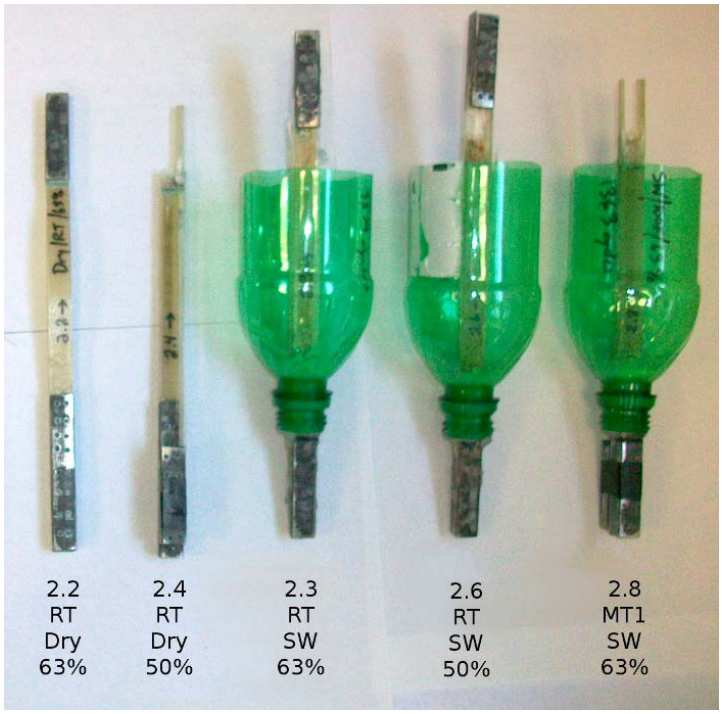

Figure 3-34 - Several Failed Tension-Tension Fatigue Samples

In Sample 2.2 the outer layers broke near the upper grips, and began slipping when the test was stopped; the layer separation runs the entire span of the gage length, and can be seen in Figure 3-35. The rest of the samples failed in a similar fashion, with the outer layers (both 0° and 90° fibers) broken near the upper grip. The inside layer of unidirectional fiber separated parallel to the fibers near both outer edges in the upper grip, usually with one or both edges slipping from between the outer layers (Figure 11 shows the separation along the inside layer). The central

fibers of the inside layer broke at or around where the outer layers had broken, leaving both outer layers and the central fibers of the inner layer still adhered to the upper steel tabs. While the failure frequently seemed to be focused in the upper grips (which is generally not a desirable location for failure), in every sample there was evidence that the lamina separation ran the entire span of the gage length, implying failure was not localized but throughout the sample.

Figure 3-35 - Layer Separation in Sample 2.2

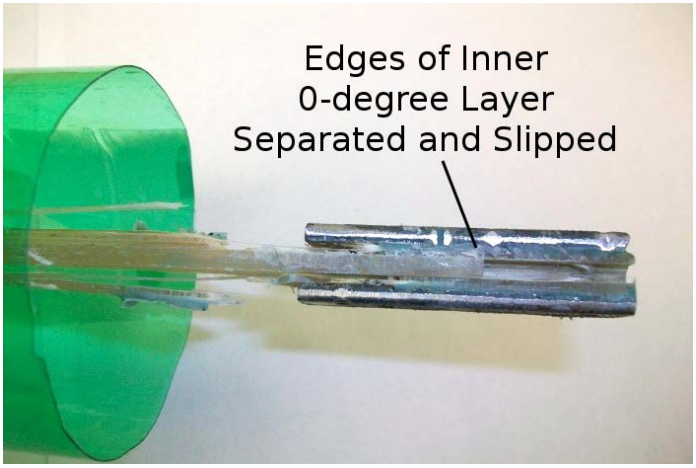

Figure 3-36 - Inner Layer Separation and Slipping in Sample 2.6

There was no salt water effect observed on the fatigue life of the material as compared to that of a dry sample under a loading level of 63% of ultimate failure load at room temperature because of its short duration (~100 minutes). The slight increase in fatigue life (from 2,925 cycles to 3,505 cycles) is a result of the scattering effect, or variation, from one sample to another. At a stress level of 50% of the ultimate load, the presence of salt water reduced the

fatigue life of the material to 43% of the value of a dry test at room temperature, from 70,772 cycles to 30,454 cycles (see Figure 3-37).

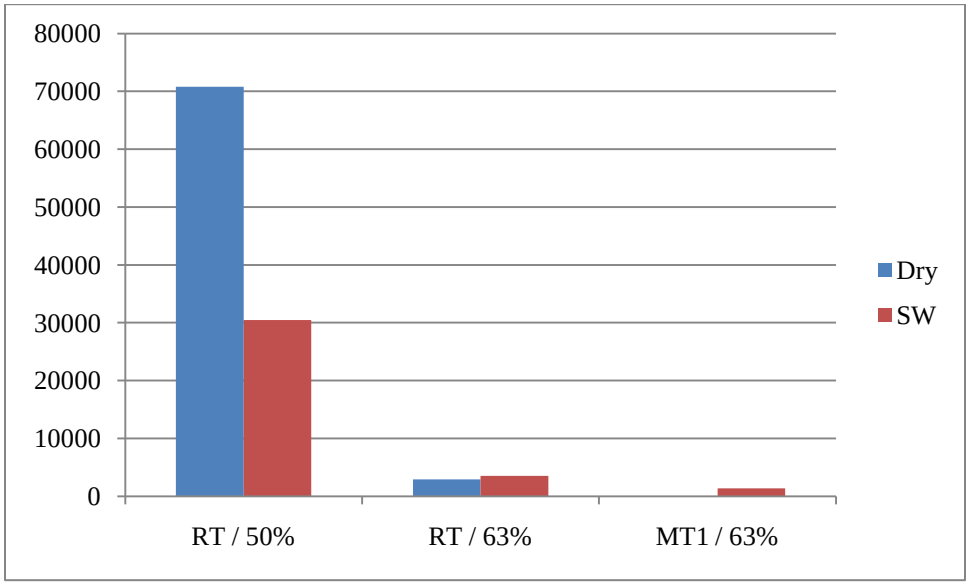

Figure 3-37 - Tension-Tension Fatigue Life Environment Comparison

A slightly elevated temperature (100F) reduced the fatigue life of the material to approximately 39% of the value at room temperature, in salt water at a stress level of 63%, from 3,505 cycles to 1,363 cycles, likely because of the viscoelastic effect of the polymer resin.

Under the same environmental conditions (room temperature, salt water), increasing the loading level from 50% to 63% resulted in a decrease in fatigue life to 12% of the original, i.e. from 30,454 cycles at 50% to 3,505 cycles at 63%. A dry test run at room temperature resulted in a decrease of fatigue life to 4% of the original, from 70,772 cycles at 50% to 2,925 cycles at 63% (see Figure 3-38).

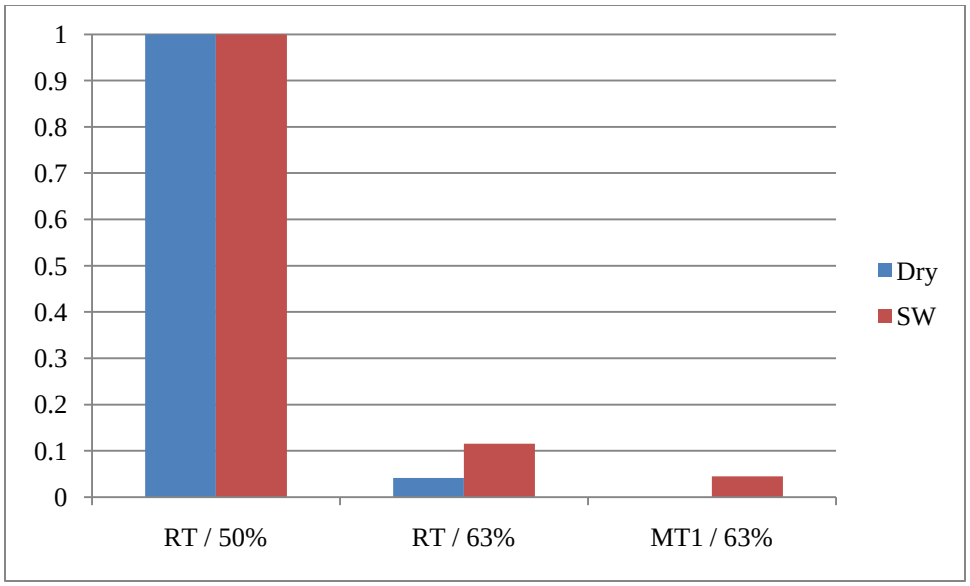

Figure 3-38 - Tension-Tension Relative % Fatigue Life Environment Comparison

As expected, the presence of salt water (over time) or elevated temperature significantly adversely affected the fatigue life of the material in tension, while reducing the loading level greatly increased its fatigue life. As compared to bending fatigue data under the same stress levels ($\sigma_{max}/\sigma_{ult}$), the tension fatigue tests lasted for fewer cycles to failure and, generally, were more susceptible to environmental effects (see Table 3-13).

Table 3-13 - Comparison of Tension-Tension Fatigue Data with Bending Fatigue Data

Presence of Salt water (at Room Temperature)					
	Baseline		**Variation**		**% Change**
	Condition	***Cycles***	***Condition***	***Cycles***	***(Variation/Baseline)***
63% Ult. Load					
Tension	Dry	2,925	Salt water	3,505	**120%**
3-pt. Bending	Dry	34,445	Salt water	28,845	**84%**
50% Ult. Load					
Tension	Dry	70,772	Salt water	30,454	**43%**
3-pt. Bending	Dry	284,360	Salt water	153,749	**54%**
Temperature Increase (in Salt water)					
	Baseline		**Variation**		**% Change**
	Condition	***Cycles***	***Condition***	***Cycles***	***(Variation/Baseline)***
63% Ult. Load					
Tension	RT (72°F)	3,505	MT1 (100°F)	1,363	**39%**
3-pt. Bending	RT	28,845	MT1	17,802	**62%**
3-pt. Bending	RT	28,845	MT2 (125°F)	13,031	**45%**
3-pt. Bending	RT	28,845	HT (150°F)	4,824	**17%**
Load Increase (at Room Temperature)					
	Baseline		**Variation**		**% Change**
	Condition	***Cycles***	***Condition***	***Cycles***	***(Variation/Baseline)***
Dry					
Tension	50% Ult. Load	70,772	63% Ult. Load	2,925	**4%**
3-pt. Bending	50%	284,360	63%	34,445	**12%**
Salt water					
Tension	50%	30,454	63%	3,505	**12%**
3-pt. Bending	50%	153,749	63%	28,845	**19%**

3.4.5 Accelerated Immersion Conditioning

A summary of the immersion conditioning results is shown in Table 3-14. One sample (sample 2.5) was conditioned at room temperature and atmospheric pressure. The first round of accelerated immersion (samples 2.9, 2.10, 2.11) was conditioned at room temperature and approximately 2500psi. The second round of accelerated immersion (samples 2.12, 2.13, 2.15) was conditioned at 100F and approximately 1700psi.

Table 3-14 - Absorption Results

Sample	Pressure (psi)	Temperature	Pre Wt. (g)	Hours Immersed	Post Wt. (g)	% Wt. Gain
2.5	atmospheric	RT	38.7665	7657	38.8235	0.147
2.9	2500	RT	39.3727	622	39.4099	0.094
2.10	2500	RT	39.5372	769	39.5739	0.093
2.11	2500	RT	39.5438	769	39.5836	0.101
2.12	1700	RT / 100°F	39.2298	1824	39.2941	0.164
2.13	1700	100°F	38.8671	863	38.9035	0.094
2.15	1700	100°F	38.7686	863	38.8067	0.098

After the first round of samples had been in the pressurized immersion chamber for several hundred hours (at room temperature and 2200 psi), it appeared that the samples had reached their saturation points (as shown in Figure 3-39). From the data, it appeared that saturation occurred around 0.1% weight gain. Since sample 2.12 was not needed in the first trio of fatigue tests, it was replaced in the pressurized immersion chamber for a second round of testing (at 100°F and 1700 psi). Unexpectedly, sample 2.12 then began to gain weight again, topping off at around 0.16% weight gain.

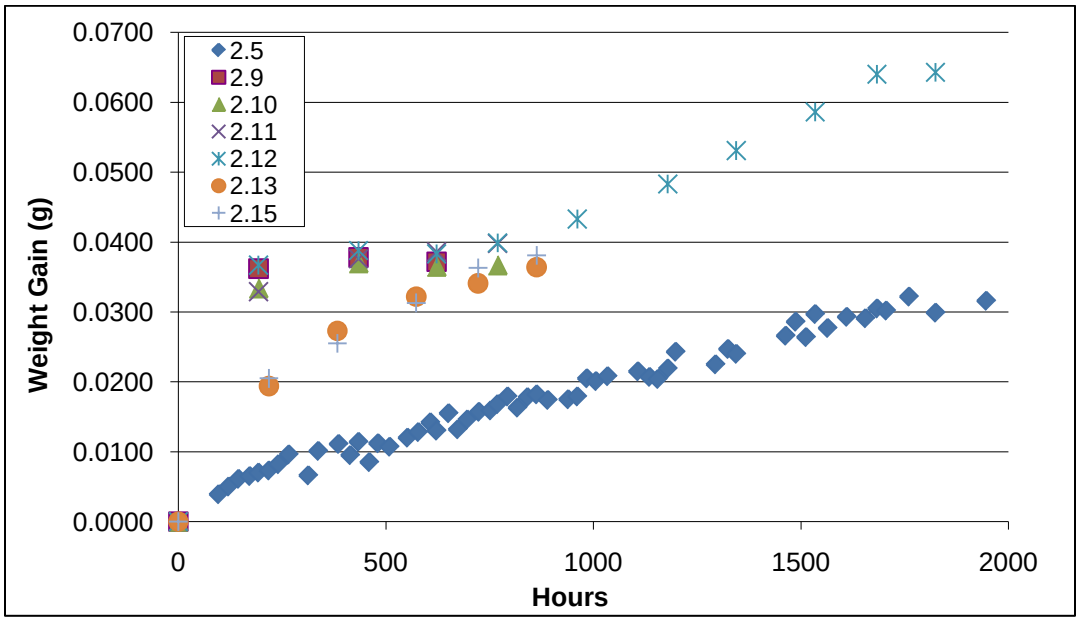

Figure 3-39 - Absorption Plot of First 2000 Hours

Liao et al. (Liao et al. 1999) also experienced some unexpected absorption behavior when they conducted their absorption tests at elevated temperatures. The researchers concluded that increased temperature resulted in faster weight gain, but was often followed by weight loss, with the elevated temperature samples eventually reaching a lower saturation than the absorption tests conducted at room temperature. The increased temperature could be responsible for the gaining of additional weight for sample 2.12, and it is possible that it would have lost weight again had the test continued beyond 2000 hours. However, the other data indicates that the second round of absorption samples actually gained weight at a *slower* rate than the samples absorbing at ambient temperatures. The only reasonable explanation for this phenomenon is that the higher average pressure on the first round of tests was of greater influence on the absorption rate than the elevated temperature on the second round of tests.

The absorption test conducted at room temperature (sample 2.5) lends credence to the higher saturation level of sample 2.12. The sample continued to gain weight for at least 8000 hours (see Figure 3-40), and seemed likely to reach a saturation point between 0.15-0.2%. With this being the case, it seems like the unexplained behavior is actually the low saturation point apparent in the first round of data. This possibly may have been due to the presence of lubricating oil in the newly manufactured pressurized immersion chamber that may have coated the samples over time and prematurely slowed absorption. For the remainder of this report and analysis, all samples will be treated as though they reached their saturation point prior to fatigue testing.

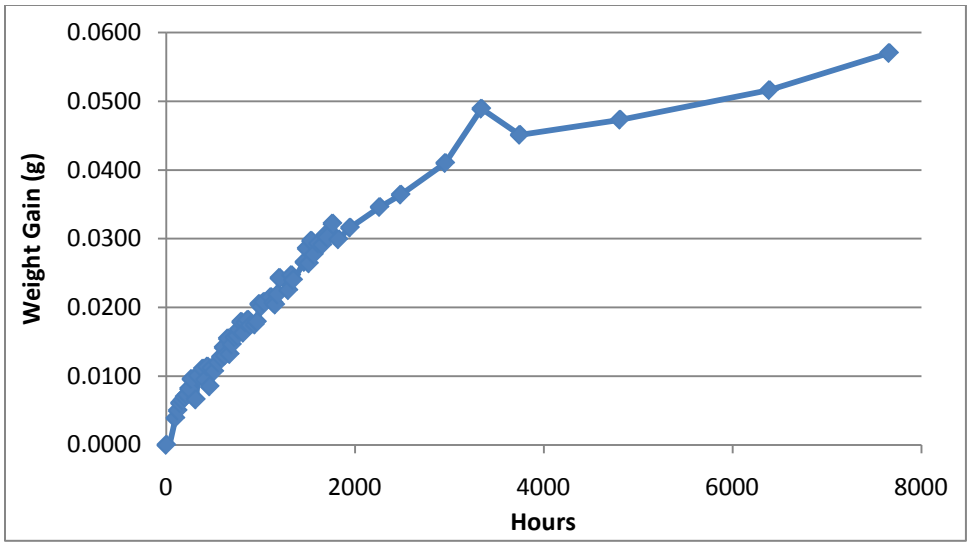

Figure 3-40 - Sample 2.5 (RT / Atmospheric) Absorption Plot

A summary of the fatigue test results is shown in Table 3-15. For each fatigue test, data plots were generated over the number of cycles for the following quantities: max/min load, max/min deflection, load range, and deflection range. The results for the tests with varying immersion conditions were compiled into the following composite plots (available in Appendix A): loading (Figure A-13), deflection maximum (Figure A-14), deflection minimum (Figure A-15), and deflection range (Figure A-16).

Table 3-15 - Tension-Tension Fatigue (Immersion) Test Results

Sample ID	**2.9**	**2.10**	**2.11**	**2.12**	**2.15**	**2.13**
Immersion Temperature (°F)	RT (72)	RT (72)	RT (72)	**MT1 (100)**	**MT1 (100)**	**MT1 (100)**
Fatigue Temperature (°F)	RT (72)	RT (72)	RT (72)	RT (72)	RT (72)	RT (72)
Salt water	**No**	Yes	Yes	**No**	Yes	Yes
Rate	0.5 Hz	0.5 Hz	0.5 Hz	0.5 Hz	0.5 Hz	0.5 Hz
Load Level	0.5	**0.63**	0.5	0.5	**0.63**	0.5
R-Ratio	0.2	0.2	0.2	0.2	0.2	0.2
Average Max Load (lbs)	6042.0	7596.6	6048.8	6051.8	7598.5	6048.7
Average Min Load (lbs)	1190.4	1490.8	1196.0	1204.5	1510.8	1200.7
Load Range (lbs)	4851.6	6105.8	4852.8	4847.3	6087.7	4848.0
Deflection Change (in)	0.0583	0.0553	0.1392	0.1282	0.0271	0.0623
Full Number of Cycles	47,454	1,663	24,880	13,686	674	8,701
Cycles to First Failure	**47,453**	**1,661**	**24,879**	**13,685**	**582**	**8,699**

As in the previous tension-tension tests, the failure mode for all of the tensile fatigue tests seemed to be a combination of lamina separation and fiber breaking. In every instance, the weakest lamina interfaces seemed to be between the thin outer layers and the thick 0° inner layer.

The inside layer of unidirectional fiber separated parallel to the fibers near both outer edges in the same grip, usually with one or both edges slipping from between the outer layers. The central fibers of the inside layer broke at or around where the outer layers had broken, leaving both outer layers and the central fibers of the inner layer still adhered to the upper steel tabs. While most often the failure seemed to be focused in the upper grips, in every sample there was evidence that the lamina separation ran the entire span of the gage length, implying failure was not localized but throughout the sample.

As seen in the previous bending and tension-tension tests, fatigue in a salt water environment at a load level of 50% ultimate results in a decrease in fatigue life to 40-55% of the fatigue life of a dry sample (see Figure 3-41). Fatiguing at room temperature / dry / 50% ultimate load level, the room temperature water immersion sample resulted in a decrease to 67% of the number of cycles for no immersion, while the 100°F immersion resulted in a decrease to 19% (see Figure 3-42). At room temperature / sea water / 63% ultimate load level, introducing room temperature immersion resulted in a decrease to 47% of the number of cycles for no immersion, while introducing 100°F immersion resulted in a decrease to 17%. At room temperature / sea water / 50% ultimate load level, the room temperature immersion resulted in an increase to 116% of the number of cycles for no immersion, while the 100°F immersion resulted in a decrease to 40%.

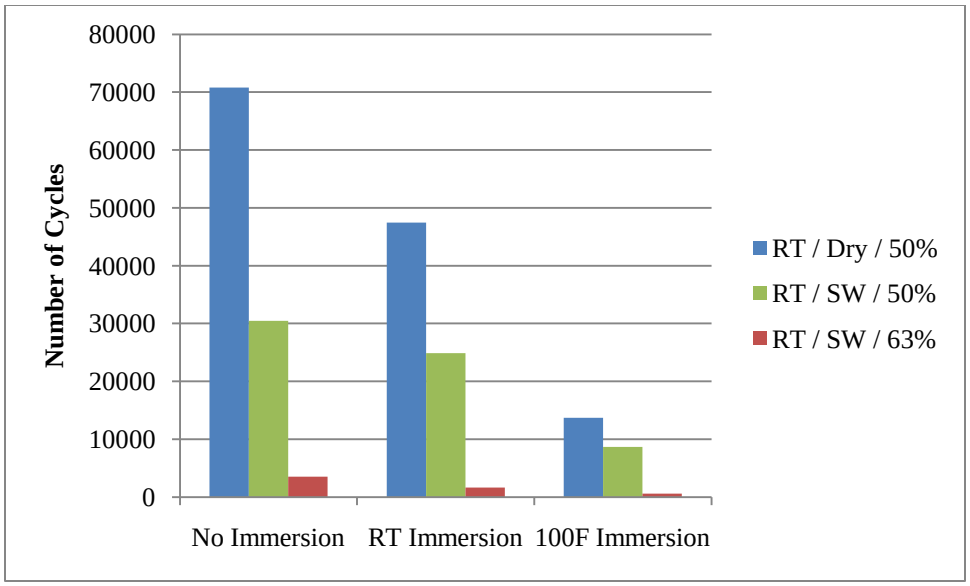

Figure 3-41 – Tension-Tension Fatigue Life Immersion Comparison

The slight increase in immersion temperature from room temperature (72°F) to 100°F resulted in a decrease in the number of cycles to failure in all three tests to approximately 33% of the number of cycles to failure for the room temperature immersion tests. Immersion testing at one or two more temperature levels would help to characterize this effect.

It appears that room temperature immersion conditioning could reduce the fatigue life of the material to 50-65%, while 100°F immersion conditioning could reduce the fatigue life of the material to 15-25% (see Figure 3-42). This significant effect should be further examined through additional and repeated testing.

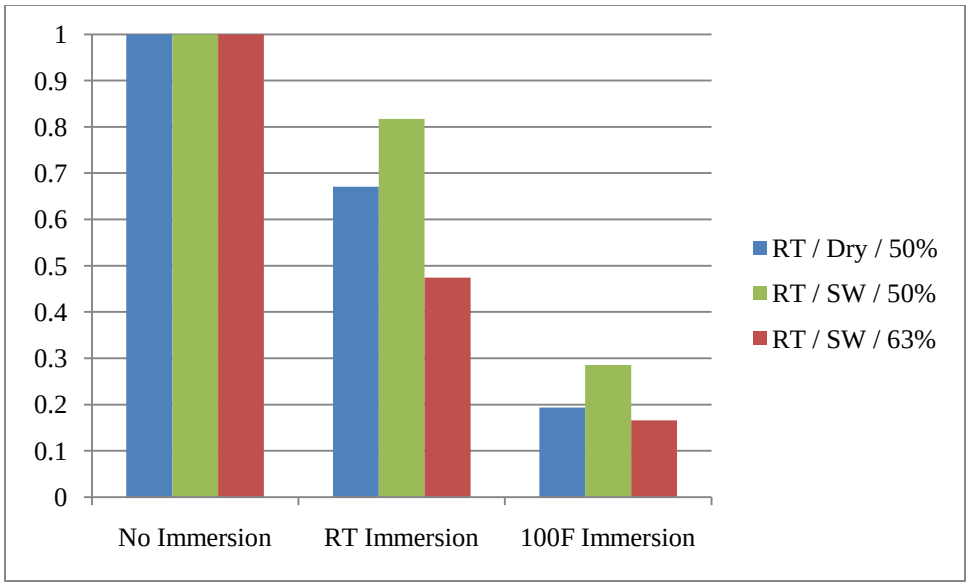

Figure 3-42 - Tension-Tension Relative % Fatigue Life Immersion Comparison

As a different way to look at the same results, the fatigue strength knockdown for a particular number of cycles due to each of the immersion conditions can be interpolated. To do this, individual plots of the number of cycles to failure for each immersion condition at each of the stress levels were generated. Assuming a simple, linear relationship on a semi-log S-N plot, the fatigue strength knockdown at approximately 3500 cycles can be found (see Figure 3-43). For this fatigue life, strength knockdowns of 6% for room temperature immersion conditioning and 14% for 100°F immersion conditioning were calculated. From this perspective, a sample designed for a particular fatigue life would not necessarily experience a significant loss in strength due to a salt water environment. It is possible that at a high enough fatigue life (and therefore, a low enough stress level) these curves may converge; this would mean that there would be an insignificant loss of fatigue strength given any reasonable immersion conditions. Further testing would provide more evidence of this effect.

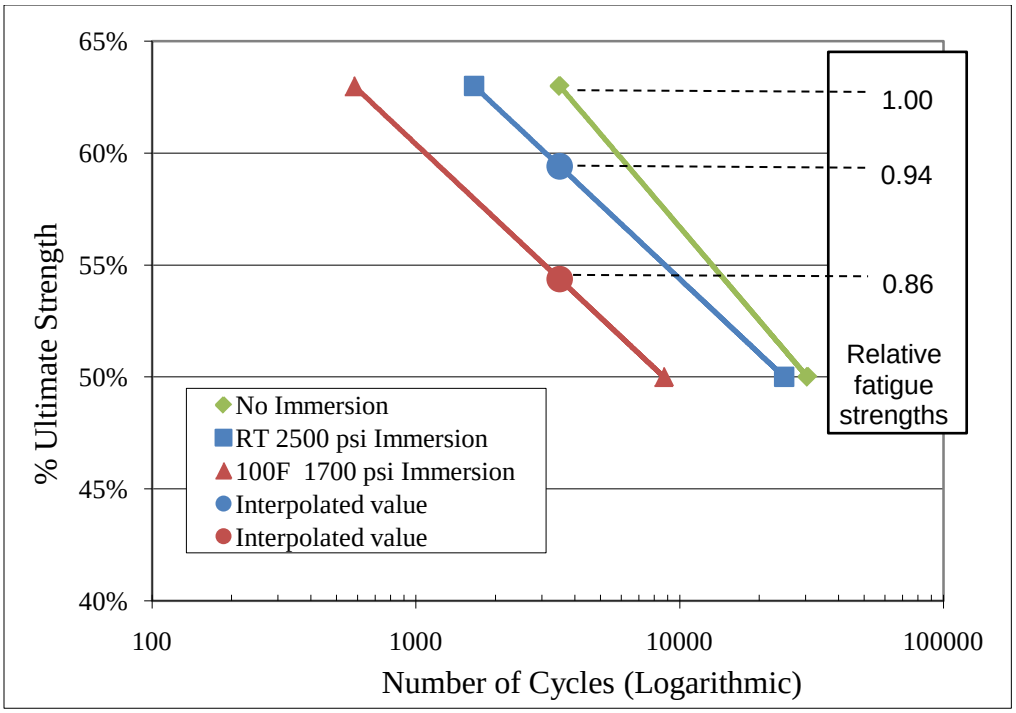

Figure 3-43 - Interpolated Immersion Knockdown Fatigue Strength

3.5 Conclusions

Through the fiber content test and the static tests, some of the characteristics and mechanical properties of the material were determined. The average fiber weight fraction was found to be 76.1% and the average fiber volume fraction was found to be 56.8%. Through the resin ignition test, it was also found that the material consisted mainly of 0° fibers in the center and along the top and bottom, with thin layers of 90° fibers in between. After conducting the static bending tests, the average adjusted flexural modulus was calculated as 6.47×10^6 psi, and the average flexural strength as 150.4 ksi. After conducting the static tension tests, the average modulus of elasticity was calculated as 5.51×10^6 psi, and the average tensile strength as 100.70 ksi.

In bending fatigue, the most common failure mode was delamination of the outer layers on the tension side of the sample, believed to be initiated by micro-cracking at the midpoint (the highest bending moment). The presence of salt water reduced the fatigue life of the material to 84% of the value of a dry test at room temperature and a stress level of 63% of ultimate load, and to 54% of the value of a dry test at room temperature and a stress level of 50%. The effect of temperature on the life of the material was found to be approximately linear (with a higher temperature leading to a reduction in fatigue life), at least on those samples which were also tested in a salt water environment. The tests confirmed that the fatigue life of the material is decreased by the presence of salt water, elevated temperature, or increased loading level.

The tension tests conducted under the room temperature and dry environmental conditions, varying only the stress, were run in order to characterize the material for application of the strain energy fatigue life prediction model. These results seemed to be well-ordered and were nearly linear when plotted on a semi-log S-N plot. The failure mode for all of the tension-tension fatigue tests seemed to be a combination of lamina separation and fiber breaking. In every instance, the weakest lamina interface seemed to be between the outer 90° laminae and the thick 0° laminae of the inner layer. While the failure frequently seemed to be focused in the upper grips (which is generally not a desirable location for failure), in every sample there was evidence that the lamina separation ran the entire span of the gage length, implying failure was not localized but throughout the sample. The presence of salt water in the 50% stress level sample reduced the fatigue life of the material to 43% of the value of a dry test, while at 63% no salt water effect was observed – this makes it clear that salt water has a larger effect over time, as the 63% load level tension test only lasted for a few hours. As compared to bending fatigue data

under the same stress levels ($\sigma_{max}/\sigma_{ult}$), the tension fatigue tests exhibited much fewer cycles to failure and, generally, were more susceptible to environmental effects.

Through the absorption tests, the salt water saturation point of the material was determined to be between 0.10% and 0.17% of the weight. The false, low saturation point observed in the first round of testing was most likely due to the presence of lubricating oil in the newly manufactured pressurized immersion chamber that may have coated the samples over time and prematurely slowed absorption. The slight increase in immersion temperature from room temperature (72°F) to 100°F resulted in a decrease in the number of cycles to failure in all three tests to 33% of the number of cycles to failure for the room temperature immersion tests. It appears that room temperature immersion conditioning could reduce the fatigue life of the material to 50-65% of the fatigue life of the pre-immersion material, while 100°F immersion conditioning could reduce the fatigue life of the material to 15-25%. The fatigue strength knockdown at approximately 3500 cycles was calculated to be 6% for room temperature immersion conditioning and 14% for 100°F immersion conditioning.

CHAPTER 4 FATIGUE LIFE PREDICTION MODEL EVALUATION

4.1 Introduction and Scope

When developing a fatigue life prediction model, it is important to evaluate how the model is able to handle a variety of materials and test conditions. Due to the time commitment and complexity involved with conducting extensive fatigue testing on a material, this has previously been difficult to do, with many researchers reanalyzing the same few fatigue data points. Thanks to the DOE/MSU Composite Material Fatigue Database, a large amount of composite fatigue test data is now freely available to researchers worldwide.

Researchers at Montana State University have compiled a large composite material fatigue test database after doing considerable fatigue testing on wind turbine blade materials for the US Department of Energy (Samborsky and Mandell 2005; Mandell and Samborsky 1997). Over 190 materials have been tested (as of Version 18.1), and over 12,000 individual tests have been conducted. Their research was focused on materials with lay-up combinations of 0°, ±45°, and 0°/±45° fabrics, manufactured by either hand lay-up or resin transfer molding (RTM). Using the simplified strain energy fatigue model presented by Natarajan (2005), all of the necessary data is available within the fatigue database to conduct a more extensive evaluation of its ability to fit and predict fatigue life.

In this chapter, the methodology used to select and analyze the materials in the DOE/MSU Fatigue Database is presented. The fatigue life prediction model was applied to a large number of samples from the fatigue database, as well as to the material tested in the previous chapter and to

a pair of composite structures tested at the WVU-CFC by Nagaraj (1994). Conclusions are drawn regarding the model's relative ease of use and its accuracy in fitting and predicting fatigue life.

4.2 Analysis Methodology

Fatigue test results were selected from the DOE/MSU Fatigue Database (Samborsky and Mandell 2005) using the following controlling criteria:

(1) Tension-Tension testing

(2) Stress Ratio, R = 0.1

(3) Minimum 3 load levels (between 25% and 75% of max stress)

(4) Minimum 5 tests run to failure with at least 100 cycles each

(5) E-glass fibers

(6) Fatigue rate $\leq$ 20 Hz

(7) Generally ordered results (if $\sigma_1 > \sigma_2$, then $N_1 < N_2$)

After applying these criteria, test results for 109 different composites (1254 individual tests) were analyzed.

Each material listing in the database included its static modulus of elasticity, static ultimate strength, and coupon dimensions, with stress load levels and number of cycles to failure for each coupon. Polyester was by far the most common matrix material, but some results for vinylester, epoxy, and thermoplastic matrices were also included. Most laminates were manufactured by resin transfer molding or lay-up techniques and a variety of fiber architectures were included.

For each composite, the fatigue coefficients (*a* and *b*) were obtained through a power regression on the criteria-selected data after plotting the results of Equations 2-26 and 2-27

(representative plot shown in Figure 4-1). Using the fatigue coefficients, the curve generated by Equation 2-28 was plotted, along with the data, on a log scale (representative plot shown in Figure 4-2).

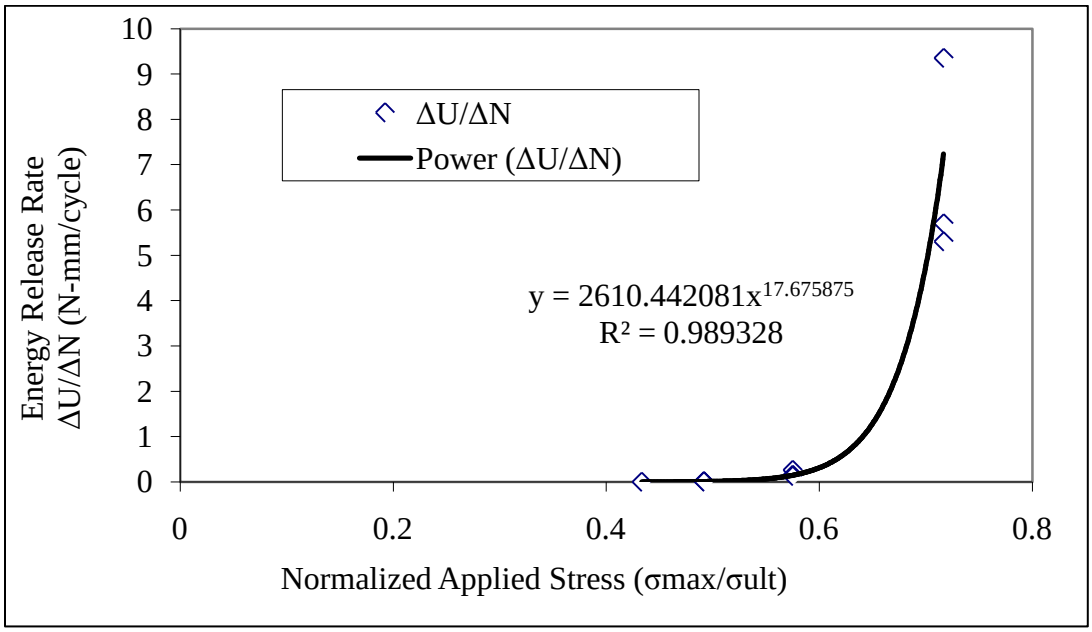

Figure 4-1 - Typical Material Energy Release Rate

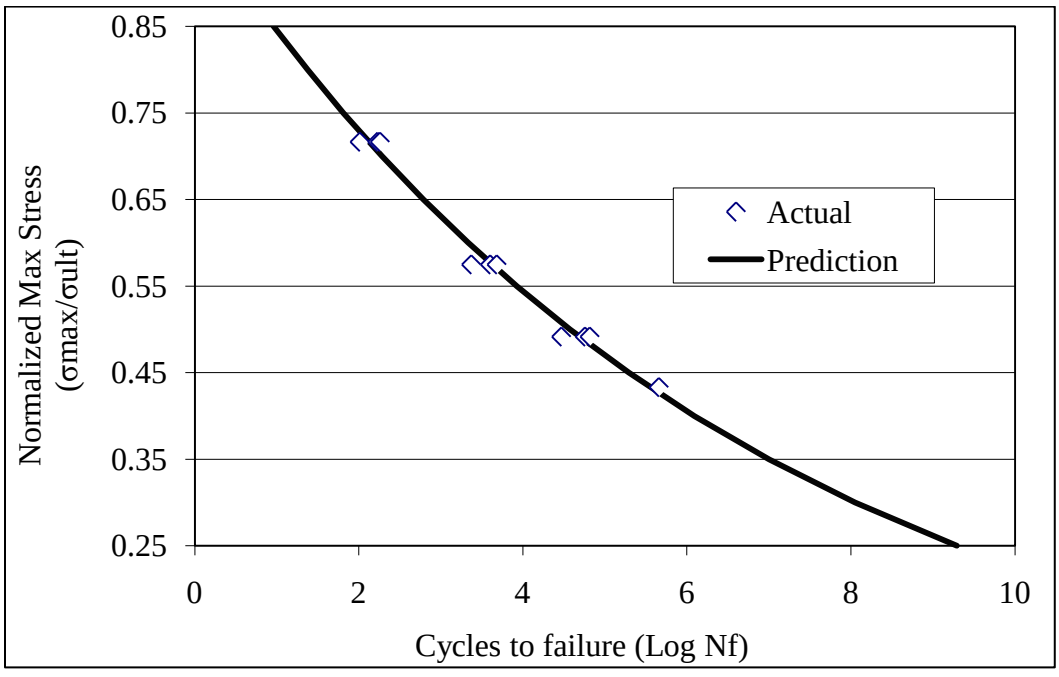

Figure 4-2 - Typical Model Fit

In order to assess the accuracy of the model in fitting data, curves of ±5% log(N_f) and ±10% log(N_f) were generated, with any data lying within these envelopes considered to be reasonably well-modeled (representative plot shown in Figure 4-3). The number of data points within each error envelope was then tallied for each sample.

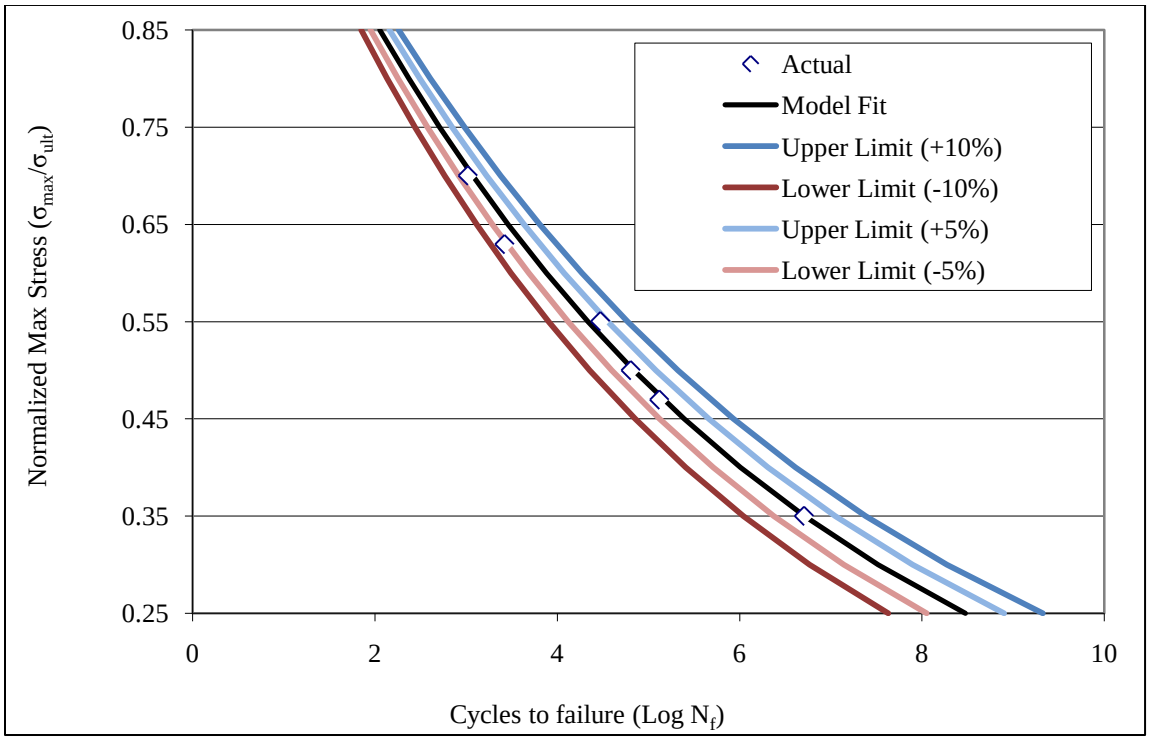

Figure 4-3 - Typical Log Error Analysis

4.3 Results and Discussion

4.3.1 DOE/MSU Fatigue Database

The results of the DOE/MSU fatigue database model analysis are shown in Table 4-1. Since data scatter is as likely as a poor-fitting model to result in data points located outside of these error envelopes, results were also considered for different correlation coefficient (R^2) values obtained from the initial power regression. A higher R^2 value would indicate less scatter;

using $R^2 > 0.98$, it can be seen in Table 4-1 that the model is able to fit over 90% of the fatigue data to within the ±5% error envelope.

Table 4-1 - Log Error Analysis Results

	Total Number	Within 5% Log Error		Within 10% Log Error	
		Number	%	Number	%
Full Data Set	1260	1034	82.1%	1222	97.0%
$R^2 > 0.9$	1201	1003	83.5%	1171	97.5%
$R^2 > 0.95$	1099	935	85.1%	1078	98.1%
$R^2 > 0.98$	623	565	90.7%	621	99.7%

Once it had been shown that the model provided good accuracy at fitting the data, another analysis was run to assess its ability to predict coupon fatigue life. For this analysis, only composites with polyester matrices and a total of 9 data points were considered, resulting in 14 laminates and a total of 126 fatigue tests. The same curve equation and error envelopes were generated for each composite, only this time using different fatigue coefficients. The power regression was performed using anywhere from 2-8 selected data points (using the highest/lowest stress levels for the 2 – usually around 25% and 75% ultimate strength, the highest/lowest and central stress levels for the 3, etc…) and the number of data points within the error envelopes was tallied. A curve was also generated for each composite using only a single data point (central, usually around 50% ultimate strength) and the loose correlation (observed from fatigue data),

$$b = 20(1 - fiber\ volume\ fraction) \tag{4-1}$$

The data was manipulated in several different ways in an attempt to determine an accurate means of estimating one or both of the material coefficients. Grouping and analyzing the data by one or more of the following characteristics at a time produced no noticeable trends:

matrix type, common fiber architecture, manufacturing process, material thickness, material cross-sectional area, modulus of elasticity, testing rate, and ultimate tensile strength. The differences in matrices may have had a slight impact on the *b*-coefficient (with epoxies averaging 11.8, polyesters 11.9, and vinylesters 12.1), but was not large enough to be significant and still did not account for the high degree of variation within each of those groups.

The linear approximation of Equation 4-1 was obtained by running linear regressions on plots of the fiber volume fraction versus the *b*-coefficient for several smaller groupings of polyester-matrix data (e.g. only unidirectional samples, only 0°/45° samples, etc…). No obvious trend was seen by looking at all of the polyester samples as a whole, but with the comparable results of each of the linear regressions of these smaller groups individually, it seemed unlikely that the trend was coincidental. Plotting the *b*-coefficient against the fiber volume fraction still does not account for the high amount of scatter (sometimes being off by as much as 4 or 5; see Figure 4-4), but does allow for a reasonable average to be obtained. An attempt was made to normalize the fiber content with respect to the 0° direction before plotting against the b-coefficient (see Figure 4-5), but based on the R^2 correlation coefficient it did not provide any better approximation. Equation 4-1 provides an approximation of the *b*-coefficient for a majority of samples only if they have polyester matrices; the error is much higher for those samples with epoxy or vinylester matrices.

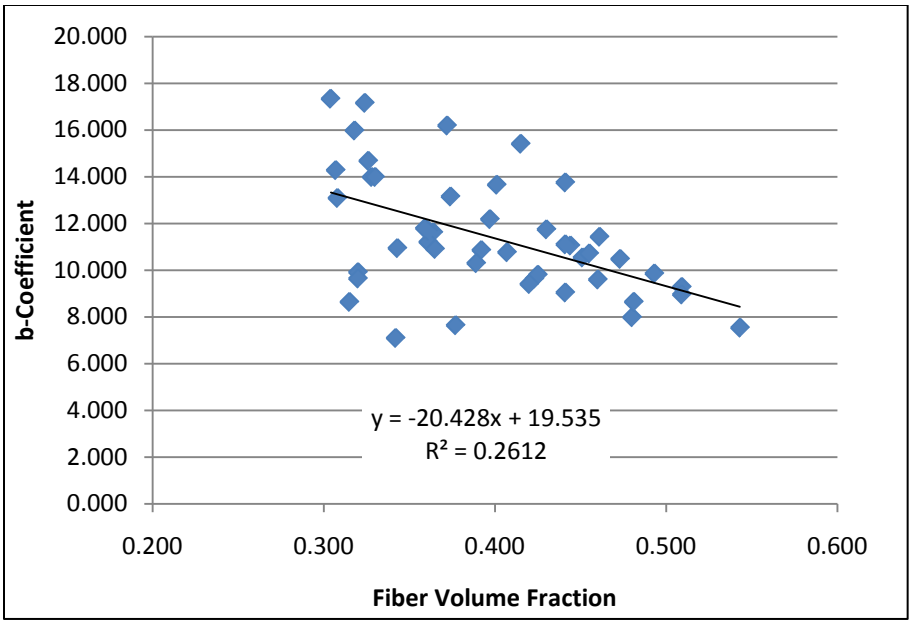

Figure 4-4 - Linear Regression on b-Coefficient vs. Fiber Volume Fraction (0/±45 fibers)

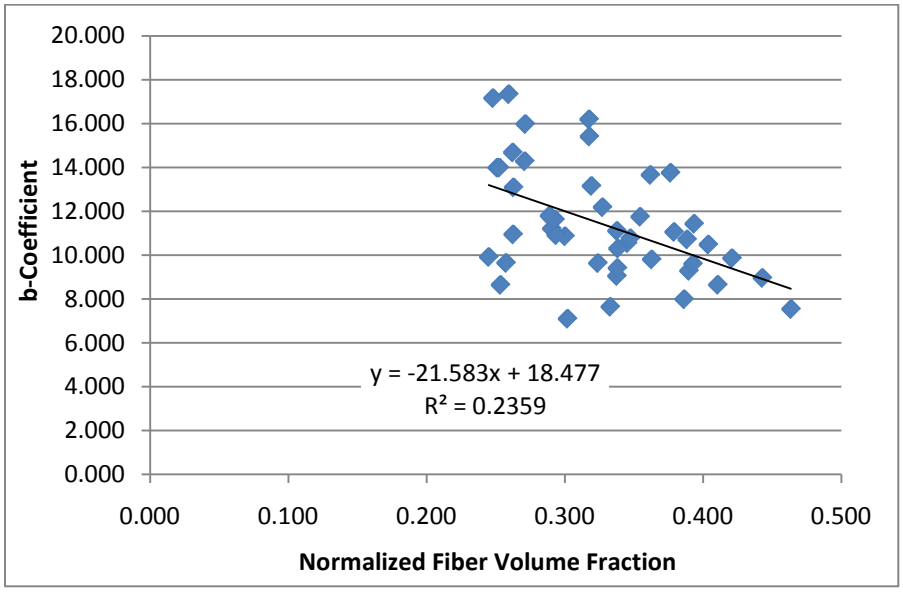

Figure 4-5 - Linear Regression on b-Coefficient vs. Normalized FVF (0/±45 fibers)

The percentages of the 126 data points that fell within the ±5% error envelope (using between 1-9 data points to obtain the fatigue coefficients) are shown in Figure 4-6; those within the ±10% error envelope are shown in Figure 4-7.

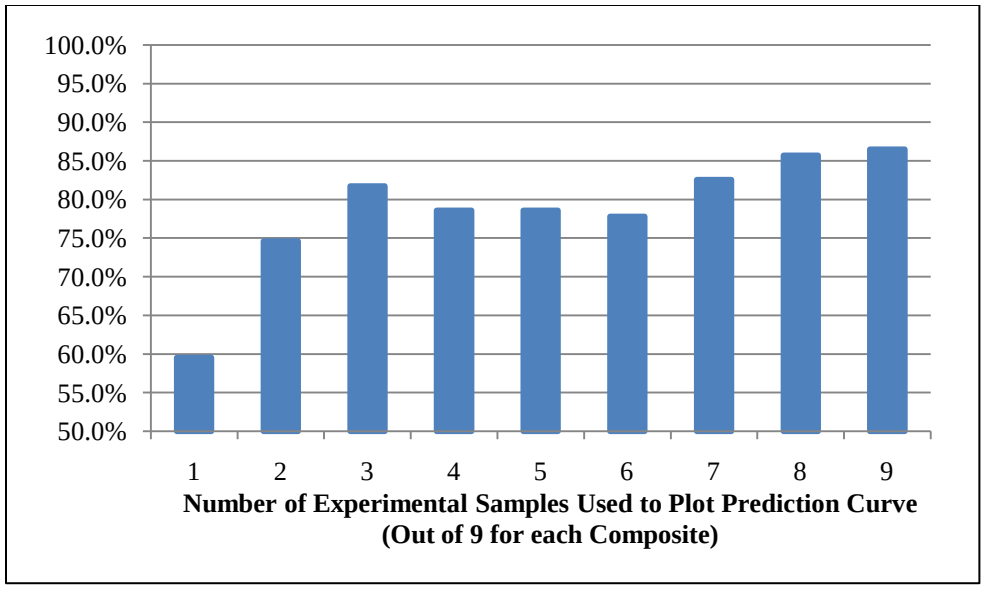

Figure 4-6 - Average % of Samples Within 5% Log Error

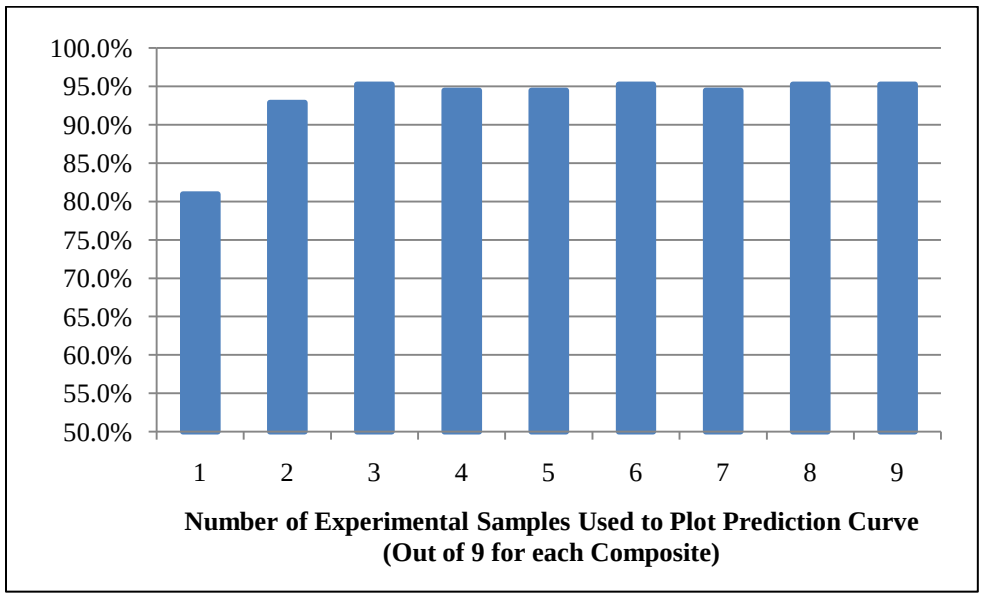

Figure 4-7 - Average % of Samples Within 10% Log Error

4.3.2 X-Strand Composite

The same logarithmic error envelope analysis was carried out on the GFRP sample tested in the previous chapter in the RT / Dry environment. Six tension-tension fatigue tests were run at six different stress levels between 35-70% of the ultimate static strength.

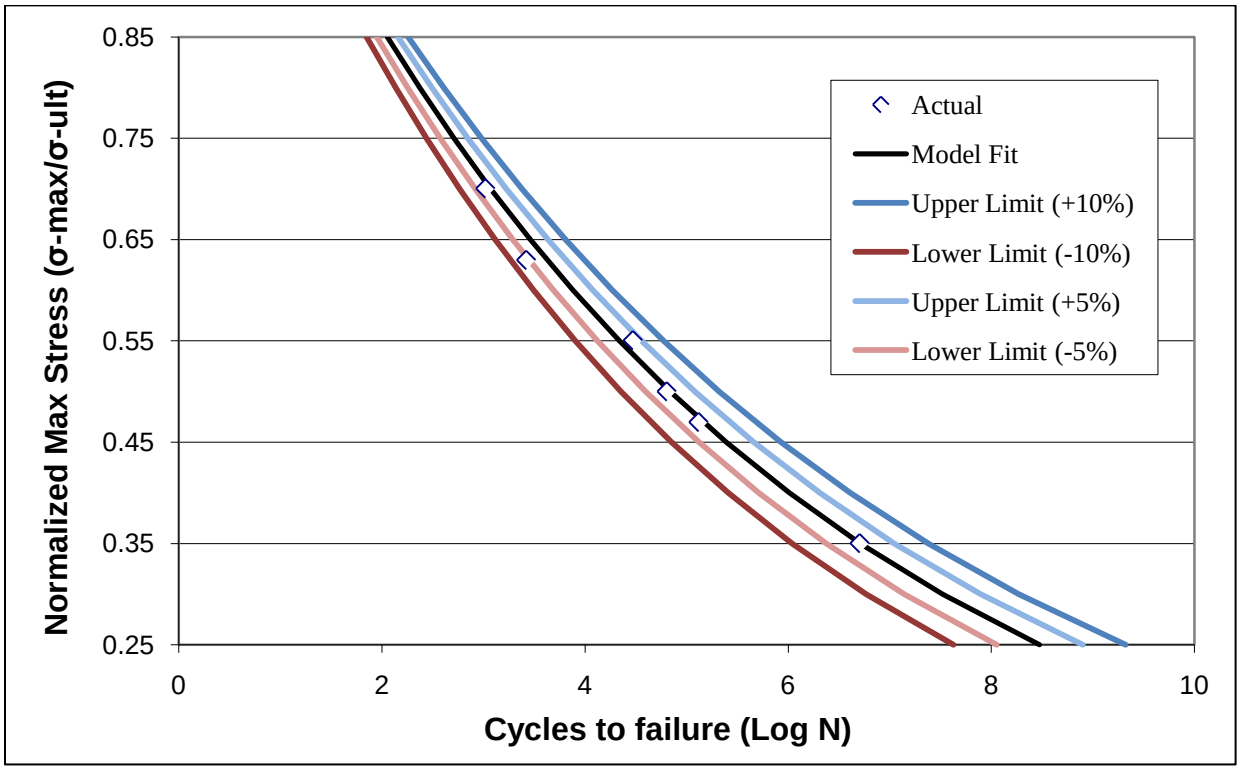

Figure 4-8 - X-Strand fatigue model fit

After performing a similar curve fit analysis as was conducted on the database materials, it was determined that the material had an R^2 value of 0.995 for the power regression and that all of the 6 data points lay within the ±5% error envelope; obviously, all 6 were also within the ±10% envelope (see Figure 4-8). After assessing the curve prediction analysis, it was found that at least 5 of the data points fell within the ±5% error envelope (all 6 within the ±10% envelope) using any number of samples (2-6) to obtain the fatigue coefficients (see Table 4-2). An

appropriate *b*-approximation has not yet been determined for vinylester resin, filament-wound composites, so a single-sample fatigue life prediction could not be obtained.

Table 4-2 - Model Coefficients and Prediction Analysis for X-Strand Composite

Number of Samples Used	*a* - coefficient	*b* - coefficient	R^2 value	within 5%	within 10%
2	5.969	14.245	1.000	6	6
3	5.998	14.246	1.000	6	6
4	4.990	14.122	0.998	5	6
5	5.006	14.085	0.997	5	6
6	6.616	14.390	0.995	6	6

4.3.3 Component Fatigue

Few fatigue tests are run to failure on composite components due to the difficulty and expense of full scale testing. Nagaraj (1994) ran 6 bending fatigue tests each on two E-glass / vinyl ester composite beams (one an I-beam, the other a box beam). Using his data and an adaptation of U_o for strain and bending (see Equation 4-2), a fit and prediction analysis could be run for full scale components. The beams tested each had 4.7 inches x 4.7 inches x ¼ inch cross sections and were fatigue tested over a span of 72 inches.

$$U_o = \frac{\varepsilon_{mean}{}^2 ILE_{static}}{6c^2} \tag{4-2}$$

The R^2 values on the power regression for the box and I-beams were 0.967 and 0.985, respectively. All 12 of the data points lay within the ±5% error envelopes; in fact, they were also all within curves of ±2.5% log(N_f) (see Figure 4-9 and Figure 4-10). The prediction analysis revealed that using anywhere from 3-6 data points to obtain the fatigue coefficients resulted in all 6 data points being within the ±2.5% error envelope for both beams. If only two data points were used to obtain the fatigue coefficients, 5 of the 6 data points were within the ±2.5% error envelope and all 6 were within the ±5% error envelope. An appropriate *b*-approximation has not

yet been determined for component fatigue, so a single-sample fatigue life prediction could not be obtained.

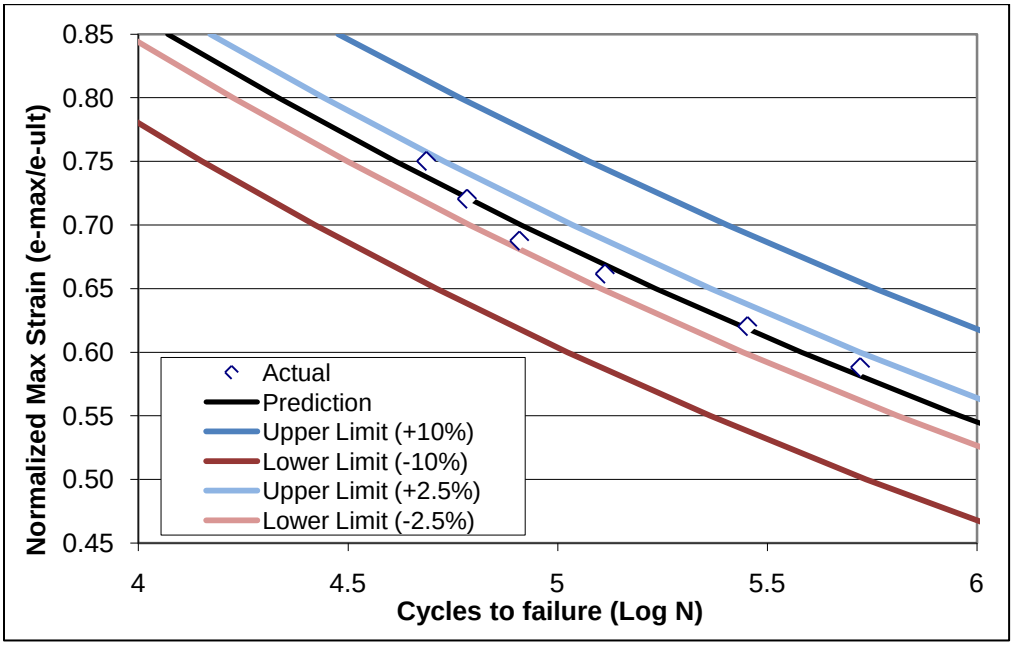

Figure 4-9 - I-Beam Fatigue Model Fit

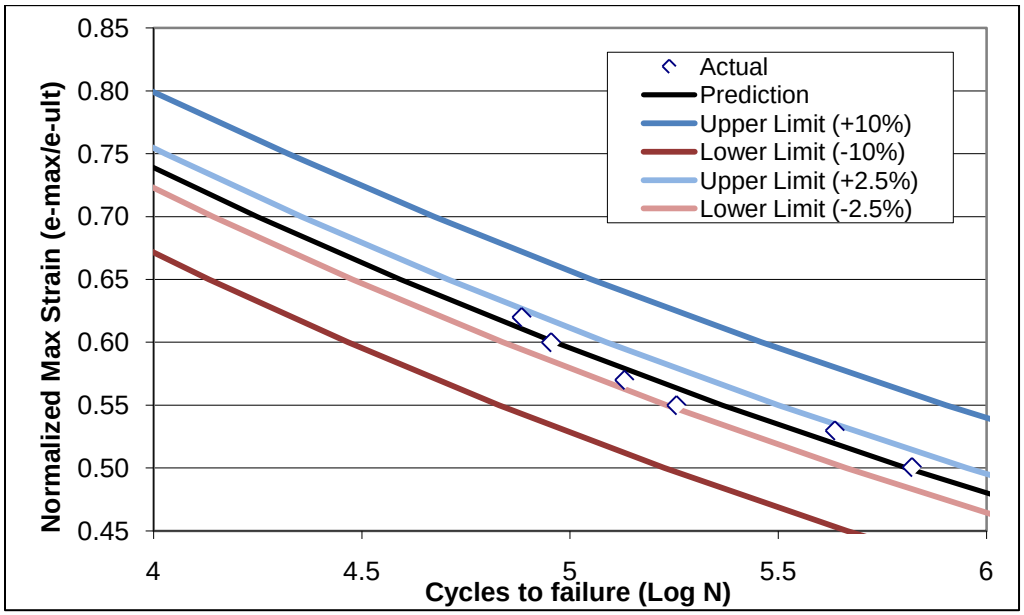

Figure 4-10 - Box Beam Fatigue Model Fit

4.4 Conclusions

The strain energy fatigue model appears to provide both a good fit and a good prediction for the fatigue life of GFRP composite materials. The large amount of data analyzed from the DOE/MSU database indicates the ability of the model to fit a variety of GFRP materials with 80-90% of the tests falling within ±5% of the log number of cycles to failure. The model was also shown to be able to predict the fatigue life of polyester GFRPs to within ±5% of the log number of cycles to failure using only two experimental values with a success rate of over 75%; using three increased the success rate to over 80%. It appears that the model can predict values nearly as accurately with nine samples as it can with only 2-3 samples, illustrating how it only requires a minimum number of experimental data points.

The tests run on the X-Strand composite produced similar results to those obtained from the analysis of the DOE/MSU database and therefore contribute to the validity of the model with reference to the database results. In light of the success of the model at fitting samples from the DOE/MSU database, this also confirms that the fatigue tests run on the X-Strand composite produced good quality results.

The analysis of the component fatigue tests indicate that the model is able to fit and predict the fatigue life for a full-scale composite component as accurately as for a coupon while maintaining the same level of simplicity. The model was able to fit and predict the fatigue life of both of the components to within ±2.5% of the log number of cycles to failure.

The strain energy fatigue model provides a simple method to predict fatigue life to within acceptable levels of accuracy for many industries. Additional work should focus on developing material and test condition-based approximations for *b*-coefficients as well as continuing to test the model against component-scale fatigue test results.

CHAPTER 5 CONCLUSIONS AND RECOMMENDATIONS

In this study, a review of published literature was conducted on FRPs on the following topics: fatigue behavior, fatigue modeling, environmental effects on mechanical performance, and environmental effects on fatigue. A series of tests was conducted on a single GFRP material in order to characterize its fatigue behavior and its fatigue response to varying environmental conditions. These tests included tests to determine the fiber content and basic architecture of the material, static tests to determine the mechanical properties of the material in bending and tension, bending and tension-tension fatigue tests in varying environmental conditions, absorption tests at different pressures and temperatures, and post-immersion conditioning fatigue tests. Finally, using a combination of the GFRP experimental test results (at room temperature and in a dry environment), test results from a previous researcher at the WVU-CFC, and test results from a published composite material fatigue database, a strain energy-based fatigue life prediction model was evaluated and shown to produce good prediction results across a wide variety of GFRPs.

5.1 Fatigue Testing of FRP Composite Coupons

The composite material was evaluated for its static and fatigue properties. More detailed results from the static tests can be found in Chapter 3; the most important results obtained were those relating to fatigue behavior and environmental conditions.

In bending fatigue, the most common failure mode was delamination on the tension side of the sample, believed to be initiated by micro-cracking at the midpoint (the highest bending moment). The failure mode for all of the tension-tension fatigue tests seemed to be a combination of lamina separation and fiber breaking. Both modes exhibited some form of

delamination near the outer surfaces of the composite, indicating that this was the weakest interface and thus the limiting factor in the material's design.

The presence of salt water reduced the fatigue life of the material to between 54% (at 50% stress level) and 84% (at 63% stress level) in bending fatigue. The presence of salt water exhibited between a 43% (at 50% stress level) reduction in tension-tension fatigue life of the material to having no effect at all (at 63% stress level). It was clear from these results that the presence of salt water can significantly reduce the fatigue life of the material, but the effect is not always observable over shorter time periods.

The reduction of fatigue life due to increased temperature was approximately linear for the bending fatigue tests. While not enough tests were run at different temperatures for the tension-tension fatigue tests to establish a similar relationship, it was observed that increased temperature significantly reduced the fatigue life of the material, indicating that one likely exists.

As a whole, compared to bending fatigue data under the same stress levels ($\sigma_{max}/\sigma_{ult}$), the tension fatigue tests exhibited much fewer cycles to failure and were more susceptible to environmental effects.

It was observed that room temperature immersion conditioning can reduce the fatigue life of the material to 50-65% of the fatigue life of the pre-immersion material, while 100°F immersion conditioning can reduce the fatigue life of the material to 15-25%. The fatigue strength knockdown at approximately 3500 cycles was calculated to be 6% for room temperature immersion conditioning and 14% for 100°F immersion conditioning. For lower stress levels, it seems likely that immersion conditioning will have less of an effect.

5.2 Fatigue Life Prediction Model Evaluation

The strain energy-based fatigue life prediction model was evaluated using data from several sources. More detailed results from evaluation can be found in Chapter 4.

Nearly all of the data analyzed was made available by researchers at Montana State University, who have compiled a composite material fatigue database after conducting a large number of fatigue tests on windmill blade materials for the US Department of energy. Results from WVU-CFC fatigue tests were also employed in the model evaluation.

From the variety of coupon fatigue data used to evaluate the model, it was found that the model was able to fit GFRP materials with over 80% of the results falling with ±5% of the log number of cycles to failure. The model was also shown to be able to predict the fatigue life of polyester GFRPs to within ±5% of the log number of cycles to failure using only two experimental values with a success rate of over 75%; using three increased the success rate to over 80%, but using more had little effect on its accuracy.

From the small amount of available component fatigue data, it appears that the model is also able to fit and predict fatigue life with at least the same accuracy as it was able to predict coupon fatigue life. However, since so few samples (and only one material) were evaluated, this is only a preliminary observation.

The strain energy fatigue model appears to provide both a good fit and a good prediction for the tension-tension fatigue life of GFRP composite materials.

5.3 Recommendations

As previously stated, fatigue characterization is made much easier with larger amounts of experimental data. In order to reinforce the conclusions drawn in the previous sections, more

experimental data would be necessary. Additional bending fatigue tests are needed at different stress levels (and applying the same range of environmental conditions). Introducing a variety of temperatures (including artificial cooling) to the tension-tension and immersion conditioned tests would provide a much better understanding of the effect of temperature and the combined effects of temperature and moisture on fatigue performance. Testing under the same conditions while varying the matrix and fiber materials would also provide a valuable environmental performance characterization between different materials.

To continue the fatigue model evaluation research, it would be ideal to apply the same data to a few other popular composite fatigue life models (if the necessary data is available in the fatigue database). Doing so would provide some more direct context as to how well the simplified strain energy-based fatigue life model compares in accuracy and ease of use to other models. Additionally, more fatigue test data on composite components is necessary before any strong conclusions can be drawn on the ability of the model to predict component fatigue life.

Additional work on the theoretical side of the strain energy fatigue life model should be focused on testing if modifications to the strain energy calculation method to account for more complex stress states would provide similar or better fatigue prediction results. While Natarajan (2003) and Munagala (2005) provided some hypotheses on which material and testing characteristics affected the *a*- and *b*-coefficients in the model, but so far the only numerical trend found was for polyester-matrix composites and was related to the fiber volume fraction. Determining a more accurate way to estimate at least the *b*-coefficient for different materials would further increase the appeal of the model by limiting or eliminating the need for experimental fatigue testing.

REFERENCES

American Society of Civil Engineers. (2009). “2009 Report Card for America’s Infrastructure.” < http://www.infrastructurereportcard.org/> (Feb. 15, 2010).

Barbero, E. J. (1999). *Introduction to Composite Material Design*. Taylor & Francis, Philadelphia, PA.

Bradley, W. L., and Grant, T. S. (1995). “The Effect of the Moisture Absorption on the Interfacial Strength of Polymeric Matrix Composites.” *J. Mater. Sci.,* 30, 5537-5542.

Curtis, P.T. (1989). “The Fatigue Behaviour of Fibrous Composite Materials.” *J. Strain Anal*., 24(4), 47-56.

Degrieck, J., and Van Paepegem, W. (2001). “Fatigue Damage Modelling of Fibre-Reinforced Composite Materials: Review.” *Appl. Mech. Rev*., 54(4), 279-300.

Dittenber, D. B., and GangaRao, H. V. S. (2010). “Evaluation of Fatigue Life Prediction Model for GFRP Composite Materials.” *Proc. ANTEC 2010*, Orlando, FL.

Ellyin, F., and El-Kadi, H. (1990). “A Fatigue Failure Criterion for Fiber Reinforced Composite Laminae.” *Composite Struct.*, 15, 61-74.

Epaarachchi, J. A. (2005). “Effects of Static-Fatigue (Tension) on the Tension-Tension Fatigue Life of Glass Fibre Reinforced Plastic Composites.” *Composite Struct*., 74, 419-425.

Epaarachchi, J. A., and Clausen, P. D. (2003). “An Empirical Model for Fatigue Behavior Prediction of Glass Fibre-reinforced Plastic Composites for Various Stress Ratios and Test Frequencies.” *Composites, Part A*, 34, 313-326.

Fawaz, Z., and Ellyin, F. (1994). “Fatigue Failure Model for Fibre-Reinforced Materials under General Loading Conditions.” *J. Compos. Mater.*, 28(15), 1432-1451.

GangaRao, H. V. S. (2009) “Fatigue Response of Fiber Reinforced Polymeric (FRP) Composite Coupons under Tension and Bending.” *Proc., SAMPE ‘09*, Baltimore, MD.

Hashin, Z., and Rotem, A. (1973). “A Fatigue Failure Criterion for Fiber Reinforced Materials.” *J. Compos. Mater*., 7(4), 448-464.

Hwang, W., and Han, K. S. (1986). “Fatigue of Composites – Fatigue Modulus Concept and Life Prediction.” *J. Compos. Mater.*, 20, 154-165.

Kelkar, A. D. (2001). “Behavior of Low Cost Manufactured Thick FRP Woven Composite Laminates under Cyclic Loading.” *Proc., Int. Conf. on FRP Compos. in Civil Eng.*, J.-G. Teng, ed., Hong Kong, CN, 235-243.

Khan, Z., Al-Sulaiman, F. A., Farooqi, J. K., and Younas, M. (2001). “Fatigue Life Predictions in Woven Carbon Fabric/Polyester Composites Based on Modulus Degradation.” *J. Reinf. Plast. Compos.*, 20(5), 377-398.

Khan, R., Khan, Z., Al-Sulaiman, F., Merah, N. (2002). “Fatigue Life Estimates in Woven Carbon Fabric/Epoxy Composites at Non-Ambient Temperatures.” *J. Compos. Mater.*, 36(22), 2517-2535.

Kim, H. S., and Zhang, J. (2001). “Fatigue Damage and Life Prediction of Glass/Vinyl Ester Composites.” *J. Reinf. Plast. Compos.*, 20(10), 834-848.

Liang, R., and GangaRao, H. V. (2004). “Applications of Fiber Reinforced Polymer Composites.” *Polymer Composites III 2004*, R. Creese and H. V. GangaRao, eds., DEStech, Lancaster, PA, 173-187.

Liao, K., Schultheisz, C. R., and Hunston, D. L. (1999). “Effects of Environmental Aging on the Properties of Pultruded GFRP.” *Composites, Part B*, 30, 485-493.

Mahadevan, S., and Mao, H. (2004). “Probabilistic Fatigue-Creep Life Prediction of Composites.” *J. Reinf. Plast. Compos.*, 23(4), 361-371.

Mandell, J. F., and Samborsky, D. D. (1997). “DOE/MSU Composite Material Fatigue Database: Test Methods, Materials, and Analysis.” *Contractor Report SAND97-3002*, Sandia National Laboratories, Albuquerque, NM.

McBagonluri, F., Garcia, K., Hayes, M., Verghese, K. N. E., Lesko, J. J. (1999). “Characterization of Fatigue and Combined Environment on Durability Performance of Glass/Vinyl Ester Composite for Infrastructure Applications.” *Int. J. Fatigue*, 22, 53-64.

Mouritz, A. P. (2005). “A Simple Fatigue Life Model for Three-Dimensional Fiber-Polymer Composites.” *J. Compos. Mater.*, 40(5), 455-469.

Munagala, P. (2005). “Fatigue Life Prediction of GFRP Composite Material at Coupon and Component Level.” M. S. Thesis, CEMR, West Virginia University, Morgantown, WV.

Murthy, H. N. N., Sreejith, M., Krishna, M., Sharma, S. C., Sheshadri, T. S. (2009). “Seawater Durability of Epoxy/Vinyl Ester Reinforced with Glass/Carbon Composites.” *J. Reinf. Plast. Compos.*, 00(00), 1-9.

Nagaraj, V. (1994). “Static and Fatigue Response of Pultruded FRP Beams without and with Splice Connections.” M. S. Thesis, West Virginia University, Morgantown, WV.

Natarajan, V. (2003). “Fatigue Response of Fabric Reinforced Polymeric Composites.” M. S. Thesis, CEMR, West Virginia University, Morgantown, WV.

Natarajan, V., GangaRao, H. V. S., Shekar, V. (2005). “Fatigue Response of Fabric-reinforced Polymeric Composites.” *J. Compos. Mater.*, 39(17), 1541-1559.

Philippidis, T. P., and Vassilopoulos, A. P. (1999). “Fatigue Strength Prediction under Multiaxial Stress.” *J. Compos. Mater.*, 33(17), 1578-1599.

Qiao, P., and Yang, M. (2006). “Fatigue Life Prediction of Pultruded E-glass/Polyurethane Composites.” *J. Compos. Mater*., 40(9), 815-837.

Reifsnider, K. L. (1990a). “Damage and Damage Mechanics.” *Fatigue of Composite Materials*, K. L. Reifsnider, ed., Elsevier, Amsterdam, NL, 11-77.

Reifsnider, K. L. (1990b). “Introduction.” *Fatigue of Composite Materials*, K. L. Reifsnider, ed., Elsevier, Amsterdam, NL, 1-9.

Reifsnider, K. L., and Gao, Z. (1991). “A Micromechanics Model for Composites under Fatigue Loading.” *Int. J. Fatigue*, 13(2), 149-156.

Samborsky, D. D., and Mandell, J. F. (2005). “DOE/MSU Composite Material Fatigue Database, Version 18.1.”

Sarkani, S., Michaelov, G., Kihl, D. P., Beach, J. E. (1999). “Stochastic Fatigue Damage Accumulation of FRP Laminates and Joints.” *J. Struct. Eng.*, 125(12), 1423-1431.

Sendeckyj, G. P. (1990). “Life Prediction for Resin-Matrix Composite Materials.” *Fatigue of Composite Materials*, K. L. Reifsnider, ed., Elsevier, Amsterdam, NL, 431-483.

Stinchcomb, W. W., and Bakis, C. E. (1990). “Fatigue Behavior of Composite Laminates.” *Fatigue of Composite Materials*, K. L. Reifsnider, ed., Elsevier, Amsterdam, NL, 105-180.

Sun, Z., Daniel, I. M., and Luo, J. J. (2003). “Modeling of Fatigue Damage in a Polymer Matrix Composite.” *Mater. Sci. Eng., A*, 361, 302-311.

Talreja, R. (1990). “Statistical Considerations.” *Fatigue of Composite Materials*, K. L. Reifsnider, ed., Elsevier, Amsterdam, NL, 485-501.

Varvani-Farahani, A., and Shirazi, A. (2007). “A Fatigue Damage Model for (0/90) FRP Composites based on Stiffness Degradation of 0° and 90° Composite Plies.” *J. Reinf. Plast. Compos.*, 26(13), 1319-1336.

Vijay, P. V., and GangaRao, H. V. S. (1999). “Accelerated and Natural Weathering of Glass Fiber Reinforced Plastic Bars.” *4th International Symposium, Fiber Reinforced Polymer Reinforcement for Reinforced Concrete Structures*, American Concrete Institute, SP 188-53, Farmington Hills, MI.

Weitsman, Y. (1990). “Moisture in Composites: Sorption and Damage.” *Fatigue of Composite Materials*, K. L. Reifsnider, ed., Elsevier, Amsterdam, NL, 385-429.

APPENDIX A – COMPOSITE FATIGUE PLOTS

Within this appendix are composite plots of the load, maximum deflection, minimum deflection, and deflection range for each of the four categories of fatigue testing: 1) Bending Fatigue, 2) Tension-Tension Fatigue (Stress Varied), 3) Tension-Tension Fatigue (Environment Varied), and 4) Tension-Tension Fatigue (Immersion Varied).

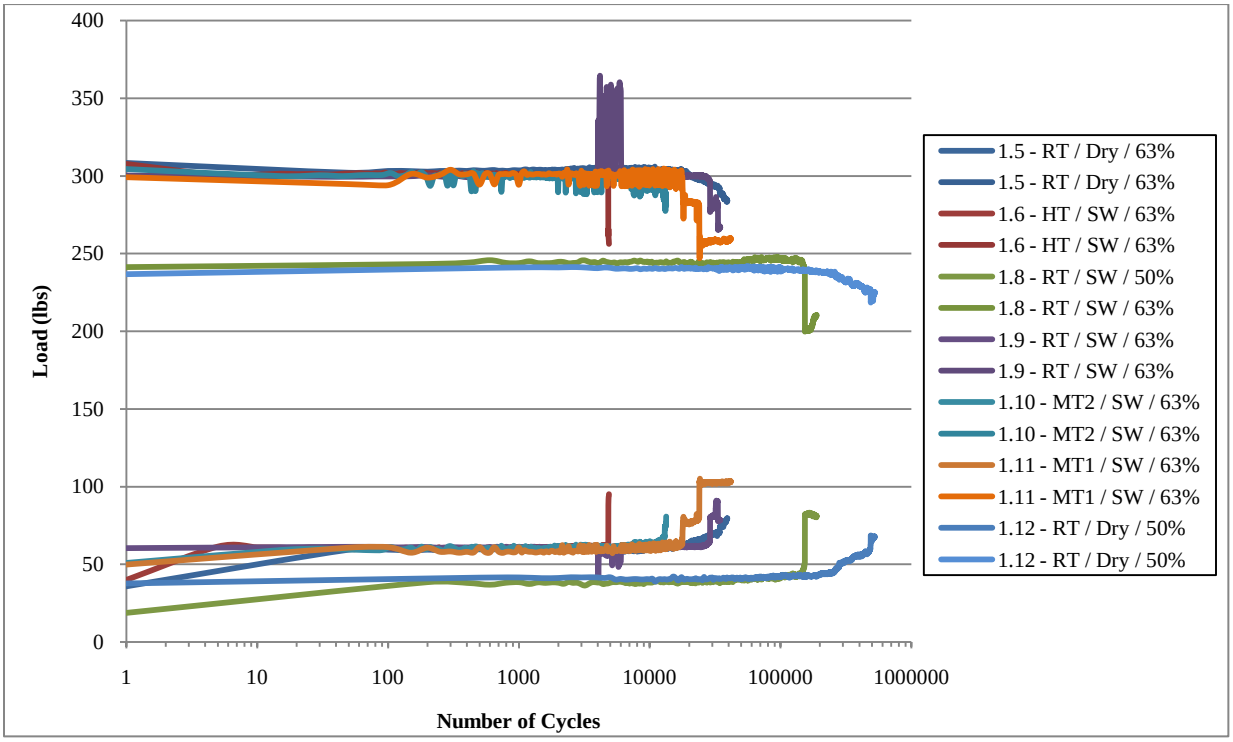

Figure A-1 - Bending Fatigue Load Plot

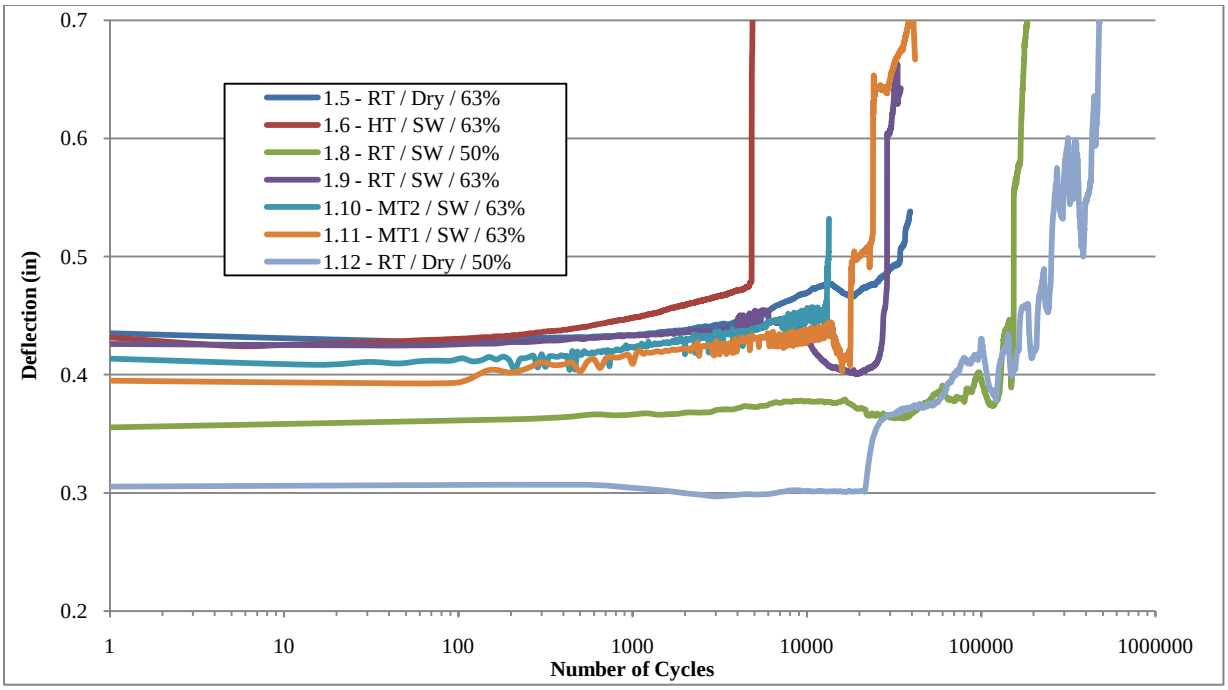

Figure A-2 - Bending Fatigue Maximum Deflection Plot

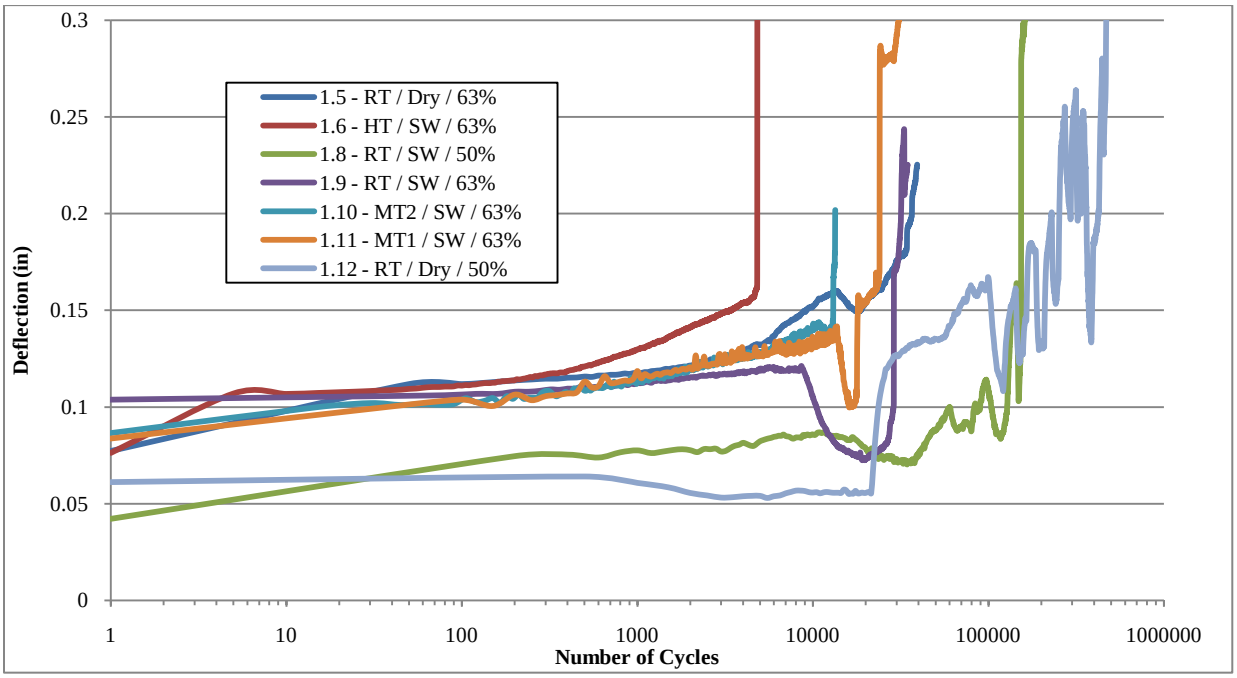

Figure A-3 - Bending Fatigue Minimum Deflection Plot

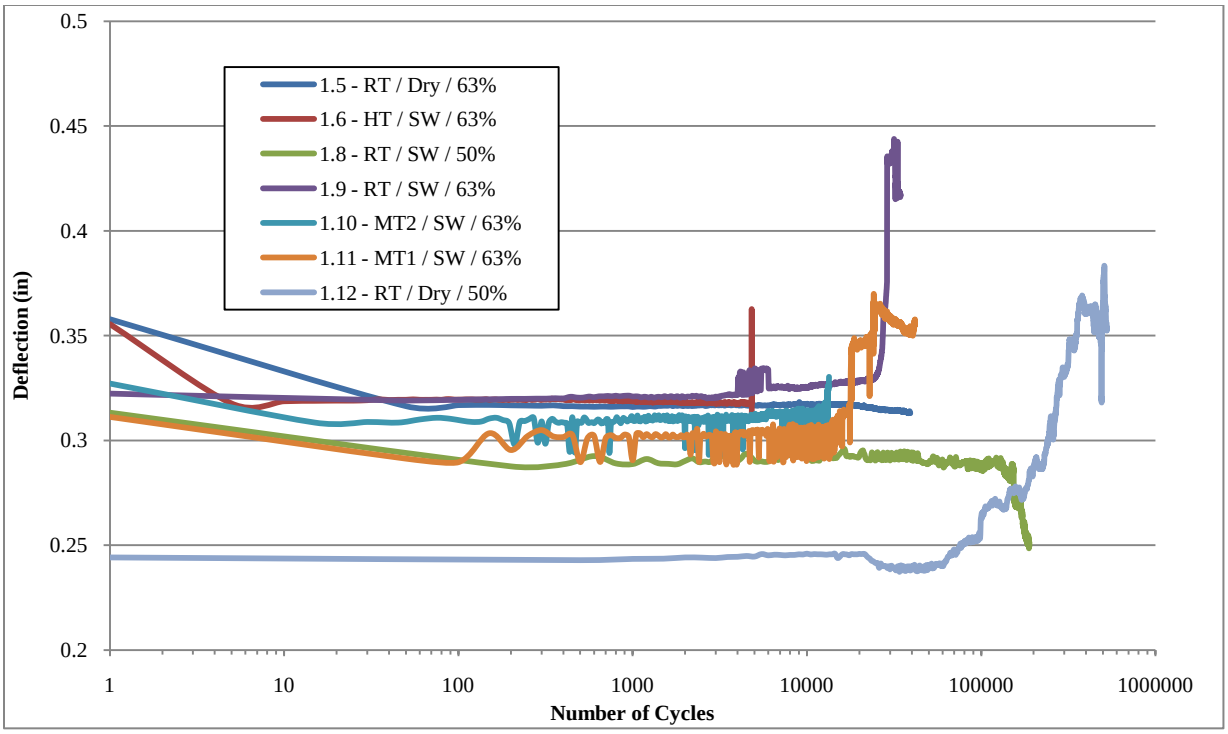

Figure A-4 - Bending Fatigue Deflection Range Plot

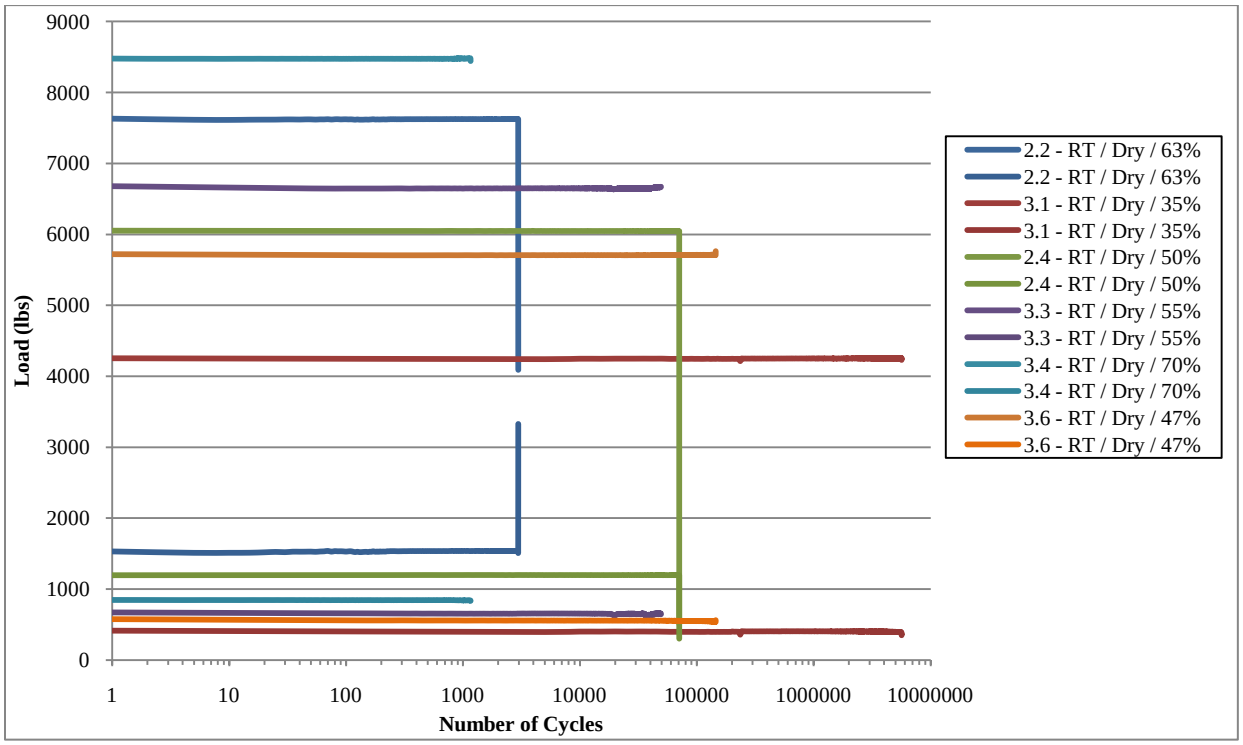

Figure A-5 - Tension-Tension Fatigue (Stress) Loading Plot

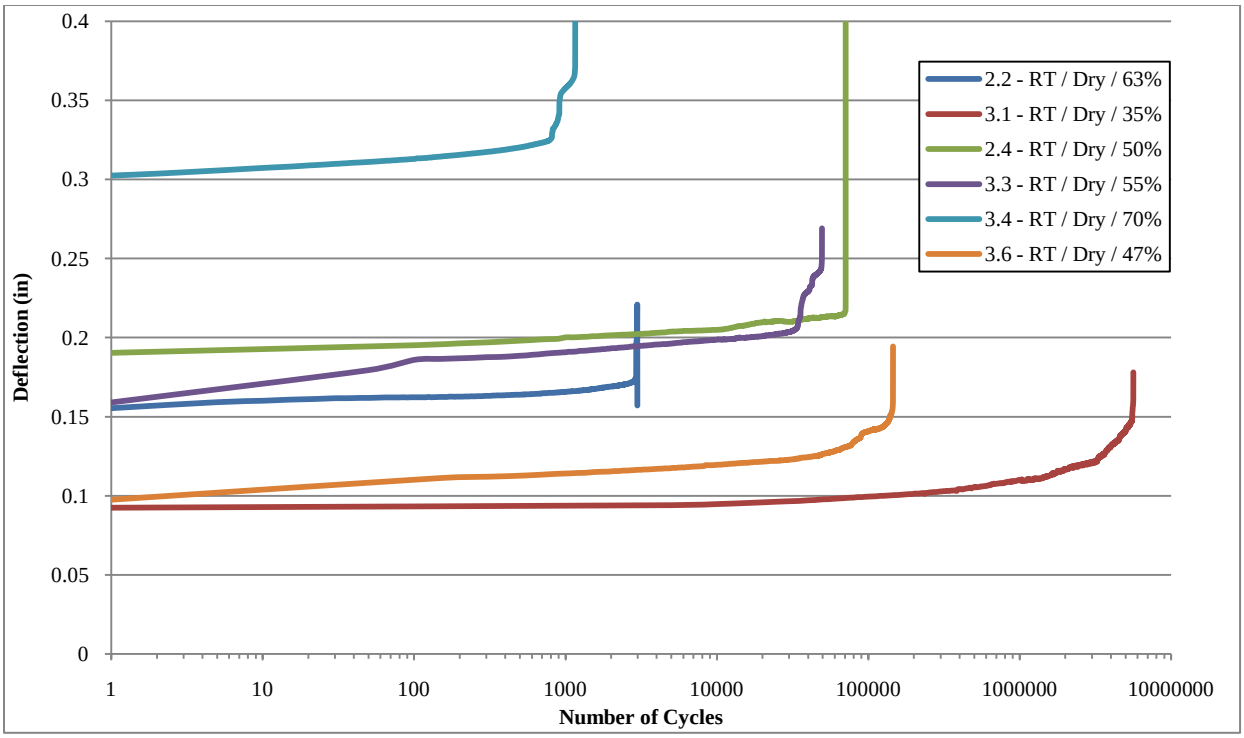

Figure A-6 - Tension-Tension Fatigue (Stress) Maximum Deflection Plot

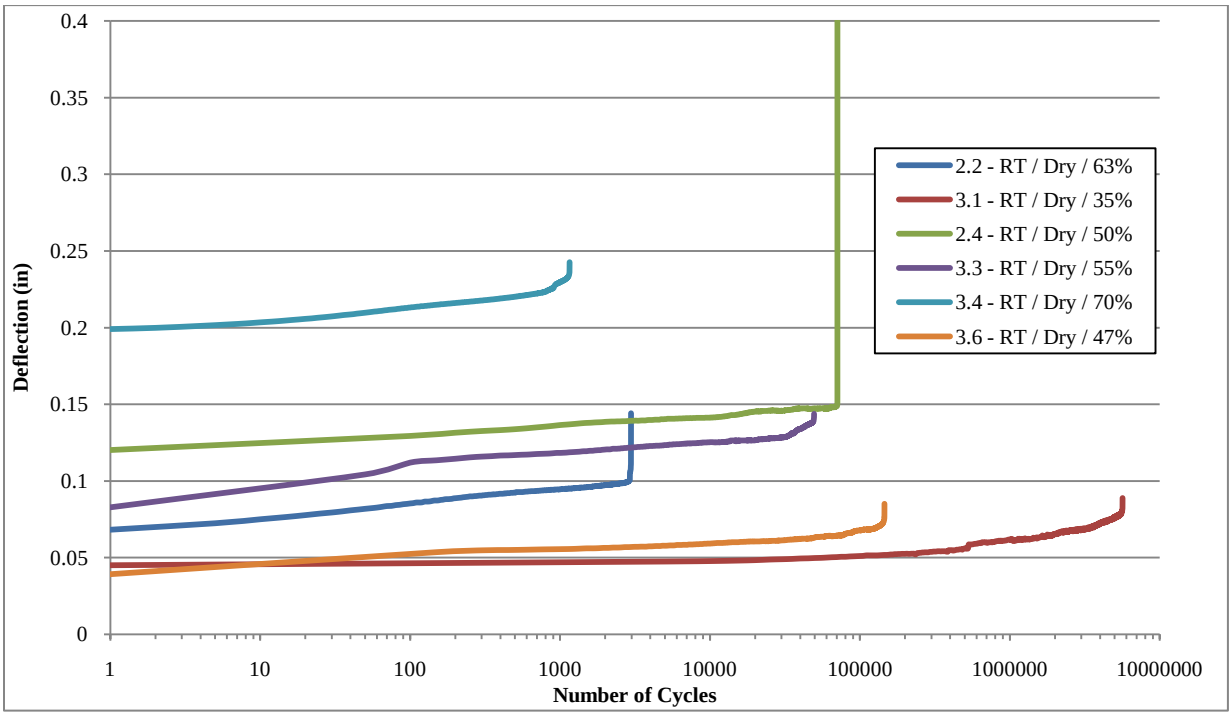

Figure A-7 - Tension-Tension Fatigue (Stress) Minimum Deflection Plot

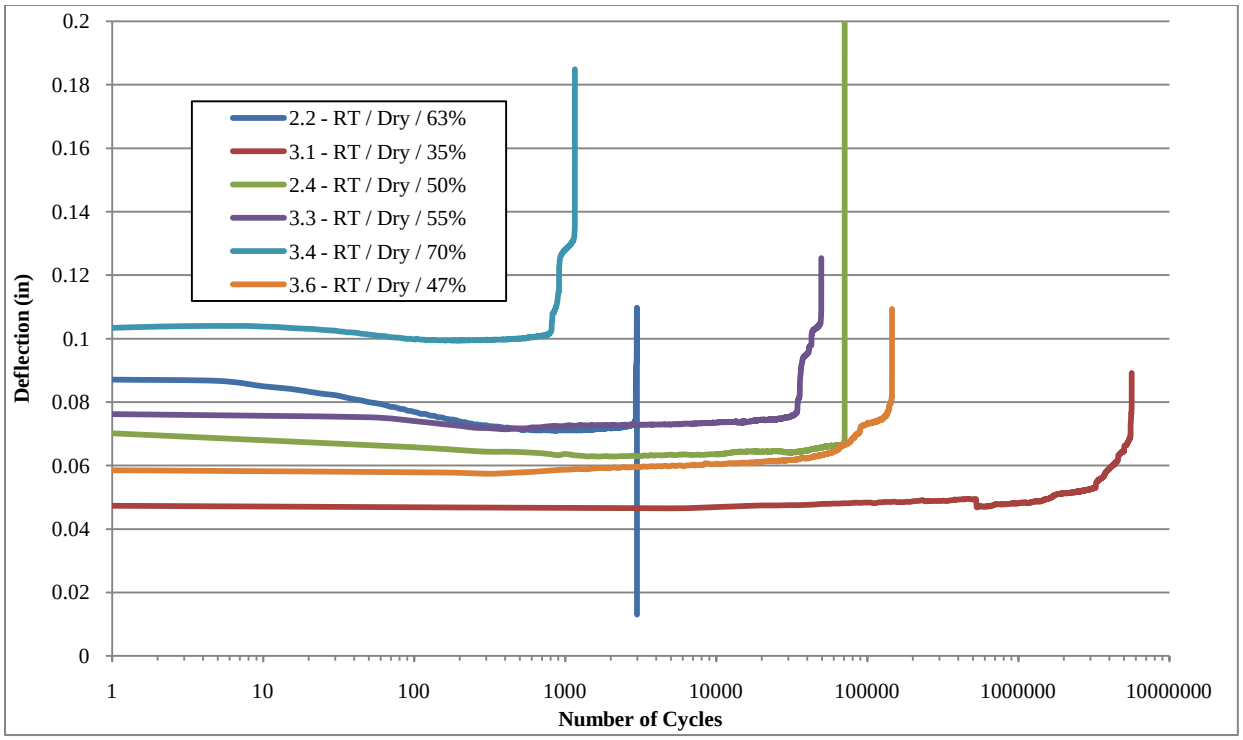

Figure A-8 - Tension-Tension Fatigue (Stress) Deflection Range Plot

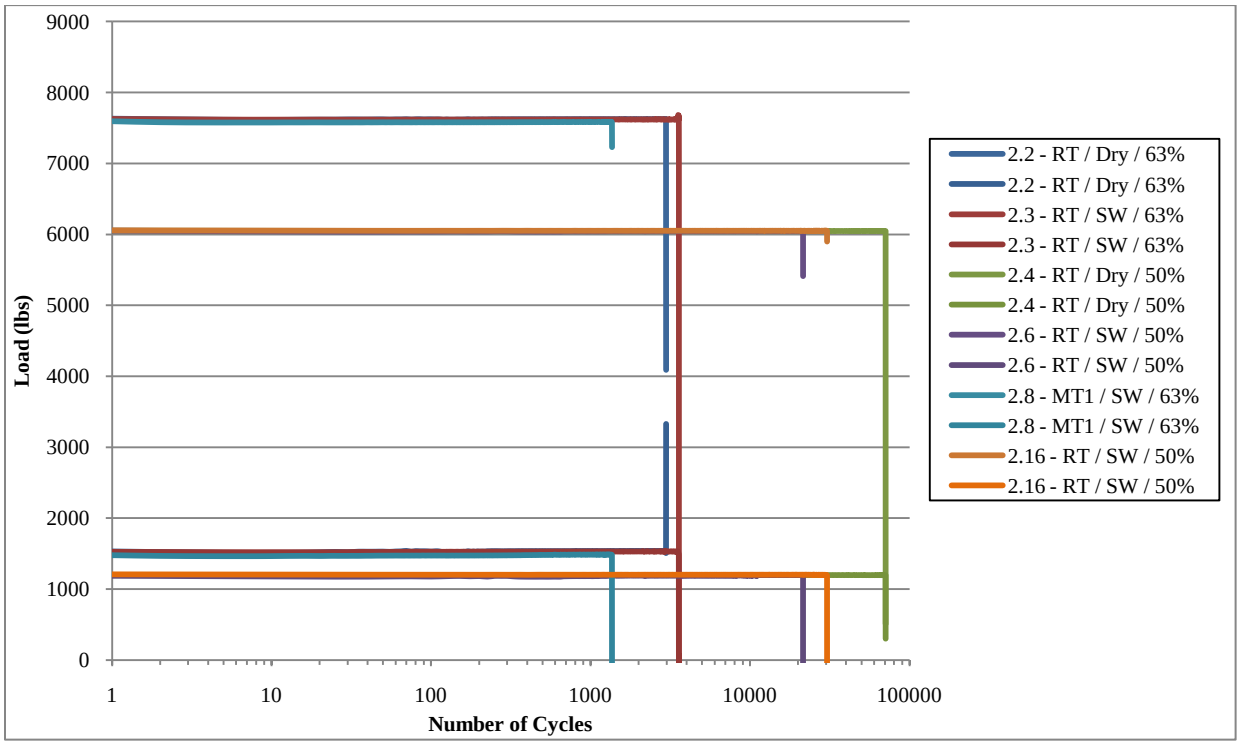

Figure A-9 - Tension-Tension Fatigue (Environment) Loading Plot

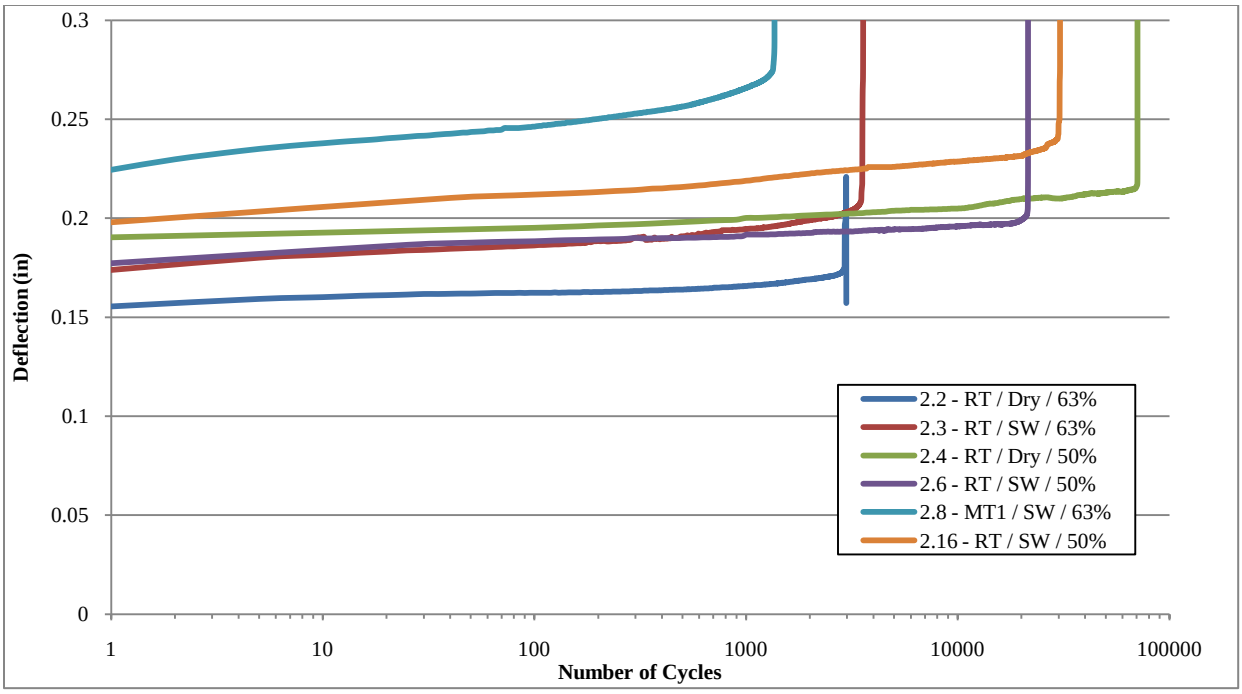

Figure A-10 - Tension-Tension Fatigue (Environment) Maximum Deflection Plot

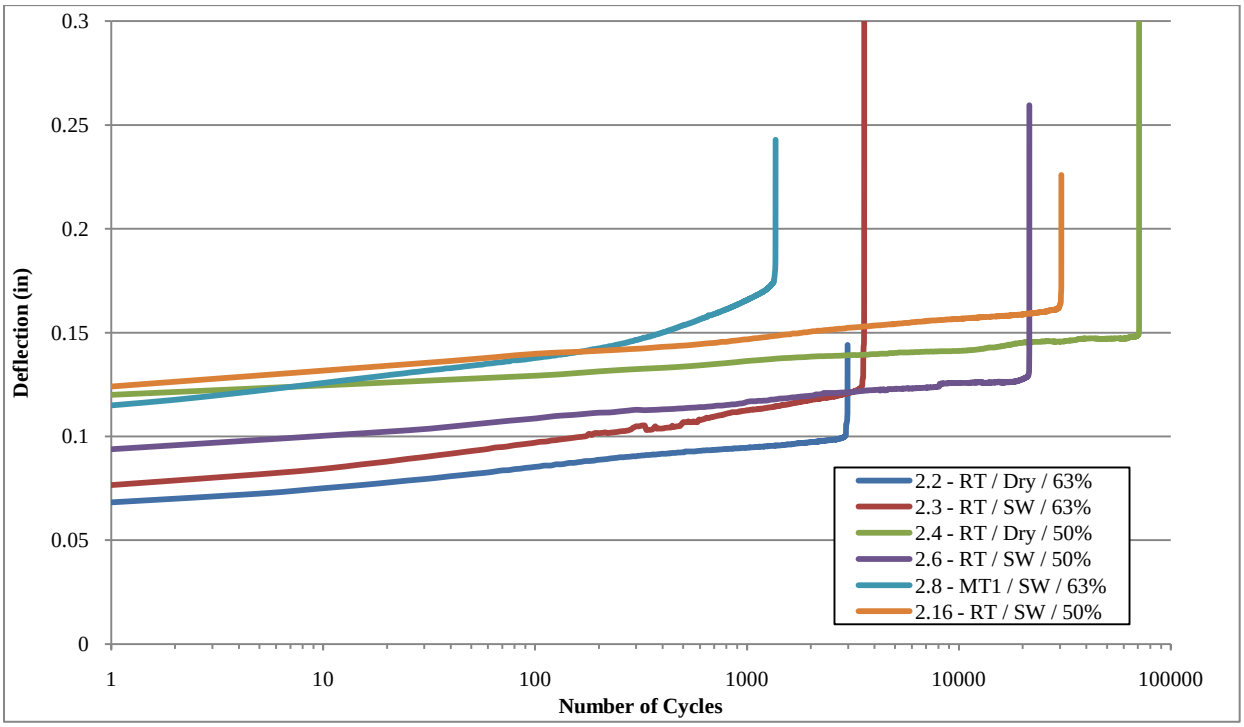

Figure A-11 - Tension-Tension Fatigue (Environment) Minimum Deflection Plot

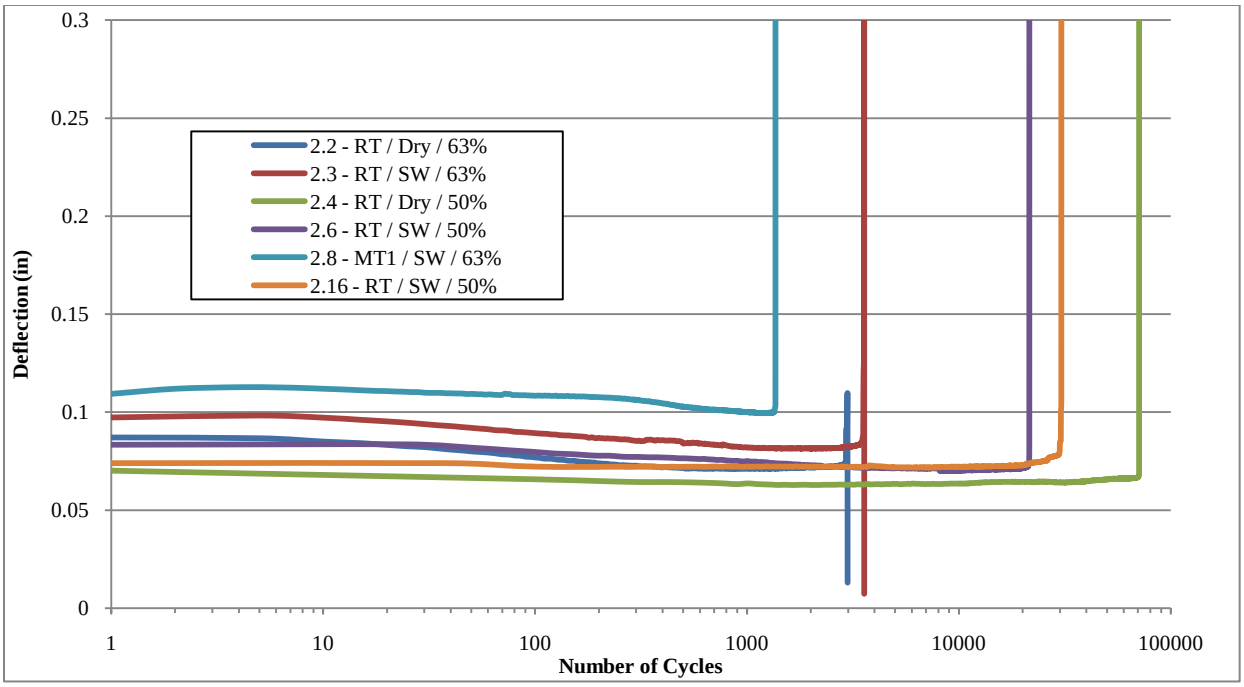

Figure A-12 - Tension-Tension Fatigue (Environment) Deflection Range Plot

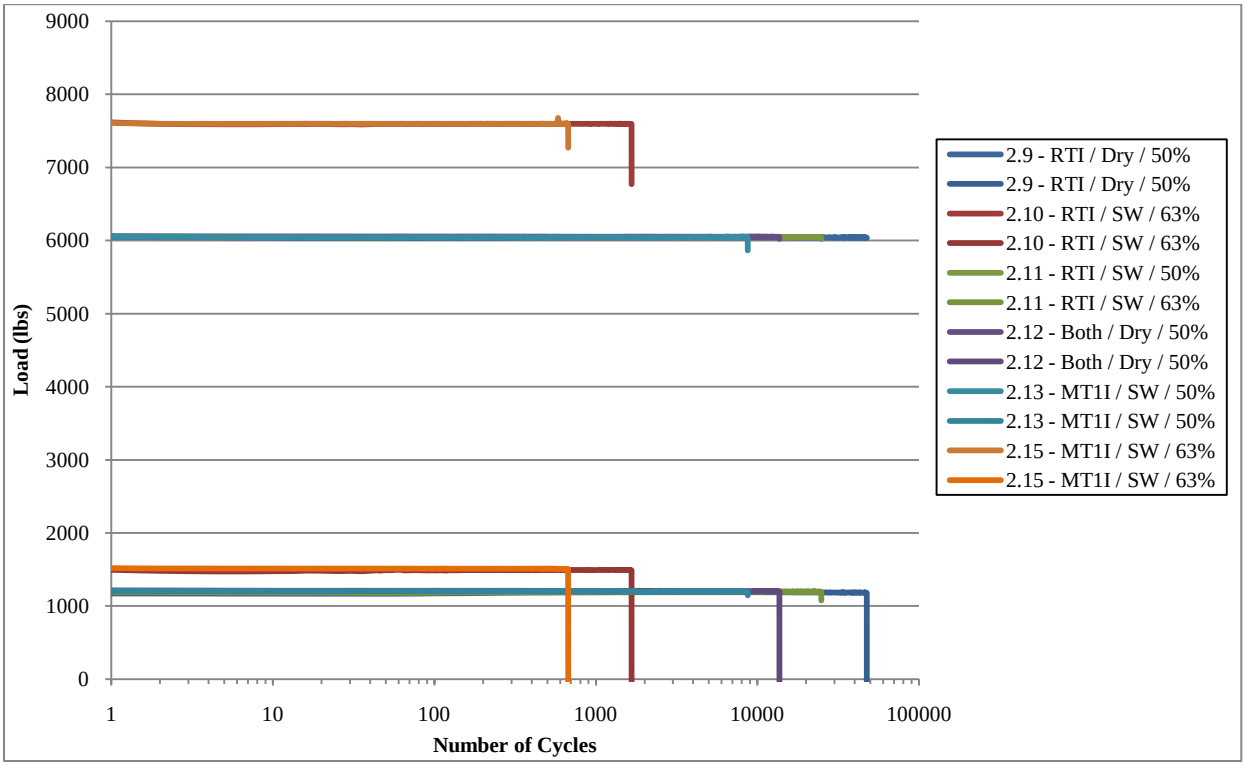

Figure A-13 - Tension-Tension Fatigue (Immersion) Loading Plot

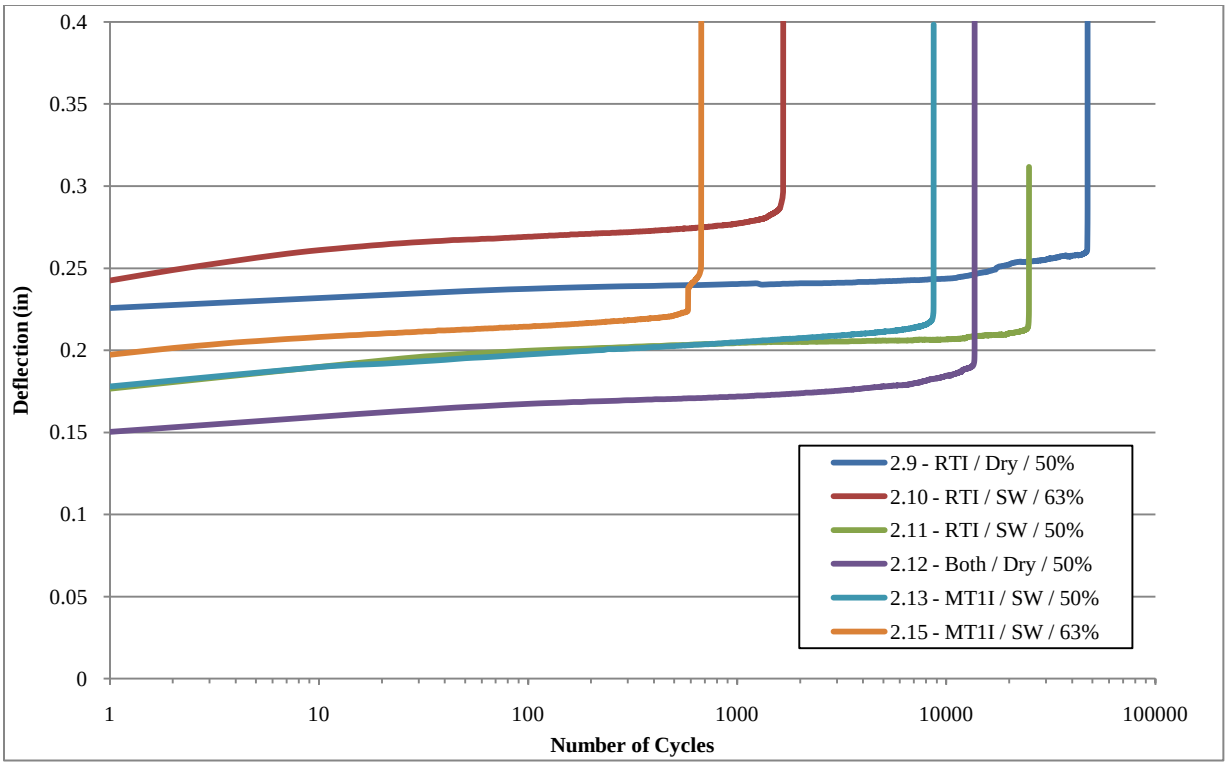

Figure A-14 - Tension-Tension Fatigue (Immersion) Maximum Deflection Plot

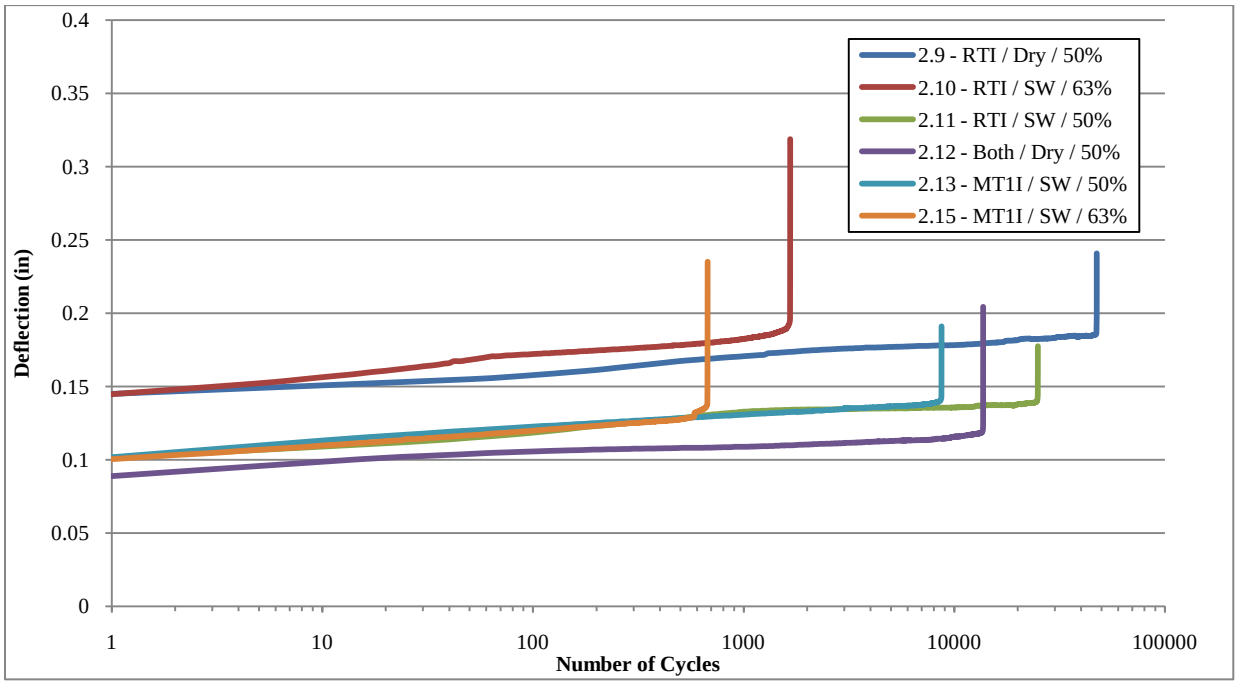

Figure A-15 - Tension-Tension Fatigue (Immersion) Minimum Deflection Plot

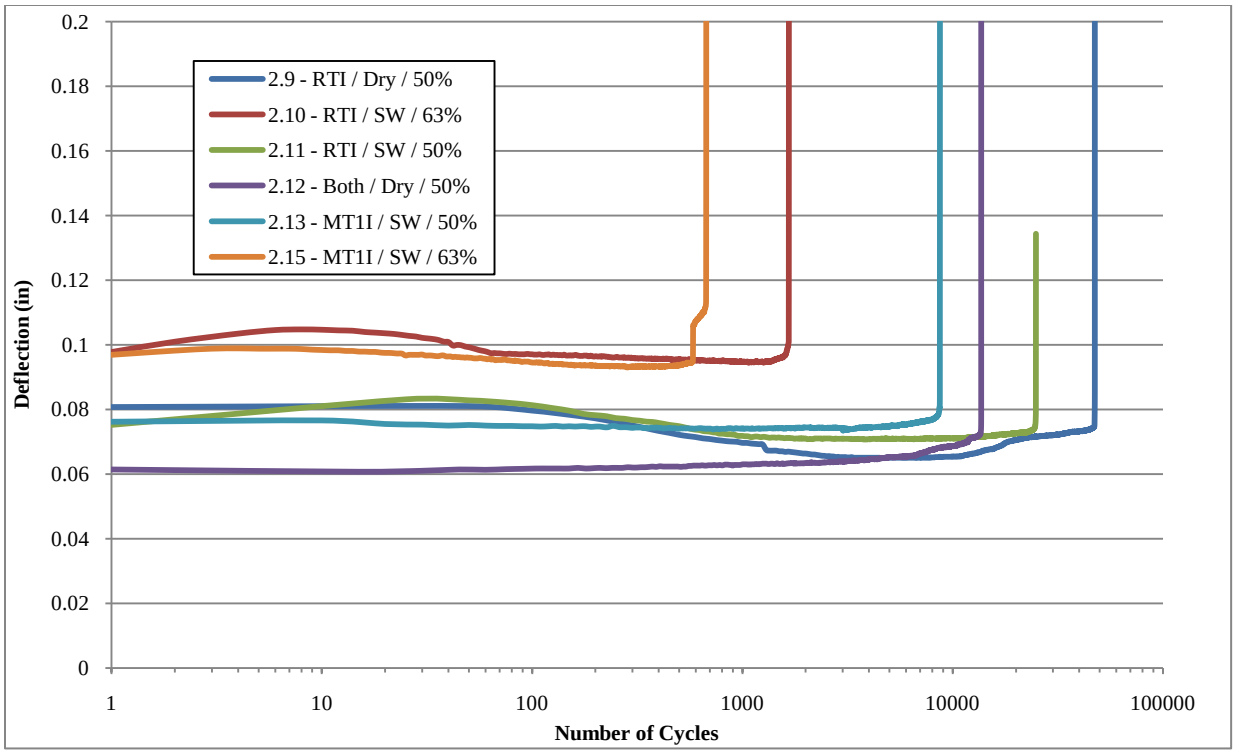

Figure A-16 - Tension-Tension Fatigue (Immersion) Deflection Range Plot

APPENDIX B – DOE/MSU FATIGUE DATABASE ANALYSIS

The following tables include all of the data taken from the DOE/MSU Composite Material Fatigue Database (Samborsky and Mandell 2005) that was used for the fatigue life prediction model evaluation conducted in CHAPTER 4, in addition to the data from the material tested in CHAPTER 3.

Table B-1 - DOE/MSU Material Properties

Material	Matrix Type	Manuf. Process	Fiber Type	Fiber Arch.
WS1	Epoxy	Lay-up	E-glass	(45/0/45) (49.4%-0)
E-LT-5500-VE	Vinylester	Lay-up	E-glass	[45/0/45/0/45] (66%-0)
E-LT-5500-EP	Epoxy	Lay-up	E-glass	[45/0/45/0/45] (66%-0)
QQ1	Epoxy	Lay-up	E-glass	[45/90/45/(90,0)4/45/90/45]
QQ2	Epoxy	Lay-up	E-glass	[45/0/45]s (64%-0)
QQ4L	Epoxy	Lay-up	E-glass	[45/0/45/0/45] (56%-0)
QQ4	Epoxy	Lay-up	E-glass	[45/0/45/0/45] (56%-0)
TT1A	Epoxy	Lay-up	E-glass	[45/0/45/0/45] (66%-0)
TT1AH	Epoxy	Lay-up	E-glass	[45/0/45/0/45] (66%-0)
TT	Vinylester	Lay-up	E-glass	[45/0/45/0/45] (66%-0)
W45	Epoxy	VARTM	E-glass	(45/45)6
SWA	Epoxy	VARTM	E-glass	(45)3s
SWB	Epoxy	VARTM	E-glass	(45)3s
B	Vinylester	Lay-up	E-glass	[0]5
L	Polyester	Lay-up	E-glass	[0]3
M	Vinylester	Lay-up	E-glass	[0/45]4
N	Polyester	Lay-up	E-glass	[0/45]4
P	Vinylester	Lay-up	E-glass	[0/45/M/0]s
R	Polyester	Lay-up	E-glass	[0/45]4
V	Polyester	Lay-up	E-glass	[0/45]5
W	Polyester	Lay-up	E-glass	[0/45]5
X	Polyester	Lay-up	E-glass	[0/M/45/0]
Y	Epoxy	Lay-up	E-glass	[0/M/45/0]
EE	Epoxy	Cut Pultruded	E-glass	[M/45/0]s
EEAV	Vinylester	Cut Pultruded	E-glass	[M/45/0]s
EEAP	Polyester	Cut Pultruded	E-glass	[M/45/0]s
EEBP	Vinylester	Cut Pultruded	E-glass	[M/45/0]s
EECP	Vinylester	Cut Pultruded	E-glass	[M/45/0]s

AA	Polyester	RTM	E-glass	[(45/0)2,(45/0),(45/0)2]
AA3	Polyester	RTM	E-glass	[(45/0)3]s
AA4	Polyester	RTM	E-glass	[(45/0)2]s
BB	Polyester	RTM	E-glass	[45/(0)2/45]s
CC	Polyester	RTM	E-glass	[45/(0)2/45]s
CC2	Polyester	RTM	E-glass	[45/(0)3/45]s
CC3	Polyester	RTM	E-glass	[0/45/(0)2/45]s
CH	Polyester	RTM	E-glass	[(45)3]s
CH2	Polyester	RTM	E-glass	[(45/0/45)]s
CH3	Polyester	RTM	E-glass	[(45/0/45)]s
CH4	Polyester	RTM	E-glass	[(45)4]s
CH5	Polyester	RTM	E-glass	[(45)3]s
CH6	Polyester	RTM	E-glass	[(45/0/45)]s
CH7	Polyester	RTM	E-glass	[(45)2]s
CH8	Polyester	RTM	E-glass	[(45)2]s
CH9	Polyester	RTM	E-glass	[(45)3]s
CH10	Polyester	RTM	E-glass	[(45)3]s
CH11	Polyester	RTM	E-glass	[(45)2]s
CH12	Polyester	RTM	E-glass	[(45/0/45)]s
CH13	Polyester	RTM	E-glass	[(45/0/45)]s
CH14	Polyester	RTM	E-glass	[(45/0/45)]s
CH15	Polyester	RTM	E-glass	[(45/0/45)]s
CH16	Polyester	RTM	E-glass	[(45/0/45)]s
CH17	Polyester	RTM	E-glass	[(45/0/45)]s
CH18	Polyester	RTM	E-glass	[(45/0/45)]s
CH19	Polyester	RTM	E-glass	[(45/0/45)]s
CH20	Polyester	RTM	E-glass	[(45)3]s
CH23	Polyester	RTM	E-glass	[(45/0/45)]s
DD	Polyester	RTM	E-glass	[0/45/(0)3/45/0]
DD2	Polyester	RTM	E-glass	[0/45/0]s
DD4	Polyester	RTM	E-glass	[0/45/0]s
DD5	Polyester	RTM	E-glass	[0/45/0]s
DD5E	Epoxy	RTM	E-glass	[0/45/0]s
DD5P	Polyester	RTM	E-glass	[0/45/0]s
DD5V	Vinylester	RTM	E-glass	[0/45/0]s
DD5V2	Vinylester	RTM	E-glass	[0/45/0]s
DD5CYC	Thermoplastic	RTM	E-glass	[0/45/0]s
DD6	Polyester	RTM	E-glass	[0/45/0]s
DD7	Polyester	RTM	E-glass	[0/45/0]s
DD8	Polyester	RTM	E-glass	[0/45/0]s

DD9	Polyester	RTM	E-glass	[0/45/0]s
DD10	Polyester	RTM	E-glass	[0/45/0]s
DD11	Polyester	RTM	E-glass	[0/45/0]s
DD12	Polyester	RTM	E-glass	[0/45/0]s
DD13	Polyester	RTM	E-glass	[0/45/0]s
DD14	Polyester	RTM	E-glass	[0/45/0]s
DD20	Polyester	RTM	E-glass	[(0)2/45/0]s
DD20A	Polyester	RTM	E-glass	[(0)2/45/0]s
DD22	Polyester	RTM	E-glass	[(0)2/45/0]s
DD24	Polyester	RTM	E-glass	[0/45/(0)3/45/0]
DD25	Polyester	RTM	E-glass	[0/45/0]s
DD25A	Polyester	RTM	E-glass	[0/45/0]s
DD25B	Polyester	RTM	E-glass	[0/45/0]s
DD26	Polyester	RTM	E-glass	[0/45/0]s
DD27A	Polyester	RTM	E-glass	[0/45]s
DD27B	Polyester	RTM	E-glass	[0/45]s
FFA	Polyester	RTM	E-glass	[45/0/0/45]s
FFB	Polyester	RTM	E-glass	[0/45/0/45/0]s
FFC	Polyester	RTM	E-glass	[0/45/45/0]s
FFD	Polyester	RTM	E-glass	[0/0/45/45]s
FFF	Polyester	RTM	E-glass	[45/45/0/0]s
GG	Polyester	RTM	E-glass	[(0)2/45/(0)2]
A060	Polyester	RTM	E-glass	[0]8
A130C	Polyester	RTM	E-glass	[0]6
A130G	Polyester	RTM	E-glass	[0]14
A260	Polyester	RTM	E-glass	[0]4
CM1701A	Polyester	RTM	E-glass	[0]5
D072A	Polyester	RTM	E-glass	[0]10
D092B	Polyester	RTM	E-glass	[0]9
D092D	Polyester	RTM	E-glass	[0]7
D092G	Polyester	RTM	E-glass	[0]14
D155B	Polyester	RTM	E-glass	[0]5
D155C	Polyester	RTM	E-glass	[0]7
D155G	Polyester	RTM	E-glass	[0]8
D155H	Polyester	RTM	E-glass	[0]7
D155J	Polyester	RTM	E-glass	[0]9
D155K	Polyester	RTM	E-glass	[0]7
ROV2	Polyester	Lay-up	E-glass	[0/90]4 roving
ROV3	Polyester	Lay-up	E-glass	[0/90]5 roving
X-Strand	Vinylester	Filament Winding	E-glass	[0/90/0/90/0]

Table B-2 - DOE/MSU Coupon Properties

Material	Thickness (mm)	Width (mm)	Rate (Hz)	FVF	Modulus (Gpa)	UTS (Mpa)
WS1	2.56	25	1-3	0.605	4.8	720
E-LT-5500-VE	4.60	25	1-5	0.550	31.0	620
E-LT-5500-EP	4.59	25	1-4	0.550	29.0	710
QQ1	4.09	25	1-10	0.520	32.5	830
QQ2	3.96	25	2-5	0.520	23.0	542
QQ4L	5.70	25	3-5	0.400	3.1	650
QQ4	4.03	25	2-4	0.560	31.5	986
TT1A	4.59	25	3-4	0.550	28.0	898
TT1AH	3.98	25	2-4	0.630	31.5	850
TT	4.60	25	3-4	0.550	29.0	850
W45	4.06	25	1-4	0.495	16.5	224
SWA	4.20	25	0.5-2	0.450	12.2	170
SWB	4.20	25	1-4	0.450	11.9	170
B	3.45	25	1-10	0.248	21.0	581
L	2.46	25	1-10	0.509	33.6	742
M	3.10	50	5-15	0.381	20.7	516
N	3.23	50	1-15	0.366	19.3	468
P	3.78	50	5-15	0.404	22.5	667
R	3.56	50	1-15	0.300	16.5	441
V	3.33	50	1-15	0.338	20.0	374
W	3.43	50	2-15	0.327	19.3	341
X	4.52	25	5-20	0.352	25.4	612
Y	4.62	25	4-25	0.345	25.0	626
EE	3.53	13	2-20	0.541	31.4	543
EEAV	3.36	20	2-20	0.480	28.2	583
EEAP	3.64	20	2-15	0.490	29.0	511
EEBP	2.90	20	2-12	0.430	26.6	515
EECP	2.48	20	2-20	0.490	28.3	526
AA	4.37	25	5-20	0.315	18.8	448
AA3	3.45	25	2-8	0.480	24.7	478
AA4	5.12	25	2-5	0.326	21.5	377
BB	2.67	25	2-20	0.430	25.2	725
CC	2.44	25	2-15	0.397	21.7	570
CC2	2.69	25	4-20	0.461	26.6	711
CC3	2.74	25	5-20	0.444	26.3	682
CH	3.86	25	2-10	0.469	13.6	145

CH2	3.78	25	2-20	0.441	16.7	362
CH3	4.19	25	2-10	0.415	16.8	336
CH4	2.92	25	2-20	0.395	11.4	155
CH5	3.05	25	2-15	0.279	8.5	139
CH6	2.26	25	2-20	0.441	21.5	502
CH7	3.86	25	2-10	0.546	17.0	114
CH8	5.89	25	2-15	0.366	10.0	93
CH9	2.13	25	2-20	0.400	10.3	151
CH10	5.56	25	1-5	0.317	8.1	120
CH11	2.41	25	4-15	0.495	13.4	134
CH12	3.00	25	2-15	0.328	17.4	398
CH13	3.28	25	1-20	0.509	23.2	423
CH14	2.49	25	1-20	0.392	21.0	517
CH15	2.51	25	2-12	0.324	14.8	309
CH16	2.36	25	1-15	0.343	18.5	360
CH17	1.96	25	2-5	0.423	17.6	359
CH18	3.10	25	2-10	0.451	17.2	294
CH19	4.60	25	2-12	0.330	11.9	193
CH20	3.76	25	2-12	0.260	10.9	133
CH23	2.95	25	2-10	0.320	18.5	394
DD	2.67	22	2-20	0.509	31.3	910
DD2	2.64	22	4-20	0.441	27.0	752
DD4	2.36	22	4-20	0.481	31.0	886
DD5	2.97	22	2-20	0.374	25.2	724
DD5E	3.10	22	1-15	0.362	23.6	674
DD5P	3.02	22	1-10	0.372	24.2	661
DD5V	3.05	22	2-15	0.368	23.7	675
DD5V2	3.18	22	3-7	0.352	22.3	787
DD5CYC	3.19	10	2-10	0.360	23.5	830
DD6	3.53	22	2-15	0.318	21.1	605
DD7	2.11	22	2-20	0.543	32.0	832
DD8	2.67	22	4-15	0.436	27.1	778
DD9	2.03	22	4-15	0.560	34.6	907
DD10	1.73	22	4-12	0.622	42.5	956
DD11	3.19	22	1-12	0.304	20.0	592
DD12	2.40	22	2-12	0.407	26.4	723
DD13	2.13	22	4-12	0.460	29.5	821
DD14	2.71	22	2-10	0.425	25.1	728
DD20	2.89	22	2-10	0.342	22.2	587
DD20A	2.66	22	3-12	0.377	25.5	639

DD22	2.86	22	3-10	0.307	19.6	549
DD24	2.59	22	8-12	0.389	23.9	730
DD25	2.89	22	2-12	0.455	28.1	743
DD25A	2.67	22	4-12	0.493	28.5	783
DD25B	4.27	22	2-10	0.308	19.3	514
DD26	2.61	22	4-12	0.473	30.0	853
DD27A	4.08	22	1-8	0.320	20.5	566
DD27B	3.16	22	1-8	0.420	25.9	617
FFA	3.78	25	2-12	0.364	24.2	716
FFB	3.81	25	2-12	0.361	23.4	621
FFC	3.81	25	1-21	0.361	22.9	624
FFD	3.83	6	2-12	0.359	23.1	636
FFF	3.77	6	1-20	0.365	23.9	664
GG	2.46	22	2-5	0.401	28.0	970
A060	1.76	25	5-12	0.463	31.4	579
A130C	2.97	25	2-10	0.356	31.6	728
A130G	4.38	25	2-8	0.550	44.4	1203
A260	3.71	25	2-10	0.368	31.1	776
CM1701A	3.20	25	2-10	0.380	30.5	796
D072A	3.30	25	4-10	0.330	28.3	799
D092B	2.76	25	4-15	0.388	33.8	908
D092D	2.64	25	2-15	0.333	25.4	731
D092G	3.25	25	1-15	0.520	44.5	1163
D155B	2.70	25	1-15	0.399	31.5	854
D155C	2.99	25	2-15	0.474	38.9	1187
D155G	2.81	25	2-12	0.584	47.0	1314
D155H	2.93	25	4-15	0.515	38.3	1121
D155J	3.54	25	5-12	0.583	47.9	1142
D155K	4.45	25	1-12	0.328	28.1	861
ROV2	4.08	25	1-10	0.353	21.5	362
ROV3	3.15	25	2-10	0.400	20.9	422
X-Strand	6.17	13	0.5-2	0.570	38.0	694

Table B-3 - DOE/MSU Prediction Model Analysis

Material	*a*-coefficient	*b*-coefficient	R^2	# of Samples	W/I 5% log	W/I 10% log
WS1	2.409	11.311	0.980	17	13	16
E-LT-5500-VE	4.145	8.307	0.990	16	15	16
E-LT-5500-EP	1.183	10.180	0.987	17	13	17
QQ1	5.999	8.319	0.993	17	15	17
QQ2	6.177	10.007	0.990	7	7	7
QQ4L	14.539	11.258	0.990	7	7	7
QQ4	106.939	9.710	0.985	7	7	7
TT1A	10.613	10.536	0.956	10	8	10
TT1AH	11.265	9.487	0.949	10	8	10
TT	2.137	9.334	0.984	5	5	5
W45	55.853	16.090	0.947	9	6	9
SWA	5.488	15.310	0.966	9	7	8
SWB	12.820	13.910	0.868	9	6	8
B	5.502	11.776	0.869	9	2	7
L	2.794	10.633	0.704	5	0	3
M	3.943	6.742	0.995	6	6	6
N	5.894	7.904	0.997	7	7	7
P	24.359	9.046	0.994	10	8	10
R	117.111	15.577	0.964	15	9	11
V	1.822	8.627	0.975	14	12	14
W	2.221	11.709	0.983	8	8	8
X	31.027	16.267	0.967	8	8	8
Y	5.827	12.650	0.943	14	7	11
EE	6.995	11.741	0.986	14	11	14
EEAV	21.489	14.820	0.986	8	8	8
EEAP	20.747	16.795	0.979	8	6	7
EEBP	19.799	15.414	0.996	7	7	7
EECP	66.971	15.500	0.990	10	7	9
AA	3.742	8.644	0.995	10	10	10
AA3	1.154	7.989	0.989	9	8	9
AA4	7.732	14.683	0.973	8	7	8
BB	59.416	11.750	0.986	18	15	18
CC	55.558	12.186	0.991	14	12	14
CC2	4.796	11.431	0.994	10	10	10
CC3	2.035	11.057	0.977	13	12	13
CH	0.401	12.325	0.972	10	8	10
CH2	6.105	11.108	0.980	13	10	13

CH3	31.552	15.411	0.994	12	12	12
CH4	4.260	12.764	0.977	12	8	12
CH5	1.440	12.185	0.983	9	8	9
CH6	2.167	9.047	0.992	19	17	19
CH7	0.395	13.163	0.993	8	8	8
CH8	0.382	12.075	0.975	10	8	10
CH9	3.018	13.360	0.981	11	9	11
CH10	23.104	17.676	0.989	10	8	10
CH11	0.905	13.559	0.993	10	10	10
CH12	2.062	13.990	0.976	11	9	11
CH13	2.757	9.284	0.984	10	8	10
CH14	10.516	10.861	0.979	13	9	13
CH15	23.287	17.162	0.974	11	6	10
CH16	3.395	10.946	0.976	14	10	12
CH17	1.797	9.636	0.986	12	10	12
CH18	2.061	10.546	0.994	12	11	12
CH19	1.513	13.991	0.987	11	10	11
CH20	0.547	11.424	0.994	8	8	8
CH23	2.369	9.916	0.995	8	8	8
DD	4.321	8.961	0.994	15	15	15
DD2	15.423	13.757	0.998	9	9	9
DD4	2.580	8.647	0.979	9	8	9
DD5	3.466	13.155	0.992	11	11	11
DD5E	28.273	15.476	0.962	9	6	8
DD5P	35.315	16.193	0.977	8	7	8
DD5V	8.383	14.332	0.978	9	7	8
DD5V2	15.751	14.439	0.980	8	8	8
DD5CYC	2.222	8.261	0.989	9	8	9
DD6	17.000	15.979	0.982	8	6	8
DD7	1.254	7.541	0.984	10	8	10
DD8	3.284	13.800	0.982	8	8	8
DD9	0.968	7.889	0.993	9	9	9
DD10	1.671	8.406	0.983	7	7	7
DD11	52.827	17.340	0.975	10	6	9
DD12	1.464	10.771	0.977	8	8	8
DD13	2.511	9.602	0.988	9	9	9
DD14	5.037	9.805	0.978	9	9	9
DD20	0.351	7.100	0.982	9	9	9
DD20A	0.936	7.645	0.936	8	5	8
DD22	4.278	14.284	0.933	6	5	6

DD24	1.895	10.303	0.957	6	6	6
DD25	11.787	10.718	0.910	9	6	7
DD25A	1.788	9.859	0.954	8	8	8
DD25B	3.421	13.091	0.887	7	6	7
DD26	4.211	10.483	0.976	10	10	10
DD27A	14.452	9.645	0.994	8	8	8
DD27B	2.288	9.409	0.995	13	13	13
FFA	39.802	11.621	0.976	14	10	13
FFB	7.617	11.209	0.981	9	6	8
FFC	11.799	11.696	0.992	12	10	12
FFD	3.124	11.799	0.989	11	11	11
FFF	1.987	10.910	0.987	12	10	12
GG	43.092	13.658	0.971	9	9	9
A060	1.209	14.308	0.936	5	3	5
A130C	40.294	18.752	0.984	10	7	10
A130G	28.591	9.987	0.969	10	6	9
A260	4.685	15.068	0.955	9	6	9
CM1701A	2.958	9.622	0.940	9	7	7
D072A	3.313	12.172	0.984	10	10	10
D092B	1.836	12.142	0.979	13	13	13
D092D	14.331	17.393	0.946	7	4	7
D092G	6.226	8.805	0.962	16	7	15
D155B	11.778	14.472	0.987	17	15	17
D155C	18.025	11.137	0.995	10	10	10
D155G	3.535	8.129	0.991	11	9	11
D155H	44.987	14.860	0.983	11	10	11
D155J	2.989	11.180	0.966	10	8	10
D155K	210.231	14.468	0.972	11	8	10
ROV2	5.714	13.477	0.974	9	6	8
ROV3	19.088	12.349	0.973	11	8	11
X-Strand	6.616	14.390	0.995	6	6	6